UNIVERSITA' VITA-SALUTE SAN RAFFAELE

CORSO DI DOTTORATO DI RICERCA INTERNAZIONALE IN MEDICINA MOLECOLARE

CURRICULUM IN IMMUNOLOGIA E ONCOLOGIA DI BASE E APPLICATA

Dissecting the mechanisms of transcriptional regulation by PML in triple-negative breast cancer

DoS: Dr. Bernardi Rosa

Second Supervisor: Dr. Collas Philippe

Tesi di DOTTORATO di RICERCA di Fracassi Cristina

matr. 013853

Ciclo di dottorato XXXIV

SSD: BIO/13

Anno Accademico 2020/2021

CONSULTAZIONE TESI DI DOTTORATO DI RICERCA

Il/la sottoscritto/*I* Fracassi Cristina

Matricola / *registration number* 013853

nat_ a/ *born at* Roma

il/*on* 20/07/1994

autore della tesi di Dottorato di ricerca dal titolo / *author of the PhD Thesis titled*

Dissecting the mechanisms of transcriptional regulation by PML in triple-negative breast cancer

☒ AUTORIZZA la Consultazione della tesi / AUTHORIZES *the public release of the thesis*

☐ NON AUTORIZZA la Consultazione della tesi per …… mesi /DOES NOT AUTHORIZE *the public release of the thesis for …… months*

a partire dalla data di conseguimento del titolo e precisamente */ from the PhD thesis date, specifically*

Dal / *from* ……/……/…… Al / *to* ……/……/……

Poiché /*because*:

□ l'intera ricerca o parti di essa sono potenzialmente soggette a brevettabilità/ *The whole project or part of it might be subject to patentability;*

□ ci sono parti di tesi che sono già state sottoposte a un editore o sono in attesa di pubblicazione/ *Parts of the thesis have been or are being submitted to a publisher or are in press;*

□ la tesi è finanziata da enti esterni che vantano dei diritti su di esse e sulla loro pubblicazione/ *the thesis project is financed by external bodies that have rights over it and on its publication.*

Data /Date 23/03/2022 Firma /Signature Fracassi Cristina

DECLARATION

This thesis has been composed by myself and has not been used in any previous application for a degree. Throughout the text I use both 'I' and 'We' interchangeably.

All the results presented here were obtained by myself, except for:

1) Bioinformatics analyses on RNA-sequencing and ChIP-sequencing data (Results, chapter 3.1 and 3.2, Figure 9B, Figure 14D, and Figure 46B), which were performed by Dr.E. Zapparoli, Center of Omics Sciences, San Raffaele Scientific Institute, Milan, Italy.

All sources of information are acknowledged by means of reference

ABSTRACT

The promyelocytic leukaemia PML protein is the molecular scaffold of phase-separated organelles known as PML nuclear bodies (PML-NBs). Existing evidence propose that PML-NBs act as nuclear platforms for the post-translational modification and activity of a large number of proteins that transit through them in a dynamic manner and upon cellular stress. Most PML interactors are transcription factors (TFs), transcriptional regulators and chromatin remodelling proteins, which implicates PML in regulation of transcription at various levels. In this respect, PML has been mainly described as an indirect regulator of transcription, by acting as a transcriptional co-activator or co-repressor of TFs, or by promoting or inhibiting the activity of chromatin modifiers. In addition, although it does not bind DNA directly, several lines of evidence suggest a more direct role of PML into transcriptional regulation, via its association with specific DNA regions or larger chromatin domains, where it may regulate epigenetic profiles, chromatin composition and chromatin architecture. In this framework, is still unclear to what extent PML regulates transcription via either direct or indirect mechanisms, or if it exerts these activities in concert.

In the context of triple-negative breast cancer (TNBC), we found that PML promotes the expression of pro-metastatic genes by influencing transcription at multiple levels and in distinct modalities. Specifically, we identified PML bound to chromatin in two distinct conformations and in opposite chromatin environments: narrow peaks found in euchromatin regions, and broad domains found in heterochromatin regions. We unveil that PML directly or indirectly regulates transcription by means of these two modalities, acting as a transcriptional co-activator or co-repressor, as well as a structural protein involved in the organization of chromatin domains. Our data demonstrate for the first time that PML may exert its transcriptional functions in multiple ways and parallelly in the same cellular context.

TABLE OF CONTENTS

ACRONYMS AND ABBREVIATIONS

ALT: Alternative length of telomeres

APBs: ALT-associated PML-NBs

APL: Acute promyelocytic leukemia

bHLH: basic-helix-loop-helix

ChIP: Chromatin immune precipitation

CBP: CREB-Binding Protein

C-TAD: C-terminal transactivation domains

DAXX/ATRX: Death domain-associated protein/α-thalassemia, mental retardation, X-linked

DSG: disuccinimidyl glutarate

EPO: glycoprotein hormone erythropoietin

EDD: Enriched Domain Detector

FIH: factor inhibiting HIF

HIFs: Hypoxia-Inducible Factors

HIFα: Hypoxia-inducible factor α-subunit

HIRA: histone cell cycle regulator

HP1: Heterochromatin Protein 1

HPTMs: Histone posttranslational modifications

HREs: hypoxia responsive elements

HSV-2: Herpesvirus protein

HSC70: Heat shock proteins 70 kilodaltons

ICP: Inductively coupled plasma

IDR: Intrinsically disordered regions

IFNγ: Interferone gamma

LINE: long interspersed nuclear element

LLPS: Liquid-liquid phase separation

MAPPS: mitotic accumulations of PML protein

MDM2: Mouse double minute 2 homolog

MEFs: Mouse Primary Embryonic Fibroblasts

MHC: Major histocompatibility complex

mRNA: messenger ribonucleic acid

ncRNA: non-coding RNA

NES: Nuclear export signal

NLS: Nuclear localization signal

NPCs: Nuclear pore complexes

NTAD: N-terminal transactivation domain

ODDD: oxygen-dependent degradation domain

OXPHOS: oxidative phosphorylation system

PADs: PML associated domains

PHD: prolyl hydroxylase domain

PML: Promyelocytic leukaemia protein

PML-NBs: Promyelocytic leukaemia nuclear bodies

PONDR: Predictor of Natural Disordered Regions

PTMs: Post-translational modifications

pVHL: von Hippel–Lindau protein

RARα: Retinoic receptor alpha

RNA: Ribonucleic acid

SAHFs: senescence-associated heterochromatin foci

SIM: SUMO-interacting motif

SINEs: Short interspersed nuclear elements

SUMO: Small Ubiquitin-like Modifier

TAD: transactivation domain

TADs: topologically associated domains

TFs: Transcription factors

TSS: Transcription start site

TNBC: Triple negative Breast Cancer

TRIM: Tripartite motif proteins

LIST OF FIGURES AND TABLES

1. INTRODUCTION

1.1 The promyelocytic leukaemia protein PML

The promyelocytic leukaemia protein PML is the molecular scaffold of phase-separated organelles known as PML nuclear bodies (PML-NBs). PML is a highly promiscuous protein able to interact with an ever-increasing number of proteins that transit through the PML-NBs in a dynamic manner and upon cellular stresses (Bernardi & Pandolfi, 2007). The PML-NBs have been initially described as nuclear scaffolds for the assembly and regulation of protein complexes, and based on the number of proteins that reside or transit through the PML-NBs, PML has been implicated in almost all biological processes. Also, PML appears to exert different functions depending on the biological context in which it operates. This is particular evident in cancer where it may exert tumour suppressive or oncogenic functions depending on the tumour context (Mazza & Pelicci, 2013).

In this chapter, I will give an overview of PML biology starting from its gene and protein structure, then describing its nuclear distribution and shortly going through its general functions, with a focus on transcription regulation and cancer. Moreover, I will describe the basic principles of genome organization and then provide a description of the physical and functional interactions of PML and the PML-NBs with chromatin.

1.1.1 Gene and protein structure of PML

PML is a member of the TRIM family of proteins which comprises proteins harbouring a conserved N-terminal motif formed by a RING finger, two B-boxes, and a coiled-coil domain (also called RBCC) and diverging C-terminal domains (Sardiello *et al*, 2008). The *PML* gene (*TRIM19*) is located on chromosome 15q22 and comprises 9 exons (figure 1). PML pre-mRNA is extensively processed via alternative splicing leading to the production of seven main isoforms (PMLI to PMLVII, figure 1) (Jensen *et al*, 2001). All PML isoforms share the first 3 exons, encoding the TRIM/RBCC motif, and arrange the following exons in a variable manner (figure 1). Exons 7 and 8 are subdivided into “a” and “b” because they contain cryptic splicing sites that undergo alternative usage, possibly accompanied by intron retention (figure 1). Moreover, all isoforms may generate additional variants due to alternative splicing of exons 4, 5 or 6 in different combinations

(Nisole *et al*, 2013), thus increasing the number of possible PML isoforms above the canonical 7 described in figure 1.

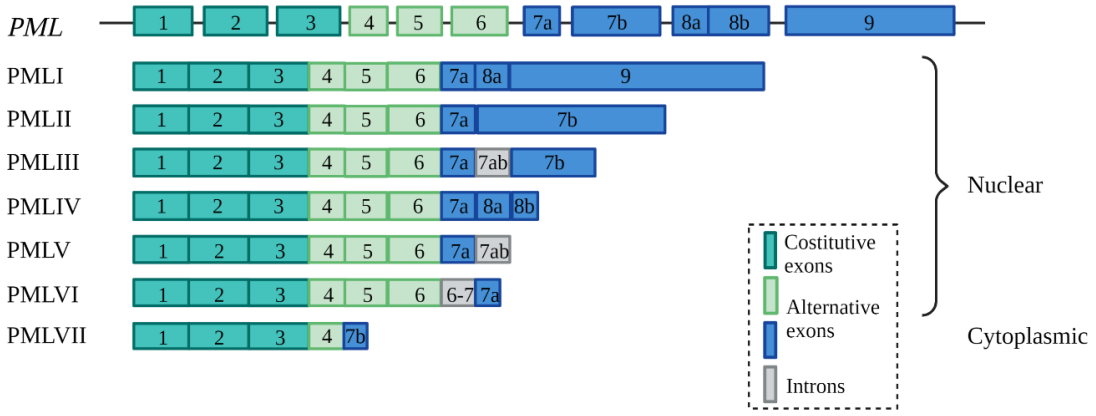

Figure 1. Structure of the PML gene and of its isoforms. *Promyelocytic leukemia (PML) gene comprises nine exons (1-9) that are alternatively spliced into seven main isoforms (I-VII). All PML isoforms contain the constitutive exons 1-3, whilst exons 4-9 are spliced in different combinations. Intron retention may occur in different alternative splicing events. Created with Biorender.*

At the protein level, the TRIM/RBCC motif promotes homo-multimerization and partakes in the self-assembly of PML-NBs (Lallemand-Breitenbach & de The, 2010). Most PML isoforms contain a nuclear localization signal (NLS) and SUMO-interacting motif (SIM), with the exception of PMLVI that lacks the SIM domain (figure 2) and PMLVII that lacks both NLS and SIM and is thus cytoplasmic (figure 2) (Mcnally *et al*, 2008) (Nisole *et al*, 2013).

PML proteins undergo multiple post-translational modifications, the most important being SUMOylation, which is involved in the formation of the PML-NBs, as described later (Geng *et al*, 2012). Although PML may be SUMOylated at different residues, the main SUMO acceptor sites are embedded in the RBCC motif and in proximity to the NLS (figure 2) (Nisole *et al*, 2013).

PML C-terminal sequences are less structured and comprise few detectable motifs, which are thought to mediate isoform specific functions and proteins interactions (Nisole *et al*, 2013). For example, PMLI contains an exonuclease-III-like motif that is partly shared by PMLIV and has been implicated in nucleolar localization under genotoxic stress (Condemine *et al*, 2007), and a nuclear export signal (NES) that promotes nuclear-

cytoplasmic shuttling (Condemine *et al*, 2006; Wang *et al*, 2019). PMLV harbours instead an α-helix that partakes in the formation of PML-NBs (Geng *et al*, 2012) (figure 2).

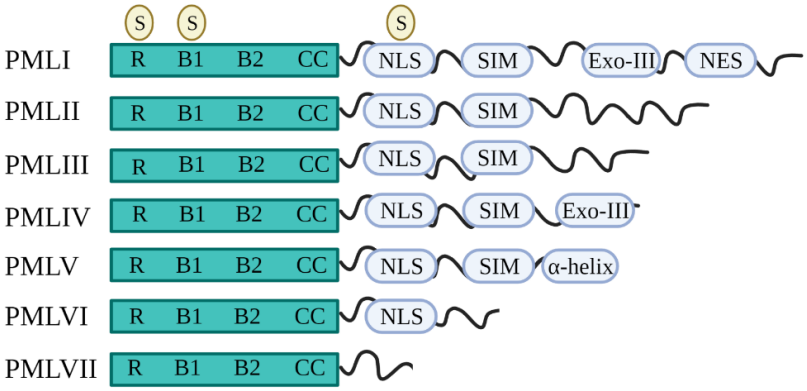

Figure 2. Protein structure of PML protein isoforms. *All isoforms share the N-terminal tripartite motif/ring finger, B box, coiled-coiled (TRIM/RBCC) domain with two main ubiquitin modifier (SUMO)ylation sites. PMLIVI contains a NLS and a SUMOylation site, and PMLI-V contain a SIM that is not present in PMLVI. PMLVII lacks both NLS and SIM and localizes to the cytoplasm. Few isoform-specific motifs have been identified in unique C-terminal regions: PMLI harbours a NES and an Exo-III domain, partly encoded by PMLIV, and PMLV contains a structural alpha helix. Created with Biorender.*

The extensive alternative splicing by which *PML* is processed is a common feature of many TRIM family members, suggesting that some evolutionary pressures may have caused the diversification of this protein family (Liao & Garcia-Blanco, 2021). Interestingly, a common trait among TRIM proteins is their involvement in viral responses and innate immunity (Versteeg *et al*, 2014). PML has been widely described as a viral restriction agent and distinct PML isoforms have been shown to physically and functionally interact with viral particles via their unique C-terminal domains. For instance, exon 9 of PMLI, which represents the C-terminal portion of the putative Exo-III motif, is essential for the interaction with the viral protein ICP0 of the Herpes Simplex Virus 1 (HSV-1) and to prevent the viral-induced degradation of the PML-NBs (Cuchet-Lourenco *et al*, 2012). In light of such evidence, it is tempting to speculate that the diversification of PML isoforms, along with the expansion of the TRIM family tree in mammals, have occurred under the genetic pressure of viral infections or demand of expanded innate immune responses in mammals (Liao & Garcia-Blanco, 2021). Perhaps supporting this hypothesis, viruses have coevolved several resistance mechanisms to

overcome PML-induced degradation. One of these mechanisms affects the splicing profile of PML pre-mRNA upon viral infection. Such is the case of the herpesvirus protein (HSV-2) ICP27 which binds PML pre-mRNA and acts as splicing silencer inhibiting skipping of intron 7ab. Importantly, retention of intron 7ab promote the switching from PMLII to PMLV and boosts HSV-2 replication, showing that the modulation of PML splicing exerted by the viral protein is aimed to enhance viral propagation (Nojima *et al*, 2009).

1.1.2 The PML-NBs and the nuclear distribution of PML

PML-NBs are dynamic and stress responsive nuclear aggregates that contain few resident proteins, such as SP100 and DAXX, and a plethora of transient clients. PML-NBs are donut-shaped 0.2-1.0 μm wide structures formed by a proteinaceous shell that surrounds a fibrillary central hole (Lallemand-Breitenbach & de The, 2010). Typically, 1 to 30 PML-NBs can be found per nucleus, with their number and distribution varying throughout the cell cycle, in different cell types, and upon stress conditions (Lallemand-Breitenbach & de The, 2010; Bernardi & Pandolfi, 2007). In the nucleus, PML-NBs localize in the intrachromosomal space (Lallemand-Breitenbach & de The, 2010) and only marginally contact chromatin via their proteinaceous outer shell (Dellaire *et al*, 2006b). From a biochemical perspective, assembly of PML-NBs begins with the self-aggregation of PML monomers, which homo-multimerize via oxidation-driven disulfide bridges and non-covalent binding of their RBCC domains. Importantly, PML mutants lacking the RBCC domain are unable to aggregate into NBs, thus suggesting that the RBCC plays a crucial in the initial assembly of PML-NBs (Sahin *et al*, 2014; Wang *et al*, 2018). As a second step, the SUMO-ligase UBC9 is recruited to PML multimers where it catalyzes the deposition of SUMO 1, 2 and 3. PML SUMOylation enhances the binding of PML homo-multimers by concatenating them via SUMO/SIM interactions. In addition, PML SUMOylation promotes the recruitment of client proteins, which often share the feature of being SUMOylated or containing a SIM domain (figure 3)(Hoischen *et al*, 2018). This array of events involves structural changes that lead to the rearrangement of PML aggregates into a hollow sphere occupied by SUMO 2/3 polymers and a surrounding proteinaceous shell formed by PML and its protein partners (figure 3).

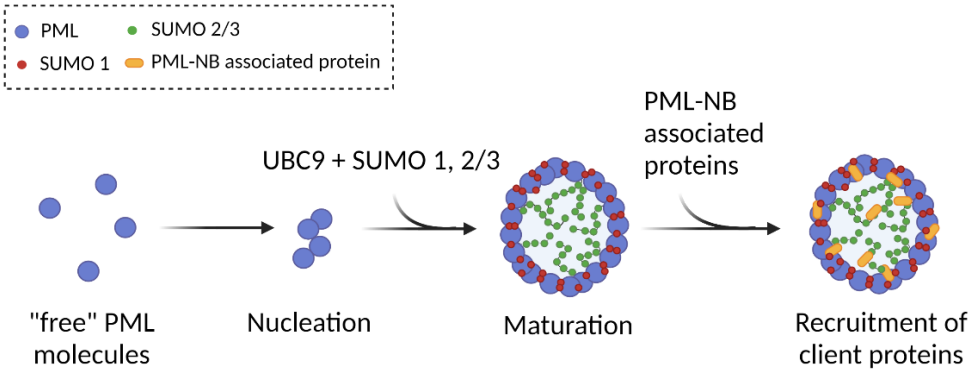

Figure 3. Biogenesis of PML-NBs. *PML-NBs assembly occurs as an ordered array of events. i) Nucleation: "free" PML molecules in the nucleoplasm homo-multimerize into small PML aggregates. ii) Maturation: UBC9 and SUMO proteins are recruited to PML multimers enhancing their associations. iii) Recruitment of client proteins: PML SUMOylation recruits constitutive and transient client proteins that distribute to the PML-NBs ring. Created with Biorender.*

While PML-NBs formation has been proposed as a clear and ordered sequence of events, more recently it is emerging that it may be far more complex. In this respect, it was recently demonstrated that PML aggregates may assemble via liquid-liquid phase separation (LLPS), a dynamic and reversible process by which two separate liquid phases coexist in the same environment (Banani *et al*, 2016; Corpet *et al*, 2020). LLPS has been recently described as a key process in the biogenesis of membraneless organelles and in the compartmentalization of nuclear processes such as transcription. The process is triggered by the increase in concentration of a specific protein, named "scaffold", in a confined region of the cell. Usually, scaffold proteins are characterized by multiple folded domains or intrinsically disordered regions (IDR) that interact and recruit "client" proteins. Most of the interactions occurring between scaffold and clients are weak and reversible, thus allowing the dynamic composition of the condensates (Banani *et al*, 2017). PML-NBs exhibit many properties of LLPS-based structures: i) PML contains IDR regions throughout its protein structure, especially in PMLI (figure 4A, data obtained by the analysis of PML amino acid sequence with PONDR, Fonin *et al*, 2021); ii) PML and clients proteins of the PML-NBs are endowed with a number of domains that establish weak interactions, including the RBCC and SIM domains (Lallemand-Breitenbach & de The, 2010); iii) PML-NBs exhibit buffering effects, by sequestering

partners proteins upon PML upregulation, as in the case of interferon induction (figure 4B, left, Everett & Chelbi-alix, 2007); iv) PML-NBs undergoes fusion/fission events in physiological or stress conditions (figure 4B, right, Eskiw *et al*, 2003); vi) clients proteins are able to shuttle in and out of the PML-NBs (figure 4B, centre).

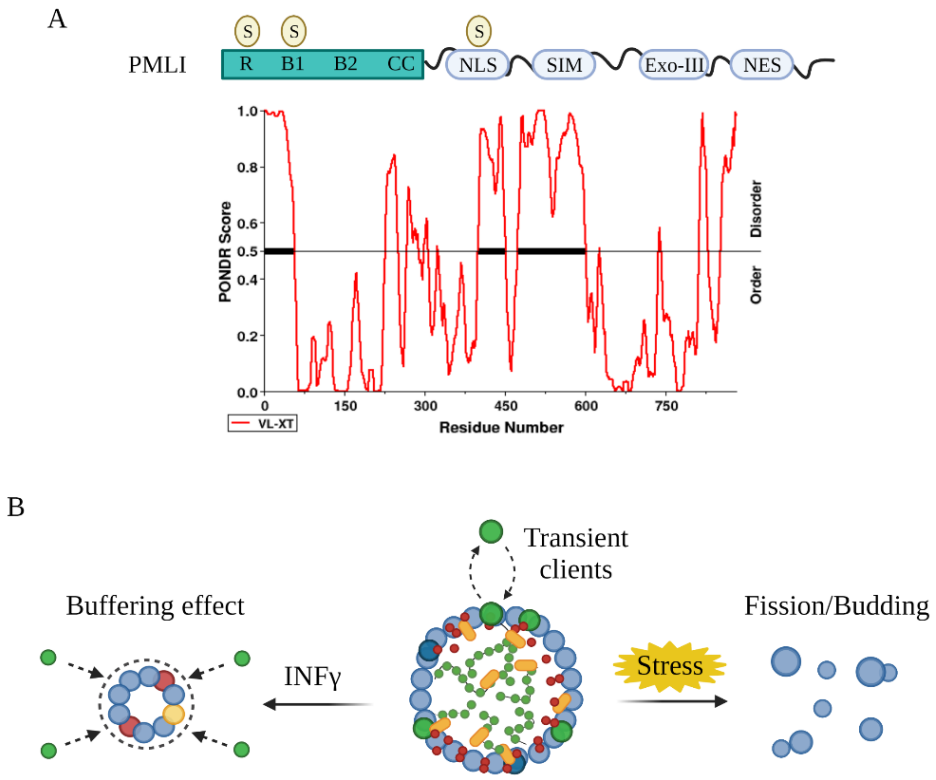

Figure 4. Biogenesis of PML-NBs based on the LLPS model. *PML-NBs assembly is influenced by different biophysical forces. A) Protein structure of PMLI and the IDR regions predicted by the PONDR algorithm. B) PML-NBs host transient client proteins, which dynamically interact with PML via weak interactions (middle); PML-NBs increase in size and number upon IFNγ treatment, leading to enhance recruitment of clients (left); in stress conditions the PML-NBs lose their integrity and break down into PML-based microstructures (right). Created with Biorender.*

Finally, another important concept that must be highlighted is that PML is also present in a free, or soluble state in the nucleus. This has been shown by biochemical fractionation, where PML is found mostly in the RIPA soluble fraction, corresponding to the nucleoplasm, with only a small fraction present in the RIPA insoluble fraction, representing the nuclear matrix (Pampin *et al*, 2006; El Mchichi *et al*, 2010). Moreover, oxidative stress induces multimerization of PML into insoluble assemblies that constitute

the PML-NBs, supporting the existence of different biochemical conformations (Jeanne *et al*, 2010; Sahin *et al*, 2014). In line with this evidence, imaging studies clearly demonstrated that PML-NBs are highly dynamic environments where proteins, including PML, shuttle in and out with different diffusion rates (Brand *et al*, 2010; Weidtkamp-Peters *et al*, 2008). Interestingly, nucleoplasmic PML has been shown to be less mobile when compared to GFP, suggesting that even outside the PML-NBs PML may be bound to an immobile structure, such as chromatin, or maybe part of large protein complexes (Hoischen *et al*, 2018). Therefore, in the context of PML-NBs biogenesis it is important to consider the contribution of the free PML molecules, which drive the nucleation of PML-NBs at any given time and place. In this respect, it is possible that in specific regions of the nucleus, such as transcriptional hubs, clusters of stress responsive proteins, DNA or RNA molecules act as seeding signals for the recruitment of free PML, thus increasing its concentration and promoting formation of a PML-NB (Corpet *et al*, 2020). Accordingly, several pieces of evidence describe *de novo* formation of PML-NBs in specific nuclear domains, such as telomeres (Loe *et al*, 2020), suggesting that tethering of PML to chromatin may induce the formation of specialized PML-NBs at targeted loci.

In conclusion, the physical properties of the PML-NBs make them highly dynamic and heterogeneous, able to adapt their structure and composition along with specific cellular processes or among different cells and tissues (Bernardi & Pandolfi, 2007). Along these lines, the multivalency of PML interactions and the specific activities of each PML isoform make it unrealistic to define the composition and biogenesis of the PML-NBs with a unifying model. In addition, the contribution of the nucleoplasmic PML molecules enlarge even more the possible conformations of PML in the nucleus and increase the possible ways in which each PML-NBs assemble and specialize.

1.1.3 Functions of PML and the PML-NBs

The functions of PML have been delineated based on the proteins that reside or transit through the PML-NBs. To date, the PML-NBs have been reported to associate with over 170 interactors, most of which are client proteins recruited upon specific stress conditions (Van Damme *et al*, 2010). Often, client proteins are post-translationally modified within the PML-NBs by a number of proteins modifying enzymes. The most relevant example

is p53, which upon cellular stresses is recruited to the PML-NBs where it is post-translationally modified by a large number of enzymes that promote its acetylation, SUMOylation and phosphorylation (Bernardi *et al*, 2008). As a consequence, PML promotes p53 transcriptional activity in different contexts, leading to senescence or apoptosis (Bernardi *et al*, 2008). Another such example is the transcriptional repressor DAXX, which is a constitutive component of PML-NBs. Under osmotic stress, the protein kinase CK2 is recruited to the PML-NBs to target DAXX for sumoylation, thus leading to repression of anti-apoptotic genes (Chang *et al*, 2011). Based on these and many other examples, the PML-NBs have been initially described as platforms for the post-translational modification of nuclear proteins (Bernardi & Pandolfi, 2007). However, along with the discovery of new PML-NBs clients it soon became evident that PML exerts many other functions. As previously described, the PML-NBs forms via LLPS and constitute an isolated nuclear compartment that increases the local concentration of its client proteins. In this way, the PML-NBs allow the isolation and exclusion of specific proteins, thereby inhibiting their nucleoplasmic functions, as well as the interaction among protein partners, thus favouring their activities. For these reasons, the PML-NBs are now generally described as scaffold domains for the dynamic assembly and regulation of nuclear protein complexes (Bernardi & Pandolfi, 2007).

The molecular functions of PML are particular evident under cellular stress conditions and environmental cues, such as growth factors and cytokines, which regulate the number and structure of PML-NBs, leading to the definition of PML-NBs as stress-responsive structures (Bernardi & Pandolfi, 2007). As already mentioned, type I and II interferons upregulate PML transcription and increase the number and size of the PML-NBs (Nisole *et al*, 2013), as well as the recruitment of PML-NBs clients proteins. Similarly, heavy metal exposure, heat shock and many other environmental stresses influence the morphology and functions of the PML-NBs (Eskiw *et al*, 2003), supporting a role of PML as a sensor of cellular stresses. Finally, PML has been more widely involved in the regulation of gene expression, by regulating the activity of transcription factors (TFs), associating non randomly with specific chromatin regions, and promoting localized transcription and/or chromatin organization (Corpet *et al.*, 2020).

Given the pleiotropism of its molecular functions, at the systemic level PML has been involved in the regulation of many biological processes. A detailed description of the many cellular functions of PML is beyond the scope of this thesis, however, I will briefly go through the most relevant examples.

Apoptosis and DNA repair:

The first evidence of PML function in apoptosis came from studies on *Pml* KO mice, which display resistance to multiple apoptotic stimuli. Accordingly, PML promotes the transcriptional activity of many pro-apoptotic factors, including p53, DAXX and c-Jun (Bernardi *et al*, 2008). In the same way, PML positively regulates the activity of checkpoint proteins after DNA damage, thereby leading to apoptosis. These proteins dynamically localize to the PML-NBs which are found proximal DNA repair and single-stranded DNA damage foci. In this concern, the PML-NBs have been also shown to partake in DNA repair via homologous recombination (Yeung *et al*, 2011; Boichuk *et al*, 2011; Vancurova *et al*, 2019) and host several DNA repair enzymes (Bernardi & Pandolfi, 2007).

Metabolism:

Another known function of PML in cell physiology is the regulation of metabolism. (Cheng *et al*, 2013; Carracedo *et al*, 2012). For instance, loss of PML in obese mouse models leads to an increased metabolic rate of glucose and fatty acids and to a reduction of obese symptoms. Nonetheless, PML has been shown to play opposing functions depending on the mouse strain, diet and age (Kim *et al*, 2011), suggesting a highly context dependent activity of PML in the regulation of fatty acid metabolism. Among other metabolic pathways, PML regulates the degradation of misfolded nuclear proteins by promoting SUMO2/3- dependent poly-sumoylation of target proteins (Guo *et al*, 2014).

Angiogenesis:

PML has been also involved in the negative regulation of angiogenesis during hypoxia. For example, PML overexpression in such context suppresses the activity of the TF HIF1α in promoting transcription of pro-angiogenic factors, such as VEGF (Bernardi *et al*, 2006). Accordingly, loss of PML results in increased neo-angiogenesis in several pathological settings (Lin *et al*, 2014; Dvorkina *et al*, 2016)

Immunity:

PML partakes in the regulation of several innate immune responses. As such, loss of PML results in impaired anti-bacterial macrophage activity under infections and downregulation of inflammatory cytokines such as IL6 and IL-1B (Lunardi *et al*, 2011; Lo *et al*, 2013). In addition, IFNs and TNF inflammatory cytokines promote PML expression, which in turn mediates the activation of their downstream signalling pathways (Cheng *et al*, 2012). This is particularly evident upon viral infection, which leads to IFNs production and PML upregulation. In this context, PML acts as a viral restricting agent by promoting transcription of interferon stimulated genes and leading to apoptosis (Crowder *et al*, 2005; Hsu *et al*, 2017). Furthermore, the PML-NBs are targeted by many viral proteins, which hijack their structure to promote viral replication, underlining the functional implication of PML in viral infection (Geoffroy & Chelbi-Alix, 2011).

In sum, many biological functions are associated to PML and they will certainly increase as new PML interactors or stress-related activities are identified. For the aim of this thesis, we are going to focus on the transcriptional functions of PML and the PML-NBs.

1.1.3.1 PML and transcription regulation

Although PML does not bind DNA directly, regulation of transcription is among the first functions associated to PML. Because a large number of transcriptional regulators localize to the PML-NBs, PML was initially described as a transcriptional co-activator or co-repressor (Zhong *et al*, 2000). As an example, PML interacts with the oncoprotein c-Fos to enhance AP-1 transcriptional activity (Vallian *et al*, 1998) and promotes c-Jun DNA binding and transcriptional activation upon UV irradiation (Salomoni *et al*, 2005). Conversely, PML interacts with STAT3 and inhibits its DNA binding and transcriptional activity (Kawasaki *et al*, 2003). These and many other proteins involved in transcriptional regulation dynamically localize to the PML-NBs.

Given the high concentration of protein modifying enzymes, the PML-NBs influence transcription by acting as platforms for the activation or repression of TFs and transcriptional regulators (Bernardi & Pandolfi, 2007). In addition, by providing domains

that confine the distribution of client proteins, PML-NBs limit their activity in the nuclear space and promote the interaction among TFs and transcriptional regulators. For instance, PML upregulation induces sequestration of the transcriptional repressor DAXX into the PML-NB, allowing transcription of DAXX-repressed genes (Li *et al*, 2000).

These and other studies have implicated the PML-NBs into transcriptional regulation mainly via indirect mechanisms, by modulating the activity of transcriptional regulatory proteins. Yet, PML has also been shown to interact with specific chromatin regions and regulate chromatin organization, suggesting a more direct role in transcriptional regulation. In addition, while PML-NBs are normally devoid of nucleic acids in their internal structure, nascent RNA (Tashiro *et al*, 2004) and highly acetylated chromatin regions (Boisvert *et al*, 2000) are found proximal to their outer proteinaceous shell. The PML-NBs were also found to associate with specific genomic regions, such as the major histocompatibility complex (MHC) locus (Shiels *et al*, 2001) and the p53 locus (Sun *et al*, 2003), as well as with transcriptionally active regions (Wang *et al*, 2004). PML is also a known interactor of the structural protein SATB1, with whom it cooperates to organize chromatin loops at the MHC class I locus and gene transcription upon IFNγ induction (Kumar *et al*, 2007). Interestingly, the association of PML to the MHC gene clusters (class I and II) has been extensively investigated and provides evidence of specific interactions that may occur between PML and chromatin (Shiels *et al*, 2001). In detail, the PML-NBs specifically interact with the centromeric end of the MHC locus independently of transcription and cell type specificity (Shiels *et al*, 2001). In addition, IFNγ regulates the nuclear localization, transcription and epigenetic memory of the MHC II locus in a PML-dependent manner (Ulbricht *et al*, 2012; Gialitakis *et al*, 2010). Upon IFNγ, the DRA gene associates with the PML-NBs, which, in cooperation with the the H3K4-methyltransferase complex MLL, promote the formation of a constitutive active chromatin state at the promoter region of the gene (Gialitakis *et al*, 2010). In opposition, PML is involved in the establishment of repressive chromatin regions, thereby inhibiting transcription. For example, the Setdb1 histone methyltransferase constitutively localize to the PML-NBs where it regulates gene repression by deposition of closed chromatin marks (Cho *et al*, 2011).

Although extensive investigations have been performed on the transcriptional functions of PML, it is still not clear whether these functions are exerted within the PML-NBs or by nucleoplasmic PML. This dualism also complicates the interpretation of studies that investigate the binding of PML to DNA by chromatin immune precipitation (ChIP). ChIP experiments have revealed that PML associates with the regulatory regions of different genes and it regulates their transcription in cooperation with specific TFs (Ponente *et al*, 2017; Sachini *et al*, 2019). Conversely, ChIP-sequencing performed in mouse primary embryonic fibroblasts (MEFs) has revealed that PML binds megabase-sized heterochromatin regions named PML associated domains (PADs), which do not contain regulated genes and do not associate with the PML-NBs. Taken together, these data demonstrate that PML can associate to different types of chromatin (eu- and heterochromatin), and that this may occur in a non-NB conformation (Delbarre *et al*, 2017). Yet, it should be highlighted that ChIP has several drawbacks that may complicate the study of DNA association by PML. First, ChIP is suitable for soluble proteins, while PML is partly found in the insoluble fraction of the nucleus (i.e. the nuclear matrix). Second, ChIP does not differentiate between the soluble and insoluble conformations of PML (Ching *et al*, 2013). To overcome these limitations novel approaches have been developed to attempt to identify chromatin regions associated with the PML-NBs. Immuno-TRAP is based on the local deposition of biotin on the DNA proximal to the PML-NBs via a PML-specific antibody, thereby allowing chromatin purification with streptavidin agarose beads (Ching *et al*, 2013; Wang *et al*, 2020). An alternative strategy uses an engineered APEX2 peroxidase fused to PML combined to deep-sequencing (ALaP-Seq) (Kurihara *et al*, 2020). With these methods, PML was found associated to the regulatory regions of active genes, as well as large DNA regions (300kb), such as the short arm of the Y chromosome (YS300) (Kurihara *et al*, 2020). Interestingly, PML does not appear to regulate the expression of genes identified by ALAP-sequencing, as the vast majority of genes identified with these protocols were not transcriptionally regulated upon PML inhibition, and conversely, genes regulated by PML were not enriched in PML-associated genes (Kurihara *et al*, 2020). However, it was reported that genes proximal to the YS300 locus, which is the most significantly enriched region in ALAP-sequencing and co-localizes with a PML-NB by DNA FISH, are regulated upon PML depletion via an indirect mechanism of exclusion of the DNA methyltransferase

DNMT3a from the proximity of PML-NBs, which creates a permissive chromatin environment that allows transcription of Y-linked genes (Kurihara *et al*, 2020). Notably, it remains unclear whether ALAP-sequencing and Immuno-TRAP enrich specifically the DNA proximal to PML-NBs, as FISH experiments utilizing such DNA as a probe identify many chromosomal regions that are not proximal to PML-NBs (Kurihara *et al*, 2020, Ching *et al*, 2013). Therefore, at the moment an experimental approach that clearly discriminates between DNA associated to PML-NBs or soluble PML moieties is still lacking.

In conclusion, transcriptional regulation via the PML-NBs has been described with two models in which the PML-NBs may act as i) depots of transcriptional regulators; ii) scaffolds for the assembly of specialized nuclear compartments (figure 5). These models need not to be mutually exclusive, as the PML-NBs may provide specialized nuclear compartments that concentrate and regulate the release of transcriptional regulators on nearby chromatin regions, although this hypothesis still needs to be addressed.

A very interesting and elusive observation is that most of the genes that are found associated to PML are not transcriptionally regulated in cells where PML has been suppressed and vice-versa, genes regulated in PML-suppressed cells minimally coincide with PML-bound genes (Kurihara *et al*, 2020; Delbarre *et al*, 2017) This confirms that PML regulates transcription via multiple mechanisms, that do not necessarily involve its association to DNA.

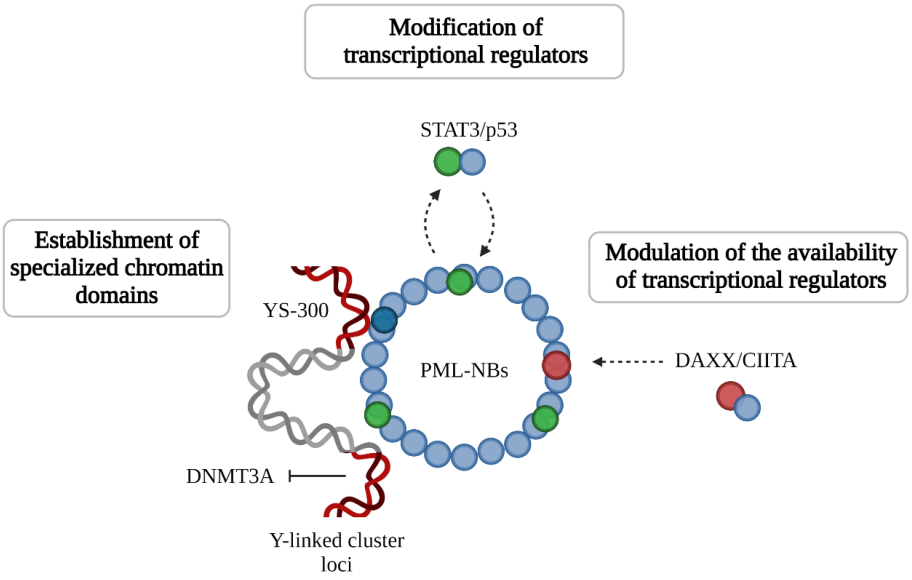

Figure 5. The role of PML-NBs in transcription regulation. *Mechanisms by which the PML-NBs modulates gene transcription: i) Modification and regulation of transcriptional regulators ii) Modulation of the availability of transcriptional regulators iii) Establishment of specialized chromatin domains. Created with Biorender.*

1.1.1.2 PML as a tumour-suppressor and oncogene

The large protein interactome of PML and its dynamic behaviour upon stress conditions contribute to its implication in a large number of biological processes, that range from DNA repair to angiogenesis and cell metabolism. Most of these processes are deregulated in cancer, thus depicting PML as fundamentally a cancer gene. Consistently, changes in the expression and activity of PML have been described in many types of tumours.

PML was originally cloned in acute promyelocytic leukemia (APL) at the breakpoint of the chromosomal translocation between chromosomes 15 and 17. In APL, the PML coding region is juxtaposed to the retinoic receptor alpha (RARα) gene leading to the production of the oncogenic protein PML- RARα (Melnick & Licht, 1999). The chimeric protein acts as a dominant-negative inhibitor of PML, impeding its homodimerization and the formation of PML-NBs. Starting from these first findings, most of the functions of PML have been studied in cancer where it was initially described as a tumour suppressor. In line with this, PML was found downregulated in a variety of tumours of different origin, such as prostate cancer and glioblastoma (Gurrieri *et al*, 2004). In addition, low PML expression levels correlate with bad prognosis and high-grade in breast and prostate

carcinomas (Gurrieri *et al*, 2004). These histopathological findings are consistent with many molecular functions attributed to PML, such as its regulation of p53 activity and inhibition of angiogenesis. Interestingly, although PML is translocated in APL, it is rarely mutated in primary tumours and human cell lines (Gurrieri *et al*, 2004).

Albeit initially described as a tumor suppressor, more recent findings show that the role of PML in cancer is highly context specific and PML is overexpressed in specific tumour subtypes where it acts as an oncogene (Mazza & Pelicci, 2013). The most remarkable example is triple negative breast cancer (TNBC), where PML overexpression correlates with early tumour recurrence (Carracedo *et al*, 2012). In this context, PML promotes survival to anoikis via the regulation of PPAR-α and fatty acid oxidation. Also, in contrast to its pro-senescent activity in other tissues, in TNBC PML blocks senescence by regulating MYC and PIM1 (Arreal *et al*, 2020). In line with these findings, our group demonstrated that PML promotes metastasis in TNBC by acting acts as a transcriptional co-activator of HIF1α towards the expression of pro-metastatic genes (Ponente *et al*, 2017). Other contexts in which PML acts as an oncogene are chronic myeloid leukaemia, where it promotes cancer stem cell maintenance via inhibition of cell proliferation (Ito *et al*, 2008) and ovarian cancer, where it sustains cancer cell growth by supporting DNA damage response pathways (Liu *et al*, 2017).

In summary, the role of PML in cancer biology seems to be highly context-dependent and probably reflects the vast range of its interactors with their tissue specific expression and function and the innate stress-responsive functions of PML. For these reasons, it is not possible to identify PML as a tumour suppressor or oncogene.

1.1.4 PML-NBs and chromatin dynamics

1.1.4.1 Hierarchical organization of chromatin

In eukaryotic cells, DNA is hierarchically organized in multiple conformations to allow proper nuclear compartmentalization and spatio-temporal regulation of gene expression. Although DNA is almost 2 m long, it can be functionally packed in a nucleus of a few micrometers in diameter, into a super-condensed state called chromatin. In this chapter I will give a brief overview on the first level of organization of chromatin, focusing on

histone modifications and chromatin compartments, and on how they might influence gene expression. I will then describe how the PML-NBs are involved in the regulation of chromatin structure at different levels.

The nucleosome:

Folding of DNA starts at the level of nucleosomes, where a stretch of 147 bp of DNA winds around a histone octamer formed by two H3–H4 and two H2A–H2B histone dimers (Prakash & Fournier, 2018). Each nucleosome is separated by a linker DNA region of variable length, bound by histone H1, giving rise to a distribution of nucleosomes over the entire length of DNA in a structure known as "beads on a string" (figure 6). Histone proteins not only act as scaffold for DNA folding but are also an important source of epigenetic information via post-translational modifications at their N-terminal tails or in the core nucleosomal structure (Prakash & Fournier, 2018; Lawrence *et al*, 2016) (figure 6). Histone post-translational modifications (HPTMs) provide information on the transcriptional status of chromatin thereby allowing the classification of chromatin in active euchromatic and inactive heterochromatic DNA regions. As a simple rule, euchromatin is characterized by high levels of histone acetylation and H3K4me1/2/3, whereas heterochromatin is marked by high levels of H3K9me2/3, H3K27me2/3. In addition, heterochromatin may be classified into constitutive and facultative heterochromatin based on H3K9me3 and H3K27me3 levels respectively (Lawrence *et al*, 2016). Although these marks may be used to generally describe the transcriptional status of chromatin, advances in sequencing and computational technologies have revealed a more complex scenario in which multiple HPTMs associate with specific gene regulatory elements (Jiang & Mortazavi, 2018). For instance, H3K4me3 marks active promoters, H3K4me1 and H3K27ac active enhancers, whereas H3K36me3 actively transcribed genes. In addition, even though H3K27me3 generally marks heterochromatin, it may be also found in close proximity to H3K4me3. This bivalent chromatin signature is defined as "poised" since it allows genes to be transcriptionally silent but ready to be activated if necessary (Jiang & Mortazavi, 2018). Finally, the epigenetic status of chromatin is also controlled by incorporation of histone variants (Henikoff & Smith, 2015) (figure 6). Histone variants are very similar to core histones and differ only in few amino acids or in the presence of additional domains. Incorporation of histone variants into DNA may have three main consequences on transcription. First, histone variants may harbour different

physical properties compared to canonical histones that change the structure and stability of the nucleosome. Second, the unique domain of each variant is recognized by specific chaperon proteins, thereby leading to the recruitment of distinct chromatin-associated complexes at specific regions of the genome. Third, histone variants are often enriched in specific or unique PTMs.

TADs and Chromatin compartments:

At a supra-nucleosomal scale, chromatin organizes into "loops" that enable interaction between distant gene regulatory regions, such as enhancers and promoters, creating contiguous globular-like structures (figure 6). In this way, chromatin loops segregate the nucleus into functionally related domains named topologically associated domains (TADs) (Dixon *et al*, 2012; Nora *et al*, 2012). TADs range from tens to hundreds of kilobases and are defined as regions of high frequency of contact among specific chromosomal loci. Multiple TADs are marked by boundaries formed by the binding of "insulator" proteins (i.e. CTCF), as well as active transcription marks, nascent transcripts, housekeeping genes and repeat elements (Dixon *et al*, 2012). The repetitive clustering of chromatin loops into TADs leads to the formation of spatially defined domains where genes tend to be co-regulated while constraining the interaction among inter-TADs elements (Bonev & Cavalli, 2016).

From one to hundreds megabase in size, TADs may be seen as clusters or compartments (figure 6). Based on their epigenetic state (or the epigenetic state of TADs herein comprised), compartments are divided into active (A) or inactive (B) compartments. A compartments represent large euchromatic DNA regions characterized by transcriptionally active genes and active histone marks, while B compartments are defined by heterochromatin and are characterized by the presence of silenced genes, repressive histone marks and late replication timing (Bonev & Cavalli, 2016). However, both A and B compartments may contain genes with divergent transcriptional activity (van Steensel & Belmont, 2017; Giorgetti *et al*, 2016). Juxtaposed A and B compartments repel each other and tend to distribute differently in the nuclear space, with A compartments localizing in the central region of the nucleus and close to the nuclear pore complexes (NPCs), and B compartments concentrating at the nuclear periphery, where they interact with components of the nuclear lamina (Buchwalter *et al*, 2019). Yet,

exceptions to this rule also exist, as B compartments can be found inside the nucleus and A compartments at the nuclear lamina.

Several mechanisms have been proposed for the segregation of euchromatin and heterochromatin, such as interaction among DNA regions with similar HPTMs and chromatin regulators, phase-separation and anchoring of heterochromatin to lamin via lamin-associated domains (LADs) (Hildebrand & Dekker, 2020). In addition, several studies suggest that repetitive DNA elements are implicated in the organization and assembly of A and B compartments (Solovei *et al*, 2016; Politz *et al*, 2013). Given the redundancy in their sequences, DNA repeats have high affinity for each other and may act as seeding points for the formation of chromatin domains (Solovei *et al*, 2016; Politz *et al*, 2013). For instance, homotypic clustering of the retrotransposon elements LINE and SINE supports the formation of hetero- and euchromatic domains respectively (Lu *et al*, 2021; Cournac *et al*, 2016).

Finally, it was recently suggested that interactions among multiple genomic loci may be facilitated by specific nuclear bodies, such as the nucleolus, Cajal bodies and the PML-NBs, which constrain their position into the nucleus (Quinodoz *et al*, 2018; Takei *et al*, 2021). Interestingly, the surface of nuclear bodies may provide a platform for the organization of multiple hubs of specific inter-chromosomal contacts. In addition, ncRNAs have been shown to regulate the assembly of chromatin territories proximal to NBs by promoting chromatin loop formation, heterochromatin maintenance and transcription (Khosraviani *et al*, 2019; Quinodoz *et al*, 2018).

In conclusion, the multiple ways in which the genome folds and spatially arranges in the nucleus critically contribute to regulation of gene expression and cell activities.

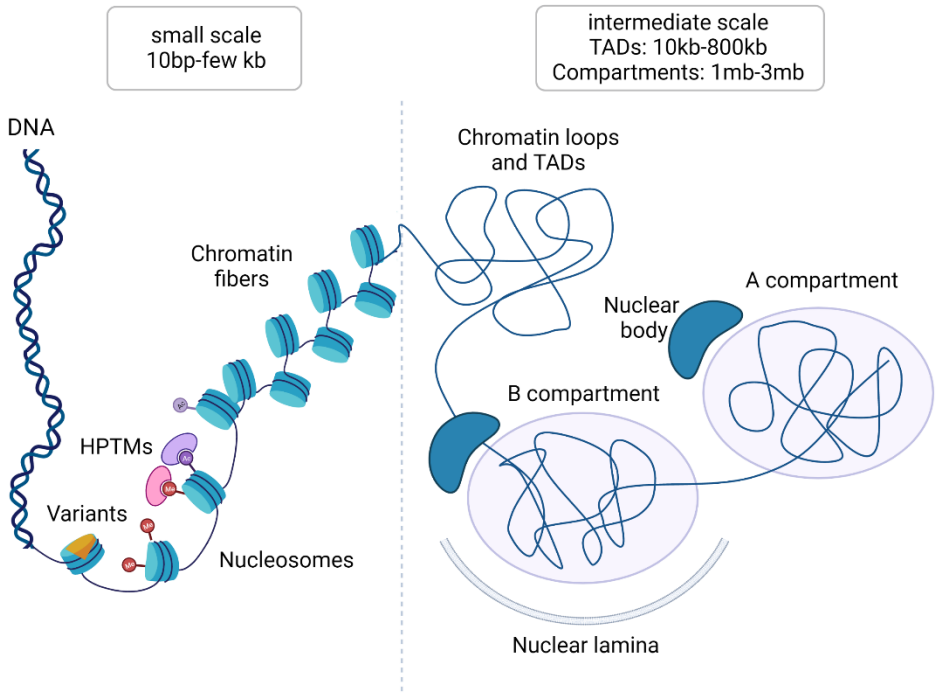

Figure 6. Hierarchical organization of chromatin structure. *The first level of chromatin organization is the nucleosome (left panel), in which DNA winds around a histone octamer. Histones are commonly modified by post-translational modifications and exist in different structural variants. Nucleosomes exhibit an array distribution on chromatin leading to the formation of fiber-like structures. Chromatin fibers further arrange in the nuclear space in higher-ordered structures (right panel). Starting from 10 kb in size, chromatin arranges in TADs. Chromatin aggregates of one to hundreds megabases in size are called clusters or compartments. Based on their epigenetic state, compartments are classified as active (A) or inactive (B). Nuclear bodies may sustain the spatial segregation of chromatin compartments and act as scaffolds for the generation of chromatin contacts. Created with Biorender.*

1.1.4.2 The physical connection of PML-NBs and chromatin

As already mentioned in the previous chapter, the PML-NBs are highly dynamic entities whose structure and nuclear localization relate to specific chromatin regions. In this concern, the link among PML-NBs goes beyond the transcriptional regulation exerted by PML on specific loci. Instead, the structural integrity of the PML-NBs is sustained by chromatin, suggesting that it may in turn regulate their formation and functions (Dellaire *et al*, 2006b). The clearest example of this crosstalk comes from imaging studies on the PML-NBs during cell cycle progression. In interphase nuclei the PML-NBs are highly stable structures which only marginally contact chromatin via their proteinaceous outer layer (Eskiw *et al*, 2004). However, as soon as chromatin unfolds to allow replication, the

PML-NBs disassemble by fission mechanism into numerous micro-bodies (Dellaire *et al*, 2006b). Contrary to PML-NBs, micro-bodies do not appear as a dense sphere of proteins but are rather small PML aggregates that spread throughout the chromatin fibres (Dellaire *et al*, 2006b). Upon entry in G2 the micro-bodies reassemble by fusion leading to the reconstitution of the parental NBs (Dellaire *et al*, 2006b). Other structural modifications occur during mitosis (M-phase). Particularly, at the onset of chromatin condensation the PML-NBs fuse and divide into larger and smaller bodies named MAPPs (mitotic accumulations of PML protein) (Dellaire *et al*, 2006c). Some of these bodies remain associated to chromosomes during cell division and have been suggested to act as seeding point for the formation of new PML-NBs at specific gene loci in G1 phase (Dellaire *et al*, 2006c). However, most of MAPPs are found into the cytoplasm where they associate with nuclear import components, which assist their transport in the nucleus of newly formed cells (Lång *et al*, 2017).

The integrity of PML-NBs may be lost also when chromatin is disrupted or change its structure upon stress condition, such as heat shock, transcriptional repression, DNA damage or oxidative stress (Nefkens *et al*, 2003; Eskiw *et al*, 2003; Dellaire *et al*, 2006a; Kepkay *et al*, 2011). For instance, during DNA damage chromatin unfolds and the PML-NBs immediately disassemble into small PML-based bodies, some of which associated with the damaged site to sustain the activation of DNA damage response pathways. (Dellaire *et al*, 2006c; Kepkay *et al*, 2011). Interestingly, histone acetylation appears to be an important signal for the formation of these PML microbodies (Dellaire *et al*, 2006c; Kepkay *et al*, 2011). Indeed, global acetylation induces chromatin de-condensation and detachment from the nuclear lamina, thus supporting the idea that chromatin surrounding the PML-NBs may exert a physical constrain that maintains their structure and position (Eskiw *et al*, 2003; Dellaire *et al*, 2006b). In line with this evidence, although the PML-NBs only marginally contact nucleic acid via their proteinaceous shell and PML is devoid of a DNA-binding domain, it seems that chromatin and its spatial distribution sustain their structural integrity. Yet, it should be also considered that most of these structural modifications occur during stress conditions or cell cycle progression, during which specialized set of proteins are activated and may be able to induce the delocalization of PML-NBs. However, regardless of whether chromatin acts directly or indirectly on the of PML-NBs, it is clear that their localization with the respect to chromatin does not

represent a random event, since each microbody reform the parental PML-NBs in the same inter-chromosomal space (Eskiw *et al*, 2003).

Altogether, these findings point out the existence of a physical connection among the PML-NBs and chromatin, that goes beyond the transcriptional functions of PML.

1.1.4.2.1 Specialized PML-NBs structures

Most of the associations between PML-NBs and chromatin have been described as spatial proximities or juxtapositions, however, in specific conditions the PML-NBs may contain DNA inside their structure. The clearest example comes from studies on telomerase-negative tumours in which telomeres are maintained by alternative mechanisms referred to as ALT (Alternative length of telomeres). In ALT cells, the PML-NBs associate with the telomeric DNA in specialized structure named ALT-associated PML-NBs (APBs) (Grobelny *et al*, 2000). Apart from canonical NBs components, such as sp100 and DAXX, APBs comprise proteins involved in telomere maintenance and DNA damage factors, as well as histone variants and heterochromatin binding proteins. APBs enclose the telomeric DNA and by the topic action of the associated proteins provide a chromatin environment that is permissive to recombination and synthesis (Draskovic *et al*, 2009; Zhang *et al*, 2019; Loe *et al*, 2020). Other specialized PML-NBs are found in specific pathological conditions. Such is the case of the giant PML-NBs found in the nuclei of ICF cells (Immunodeficiency, Centromeric region instability, and Facial anomalies syndrome) (Luciani *et al*, 2006). ICF is a rare autosomal recessive disorder characterized by a loss of function in the DNA-methyltransferase *DNMT3B* gene that leads to hypo-methylation and de-condensation of the heterochromatic satellite DNA. Similar to APBs, the giant PML-NBs organize around the under-condensed chromatin and, by concentrating heterochromatin modifiers, restore a closed chromatin conformation at the satellite DNA (Luciani *et al*, 2006). Additional examples of specialized PML-NBs, come from studies on the antiviral functions of PML. Particularly, the PML-NBs act as important sites for the restriction of viral DNA and RNA molecules, thereby inhibiting viral infection (Ching *et al*, 2005). In this context, a particular interaction has been described between the PML-NBs and the HSV-1 genome (Catez *et al*, 2012), which upon infection is entrapped in PML-based structures named viral DNA- containing PML NBs

(vDCP-NBs). Inside the vDCP-NBs the HSV-1 genome is transcriptionally repressed leading to the establishment of viral latency and quiescence (Cohen *et al*, 2018). Finally, PML-NBs may associate to DNA even in non-canonical NB structures. In human embryonic stem cells, PML organizes around centromeres in structure that resemble "rosettes" (Butler *et al*, 2009). These assemblies are not confined just to one centromeric region but cross the nucleus, like bridges that connect opposite poles of cells. Conversely to APBs, giant PML-NBs and vDCP-NBs, "rosettes" NBs do not contain canonical NBs components and associate with the nuclear lamina, suggesting a specialized and perhaps developmentally regulated role of these PML-based structures (Butler *et al*, 2009).

In the end, in specific contexts the PML may assemble in non-canonical NBs structures that act as specialized nuclear compartments. These PML-NBs commonly share the ability to enclose chromatin in their structure, suggesting that PML has a strong physical connection with chromatin and with specific DNA sequences.

1.1.4.3 PML and the regulation of epigenetic signatures

The connection of PML with the regulation of chromatin dynamics emerged from the identification of numerous chromatin-modifying factors within the PML-NBs. For example, well-known constitutive components of the PML-NBs are the CREB-Binding Protein (CBP), a histone acetyltransferase, and the heterochromatin protein 1(HP1, Corpet *et al*, 2020). Moreover, several studies indicate that PML may influence chromatin by modulating the epigenetic code, as detailed later. Thus, the PML-NBs have been proposed to act as scaffolds for the organization of specific chromatin domains either by concentrating or excluding proteins from chromatin regions (Kurihara *et al*, 2020, Delbarre *et al*, 2017).

Several resident clients of the PML-NBs are involved in the deposition and regulation of the histone variant H3.3 into chromatin (Delbarre & Janicki, 2021). Chief among them is the DAXX-ATRX complex, which regulates deposition of H3.3 into heterochromatic regions like telomeres, endogenous retroviral elements (ERVs) and methylated DNA (Voon & Wong, 2016). Deposition of H3.3 is required for the establishment of the

heterochromatic H3K9me3 histone mark and to maintain DNA regions transcriptionally silent.

In pluripotent mouse ES cells, DAXX-ATRX and H3.3 are recruited and maintained at telomeres in a PML-dependent manner (Chang *et al*, 2013). The PML-NBs localize at telomeres and promote the recruitment of DAXX-ATRX during S-phase where they regulate deposition of H3.3 into chromatin to ensure genome stability. In addition, silencing of PML leads to changes in the HPTMs of telomeric chromatin, suggesting that PML regulates the epigenetic state of these loci at different levels (Chang *et al*, 2013). PML also promotes the recruitment of DAXX and ATRX at the genomes of HSV-1 viruses (Cohen *et al*, 2018). As described above, HSV-1 infection induces the assembly of specialized PML structures named vDCP-NBs. vDCP-NBs contain both DAXX and ATRX and mediate the deposition of H3.3 into the viral genome, followed by deposition of the heterochromatic mark K9me3 (H3.3K9me3), transcriptional silencing and establishment of viral latency (Cohen *et al*, 2018).

Conversely however, PML has been shown to restrict H3.3 incorporation at specific loci. As an example, live cell imaging showed that DAXX, ATRX and H3.3 associate to a transgene array containing repetitive elements and stably integrated into Hela cells throughout the cell cycle, while PML associates only during S-phase. Upon binding to the transgene, PML antagonizes the activity of DAXX in mediating H3.3 deposition at specific regions of the transgene, i.e. the promoter and the gene body of the transgene array, promoting in this way spreading of H3K9me3. Accordingly, loss of PML induces a decrease in H3K9me3 levels and an increase in H3.3 over the entire transgene array (Shastrula *et al*, 2019). Similarly, PML was shown to exclude H3.3 deposition from specific genomic regions in MEFs (Delbarre *et al*, 2017). In detail, in these cells PML binds large heterochromatic and gene poor domains named PADs (PML-associated domains) where it maintains high levels of H3K9me3 levels while blocking H3.3 deposition. Interestingly, loss of PML leads to a decrease in H3K9me3 and increase of H3.3 and H3K27me3 in PADs, suggesting that compensatory mechanisms (i.e., the PRC2 complex) become activated to safeguard the integrity of these heterochromatic regions (Delbarre *et al*, 2017).

These findings demonstrate that PML mediates heterochromatinization of specific DNA regions and indicate that depending on the specific circumstance it may do so via different

mechanisms (i.e. by promoting or inhibiting H3.3 deposition, by cooperating with or inhibiting DAXX). Also, these studies underline the complexity of chromatin regulation, where the same epigenetic modification may have different outputs and may be regulated by different means, depending perhaps on the genomic context and/or the presence of external factors and adaptive processes.

Along these lines, H3.3 is also found at open chromatin regions where it usually marks promoters, gene bodies, and enhancers. The bivalent activity of the histone variant H3.3 is partly due to the different chaperons that mediate its incorporation into chromatin. Apart from DAXX, the histone cell cycle regulator (HIRA) mediates incorporation of H3.3 in both euchromatic and heterochromatic regions. HIRA also localizes to PML-NBs under certain stress conditions, such as senescence, exposure to IFNs and generally during viral infections (McFarlane *et al*, 2019, Rai *et al*, 2014; Zhang *et al*, 2005; Cohen *et al*, 2018). Although, the molecular mechanisms of PML and HIRA mediated H3.3 deposition are still under investigations, recent findings suggest that HIRA localize in PML-NBs to retrieve soluble H3.3-H4 dimers, which are essential to mediate H3.3 deposition in actively transcribed regions (Kleijwegt *et al*, 2021). Also, HIRA has been shown to promote viral silencing in cooperation with PML, underlining the highly context dependent activity of HIRA in H3.3 deposition (McFarlane *et al*, 2019, Cohen *et al*, 2018).

Other studies confirm the role of PML in promoting the establishment of heterochromatin. As already mentioned, in specific pathological conditions PML may arrange in specialized NBs, such as APBs and the Giant PML-NBs of ICF cells, which associate with and regulate the heterochromatinization of specific DNA sequences (Luciani *et al*, 2006). The PML-NBs are also fundamental for the assembly of senescence- associated heterochromatin foci (SAHFs) (Corpet & Stucki, 2014). Even if SAHFs are not adjacent to the PML-NBs, their structural integrity is dependent on the presence of PML. In this context, the PML-NBs create specialized nuclear compartments for the concentration of senescence regulatory proteins. For instance, HP1a and HIRA, which are essential for the assembly of SAHFs, transiently localize to the PML-NBs during the early stages of senescence. This transition is necessary for the formation of SAHFs, suggesting that the PML-NBs act as nuclear platforms for the activation of these proteins (Corpet & Stucki, 2014).

In summary, many proteins localizing to the PML NBs regulate chromatin structure, in particular establishment and maintenance of heterochromatin (e.g., DAXX, ATRX, HP1, SETDB1), and PML was found to regulate several epigenetic mechanisms. Accordingly, it has been suggested that the PML-NBs may act as meeting points for chromatin loci and specific proteins, thus creating confined nuclear compartments which assist chromatin remodelling process (Corpet *et al*, 2020).

1.2 Hypoxia inducible factor 1α (HIF1α)

Since the evolution of photosynthesis, organisms have evolved specialized mechanisms to convert reactive oxygen species into energy. Oxygen is important for most physiological functions and its deficiency compromises the survival of an organism. Drops in oxygen levels below the normal physiological state in a cell or organism is known as hypoxia (Taylor & McElwain, 2010). Besides being a pathological condition, hypoxia also occurs physiologically and regulates a large range of biological processes, like new blood vessel formation during wound healing, development and organogenesis (Dunwoodie, 2009). To sense and regulate cellular responses to changes in oxygen concentrations, organisms have developed molecular mechanisms that depend on oxygen-dependent molecules. The main pathway that coordinates this response in all metazoans involves the hypoxia-inducible transcription factors HIFs. HIFs are heterodimeric transcription factors composed of an oxygen-regulated HIFα subunit and the constitutively expressed HIF1β subunit. For the aim of this thesis, I will mainly focus on the HIF1α oxygen-dependent subunit (Dengler *et al*, 2014).

Since its discovery as a transcriptional regulator of the erythropoietin (*EPO*) gene, HIF1α has been linked to many biological processes involved in maintaining oxygen homeostasis, including cell metabolism and angiogenesis. However, further studies linked HIF1α also to the regulation of pathways which are not involved in maintaining oxygen homeostasis, such as autophagy, apoptosis, inflammation and immunity, stemness and self-renewal, and migration (Dengler *et al*, 2014).

Hypoxia is one crucial hallmark of cancer. As tumour cells rapidly proliferate, they deprive the microenvironment of nutrients and oxygen, and promote the formation of a poorly vascularized and hypoxic microenvironment. This is particular evident in solid

tumours where indeed HIF1α is often overexpressed and correlates with poor clinical prognosis (Semenza, 2003). Stabilization of HIF1α promotes the activation of a broad range of cellular pathways, which play key roles in promoting cancer progression. Relevant examples include angiogenesis, metabolic reprogramming and metastasis (Semenza, 2003).

In this chapter, I will briefly describe the biology of HIF factors, focusing on the HIF1α subunit. I will start with the gene and protein structure of HIFs and then describe the oxygen-dependent and -independent regulation of the HIF1α subunit. Finally, I will briefly overview the transcriptional and cellular functions of HIF1α. In describing the cellular functions of HIF1α, I will focus on its role in triple-negative breast cancer (TNBC) because in our laboratory PML was described as an activator of HIF1α transcription in this context (Ponente *et al*, 2017).

1.2.1 Gene and protein structure of HIF factors

HIFs are heterodimeric transcription factors composed of two basic-helix-loop-helix (bHLH) proteins of the PAS family: an oxygen-regulated HIFα subunit and the constitutively expressed HIF1β subunit (also known as aryl hydrocarbon receptor nuclear translocator, ARNT) (Dengler *et al*, 2014). In mammals, three genes encode HIFα subunits: *HIF1A*, *EPAS1* (also known as and hereinafter referred to as *HIF2A*), and *HIF3A*. The HIF1β subunit is encoded by two genes *ARNT1* and *ARNT2*. Structurally, all HIFs possess a conserved N-terminal bHLH DNA binding domain and two PAS domains (PAS-A and PAS-B, figure 7) that are required for protein heterodimerization. At the C-terminal, both HIFα subunits and HIF1β harbour a transactivation domain (TAD) named C-TAD, which mediates the interaction with transcriptional coactivators, like CBP and p300. HIFα subunits also carry a unique N-TAD involved in the activation of specific target genes and interaction with isoform-specific partner proteins (figure 7). Moreover, the N-TAD overlaps with an oxygen-dependent degradation domain (ODDD), which regulates oxygen-dependent protein stability (figure 7). Specifically, the ODDD domain harbours two conserved prolyl-residues (P402/P564 and P405/P531 in human HIF1α and HIF2α, respectively) that are targeted for hydroxylation by prolyl-hydroxylases of the PHD family and lead to HIFα degradation by the proteasome (figure 8). In addition, the

C-TAD contains an amino acid residue (Asn803/851) that confers additional oxygen-dependent regulation: this residue is recognized and hydroxylated by the factor inhibiting HIF (FIH), which inhibits the binding of coactivator proteins (Dengler *et al*, 2014).
HIF1α and HIF2α dimerise with HIF1β to form an active transcriptional complex that binds DNA at specific hypoxia responsive elements (HREs) at target gene promoters (figure 8, Schödel *et al*, 2011). Conversely, HIF3α is less characterized and has been shown to antagonize HIF1α- and HIF2α-mediated gene expression by competing with HIF1β binding (Duan, 2016).

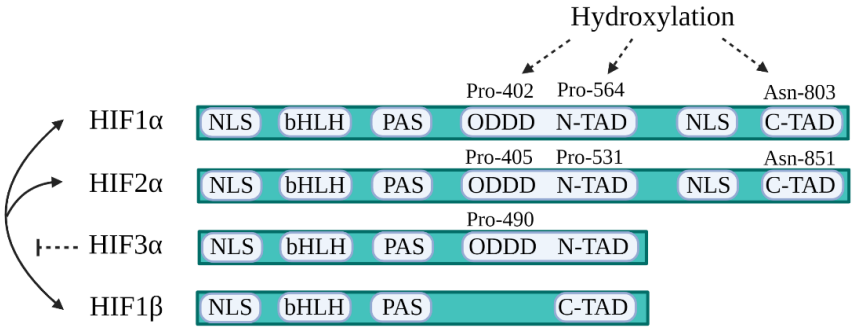

Figure 7. HIFs protein structures. *All HIFs harbour at their N-terminal an NLS followed by a bHLH and two PAS domains which mediate DNA binding and protein-protein interaction respectively. In addition, HIFα subunits contain an ODDD domain, and two TADs (N-TAD and C-TAD) and a second NLS. HIF1β also possesses a C-TAD-that mediates interactions with transcriptional activator proteins. Conversely, HIF3α only contains the N-TAD. HIF1α and HIF2α interact with HIF1β to form an active transcriptional complex. All HIFα subunits are regulated by site-specific hydroxylations, which can either occur at proline (Pro) residues in their ODDD domains, or at an asparagine (Asn) residue in the C-TAD. Those modifications regulate HIFa degradation and HIF heterodimeric complex transcriptional function in an oxygen-dependent manner. Created with Biorender.*

1.2.2 HIFα oxygen-dependent and oxygen-independent regulation

In many physiological conditions, oxygen tension is ≥5% and HIFα subunits are degraded in the cytoplasm. Under these conditions, PHDs hydroxylate the proline and asparagine residues located in the ODDD domain leading to recruitment of the von Hippel-Lindau (pVHL) E3 ubiquitin ligase, which induces ubiquitination and proteasomal degradation of HIFα subunits (figure 8, left, Dengler *et al*, 2014). PHDs use oxygen as substrate, therefore their activity is inhibited under hypoxic conditions. Accordingly, when oxygen levels decrease (< 5%), HIFα subunits are stabilized and translocate into the nucleus,

where they dimerize with HIF1β and bind target DNA regions (figure 8, right, Dengler *et al*, 2014).

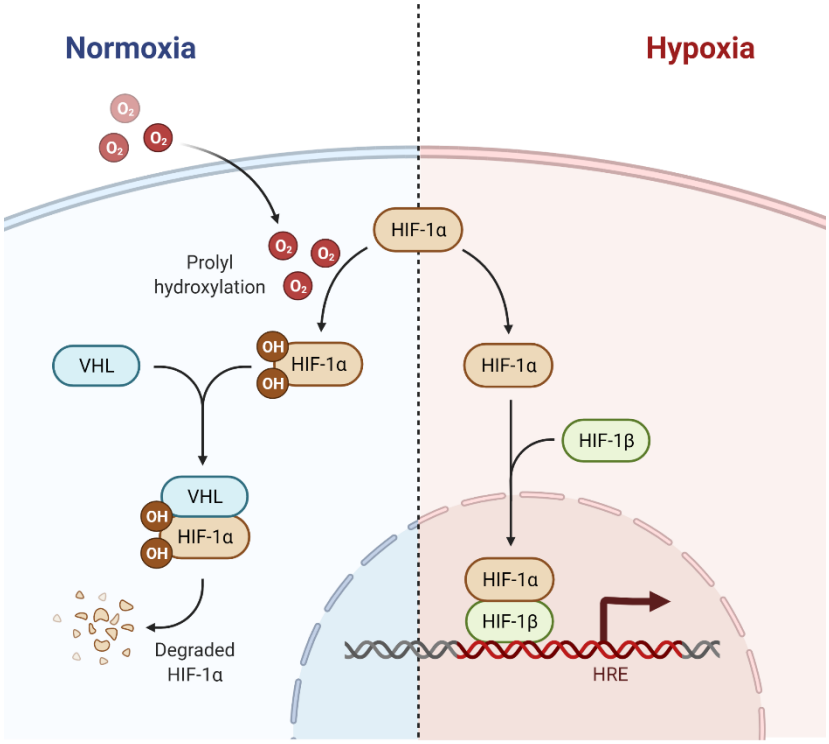

Figure 8. Oxygen-dependent HIF1α regulation*. In normoxia, PHDs hydroxylate the HIF1α subunits in the cytoplasm promoting its ubiquitination by pVHL and degradation. Conversely, in hypoxia PHDs are inactive, thus HIF1α is stabilized and able to shuttle in the nucleus.In the nucleus HIF1 α complex with HIF1β to form a transcriptionally active complex, which binds to HRE regions inducing transcription of target genes. Created with Biorender.*

Apart from well-described oxygen-dependent mechanisms, HIFs activity is regulated by other pathways that act independently of oxygen tension and are often deregulated in cancer. Activation of these pathways is particularly evident in cancer upon activation of oncogenes, loss of tumor-suppressors, and growth factors hyperstimulation (Iommarini *et al*, 2017). Given their ability to stabilize and activate HIFα independently of the oxygen tension, these conditions have been described as pseudo-hypoxic (Iommarini *et al*, 2017; Hayashi *et al*, 2019).

A remarkable example of pseudo-hypoxic regulation of HIF1α can be observed in TNBC. In this tumour context, HIF1α is transcriptionally active in normoxic conditions and acts as an oncogene by promoting the expression of metastatic, survival and immune

regulatory genes. TNBC cells overly stabilise HIF1α via multiple mechanisms. Within them, expression of a Long Intergenic Noncoding RNA for Kinase Activation (LINK-A) leads to the enzymatic activation of BRK, which phosphorylates HIF1α at Tyr565. HIF1α phosphorylation inhibits N-TAD hydroxylation and its PHD-mediated degradation (Lin *et al,* 2016). Additionally, HIF1α is stabilized by the paracrine activity of glutamate, which acts as an oncometabolite by inhibiting the activity of the prolyl-hydroxylates EglN (Briggs *et al,* 2016). Also, TNBC samples show a decreased expression of the FBXL16 protein-ubiquitin ligase, identified as a novel mediator of HIF1α degradation. Downregulation of FBXL16 contributes to HIF1α stabilization and expression of metastatic genes under normoxic conditions (Kim *et al*, 2021).

Other examples of oxygen-independent pathways that activate HIF1α in cancer involve the PI3K/Akt/mTOR, ERK/MAPK and JAK/STAT signalling pathways (Iommarini *et al*, 2017). In particular, hyperactivation of PI3K/Akt/mTOR axis increases HIF1α translation, which results in a higher amount of HIF1α protein and in a lower activity of pVHL in mediating HIF degradation under non-hypoxic conditions (Laughner *et al*, 2001). Similarly, STAT3, a TF involved in the JAK/STAT pathway, directly binds the promoter of *HIF1α* increasing its expression (Niu *et al*, 2008). Finally, the ERK/MAPK signalling pathway enhances HIF1α transcriptional activity by promoting p300/CBP phosphorylation (Kietzmann *et al*, 2016).

1.2.3 HIF1α transcriptional program

As previously described, under hypoxia HIF1α is stabilized and able to translocate in the nucleus where it dimerises with HIF1b to bind hypoxia inducible target genes. Specifically, heterodimeric HIF complexes recognize a core consensus sequence 5'-(A/G)CGTG-3', known as hypoxia-response element (HRE). For long time, the presence of an HRE was considered the main readout of HIF binding to DNA. However, although HRE sequences are widely spread across the genome, less than 1% are directly bound by HIFs at the promoter region of hypoxia-inducible genes (Mole *et al*, 2009). Rather, pan-genomic analyses revealed that HIF1α binding sites are mostly located 10 kb away from their nearest gene (Schödel *et al*, 2011). These intergenic regions are marked by H3K4me1 and promote the formation of chromatin-chromatin interactions with

promoters of hypoxia responsive genes. Interestingly, these interactions are already established in normoxia and support a model in which HIF1α binds to pre-established chromatin loops to promote a rapid transcriptional response to hypoxic stress. In addition, HREs are often proximal to or overlap with other TF motifs (like those of FOS, CREB, E2F and MYC), suggesting that HIF1α may also regulate target genes transcription in a cooperative manner. In line with this hypothesis, it was found that HIF1α and STAT3 cooperatively bind and recruit RNApol2 to promoters of some hypoxia-inducible genes, such as *VEGF*, *CA9*, and *PGK1* (Pawlus et al., 2013). Moreover, HIF1α has been shown to indirectly participate in the regulation of gene expression by working as cofactor of other DNA-binding proteins via binding with its N- or C-TAD domains (Fortini, 2009; Galbraith *et al*, 2013).

N- and C-TADs also drive different transcriptional activation of HIFα proteins in hypoxia. As previously mentioned, PHDs promote HIF1α degradation by hydroxylation at conserved proline residues contained within the N-TAD, while the C-TAD is modulated by hydroxylation of an asparagine residue by FIH. PHDs and FIH show distinct sensitivity for oxygen, with PHDs displaying lower affinity for oxygen than FIH and being inactive at moderate hypoxic conditions, thus allowing HIF1α stabilization. However, at moderate hypoxia the C-TAD is still masked by hydroxylation driven by FIH, which is inactivated only at lower oxygen concentrations compared to PHDs (Hirsilä *et al*, 2003; Koivunen *et al*, 2004). As a result, HIF1α proteins exhibit a bifunctional transcriptional activity depending on the available TAD. As an example, the HIF1α PDK target gene may be activated in normoxic condition only by silencing of PHDs and not of FIH (Bracken *et al*, 2006; Dayan *et al*, 2006). Hence, HIF1α TADs can impact transcription under different oxygen concentrations, enlarging even more the transcriptional functions of HIF1α. Whether or not their differential activity may also occur in pseudo-hypoxic conditions is not clear.

1.2.3.1 HIF1α target genes and cellular functions

Since HIF1α has evolved to regulate the response to fluctuation in oxygen concentration, most of its target genes are involved in the regulation of oxygen homeostasis. Among them, we found several glycolytic enzymes and molecules that mediate the delivery and distribution of oxygen, such as EPO, VEGF and its receptors FLT1 and FLK1, as well as

END1 and ANGPT1. Nonetheless, HIF1α is also involved in the regulation of pathways which do not maintain oxygen homeostasis. As such, HIF1α promotes the expression of genes involved in epithelial to mesenchymal transition (EMT) during development, such as *LOX*, *MMP1* and *TWIST*. However, hypoxia is a hallmark of cancer and HIF1α target genes are often deregulated in this context. Here, I will briefly go through the most relevant examples of HIF1α transcriptionally regulated pathways that are often deregulated in cancer, and I will highlight their relevance in TNBC pathogenesis.

Angiogenesis:

One of the first transcriptional programme associated to HIF1α regulation is angiogenesis. Accordingly, HIF1α is essential in the development of the embryonic vascular system, as well as in promoting angiogenesis in different pathological conditions (Majmundar *et al*, 2010). As such, solid tumours often express hypoxic areas characterized by a discontinuous and leaky vascular network with limited oxygen diffusion. In this context, HIF1α overexpression promotes the transcription of several pro-angiogenic factors, such as VEGF, SDF1, ANGPT2, PGF, and SCF, which enhance the uncontrolled growth of the tumour vasculature, thereby favouring cancer growth (de Heer *et al*, 2020). Interestingly, in TNBC, angiogenesis is an essential step in the initiation of cancer metastasis. As an example, HIF1α has been shown to increase the expression of ANGPTL4, which upon secretion in the microenvironment enhances cancer cells extravasation and migration (Zhang *et al*, 2012)

Metabolism:

HIF1α is involved in the rewiring of cell metabolism during hypoxia and its function is essential to switch from cellular respiration to aerobic glycolysis (Majmundar *et al*, 2010). HIF1α sustains this metabolic switch by promoting the expression of glucose transporters, glycolytic enzymes, LDHA, and PDK1, which use extracellular glucose as a source of energy in lack of oxygen. As an additional source of glucose, HIF1α also regulates glycogen synthesis and breakdown, and this mechanism has been linked to the invasiveness potential of TNBC cells (Altemus *et al*, 2019). Moreover, HIF1α promotes transcription of lactate transporters that allow lactate release in the microenvironment,

thus preventing reduction of intracellular pH levels while leading to the formation of an acidic and immunosuppressive tumour microenvironment (de Heer *et al*, 2020).

Metastasis:

Metastasis is a complex and multistep process that leads to the development of secondary tumours in parts of the body that are far from the original primary tumour mass (Hanahan & Weinberg, 2011). The steps involved in metastasis establishment and progression are: i) epithelial-mesenchymal transition (EMT); ii) degradation and remodelling of extracellular matrix (ECM); iii) intravasation of cancer cells into blood vessels and in the circulation; iv) homing and survival of cancer cells within the circulation; v) extravasation of cancer cells from the blood stream to distant organs; and, vi) metastatic niche formation at the metastatic site to create an environment that is favourable for cancer cells growth (Hanahan & Weinberg, 2011). In TNBC, HIF1α has been shown to sustain the metastatic process at multiple levels. First, HIF1α promotes EMT via upregulation of EMT-associated transcription factors, signalling pathways and inflammatory cytokines. For instance, HIF1α promotes the downregulation of E-cadherin by inducing expression of *SNAIL2*, *ZEB1*, *ZEB2*, *TWIST* and *TCF3* genes, transcription factors that activate the expression of mesenchymal markers to promote cell motility (Gilkes & Semenza, 2013). Additionally, HIF1α regulates the degradation and remodelling of the ECM by promoting the expression of matrix metallo-proteinases (MMPs), such as MMP-9 and MMP-2 (Gilkes & Semenza, 2013). Second, HIF1α regulates the synthesis and assembly of collagen via transcription of pro-collagen prolyl (P4HA1 and P4HA2) and lysyl (PLOD1, PLOD2, LOX and LOXL2) hydroxylases, thereby leading to the formation of straight and aligned collagen fibres that facilitate cancer cells migration. Third, by inducing the expression and release of VEGF-A, HIF1α stimulates angiogenesis, blood vessels permeability and cancer cells intravasation (Jin *et al*, 2012). In addition, HIF1α sustains cancer cells extravasation by mediating the downregulation of endothelial cell junctions and upregulation of adhesion molecules between cancer and endothelial cells (Zhang *et al*, 2012). As such, under hypoxia, HIF1α induces secretion of ANGPTL4 and expression of L1CAM which increase vascular permeability and enhance adhesion of cancer to endothelial cells (Zhang *et al*, 2012). Finally, HIF1α regulates the formation of premetastatic niches by inducing the expression of collagen lysyl oxidase (i.e. LOX and

LOXL2) that once released in the circulation are able to reach the site of metastasis, where they remodel ECM and promote the establishment of a premetastatic niche (Gilkes & Semenza, 2013)

Finally, besides mediating the hypoxia-induced expression of mRNA-encoding genes, HIF1α also partakes in microRNA (Kulshreshtha *et al*, 2007) and long non-coding RNA networks (Choudhry *et al*, 2015), as well as multiple epigenetic and secondary transcriptional cascades (Lendahl *et al*, 2009).

In summary, HIF1α regulates transcription of a wide range of genes influencing a broad range of cellular processes, which are often deregulated in cancer. Although HIFα factors are canonically active during hypoxia, in cancer, they may be stabilized by a variety of oxygen-independent mechanisms. This is particular evident in TNBC where HIF1α is constitutively express under normoxic conditions and promotes angiogenesis, metabolic reprogramming, and metastasis.

2. AIM OF THE WORK

Existing evidence describe the PML-NBs as nuclear platforms for the post-translational modification and activity of a large number of proteins, mostly involved in transcriptional regulation. As a consequence, PML has been shown to act as a transcriptional co-activator or co-repressor depending on the cellular and experimental conditions. In addition, the PML-NBs frequently associate with transcribed regions, with specific genomic loci and with epigenetic modifiers, thus suggesting that PML is also involved in chromatin organization and epigenetic regulation.

Our group has recently demonstrated that PML acts as an oncogene in triple negative breast cancer (TNBC), by promoting the expression of a specific HIF1α transcriptional program that triggers metastatic dissemination. Interestingly, this occurs specifically in TNBC cells and not in other breast cancer cell lines, thus revealing cell type-specific transcriptional regulation by PML in the breast cancer context (Ponente *et al*, 2017). However, a number of questions have been raised by this study. First, the full extent of PML-mediated transcriptional output in TNBC has not been defined. Also, the molecular mechanisms of PML transcriptional cooperation with HIF1α in this tumor type have not been fully elucidated. These questions are connected to the wider open field of the fine molecular mechanisms of transcriptional regulation by PML, as it is still unclear to what extent PML regulates transcription via: i) indirect activation or inhibition of transcription factors, ii) co-activation or -repression of transcription factors on DNA, iii) regulation of epigenetic and chromatin organization states, iv) organization of chromatin states at specific genomic loci, v) all of the above. Connected to these questions are the issues of tissue specificity and biochemical complexity of PML states.

To begin to answer to these questions via a reductionistic approach, in a cell type where a full understanding of PML transcriptional functions may lead to therapeutic implications, we aimed to:

Aim 1- Dissect the mechanisms of transcriptional regulation by PML in triple-negative breast cancer

Aim 2- Characterize the functional interaction of PML and HIF1α in TNBC

3. RESULTS

3.1 Aim 1. Dissect the mechanisms of transcriptional regulation by PML in triple-negative breast cancer

3.1.1 Gene regulation by PML in TNBC

To define unbiasedly the transcriptional programs regulated by PML in TNBC, we performed RNA-sequencing in TNBC MDA-MB-231 cells upon PML silencing *via* stable shRNA expression (figure 9A). PML silencing leads to a mild proliferative delay in MDA-MB-231, with a more pronounced defect in cell migration, invasion and *in vivo* metastasis (Ponente *et al*, 2017). Three experimental triplicates were analysed, obtained as independent lentiviral infections of vectors containing validated PML-specific or control shRNA sequences (figure 9B, left panel).

Silencing of PML led to the identification of two classes of deregulated genes compared to control cells (shCTRL): genes downregulated upon PML silencing (i.e. genes that are positively regulated by PML; DOWN in figure 9B, right panel) and genes that are upregulated when PML expression is suppressed (i.e. genes that are negatively regulated by PML; UP in figure 9B). To avoid confusion, from now on genes downregulated or upregulated upon PML silencing in our RNA-sequencing experiment will be defined "activated" and "repressed" by PML, respectively.

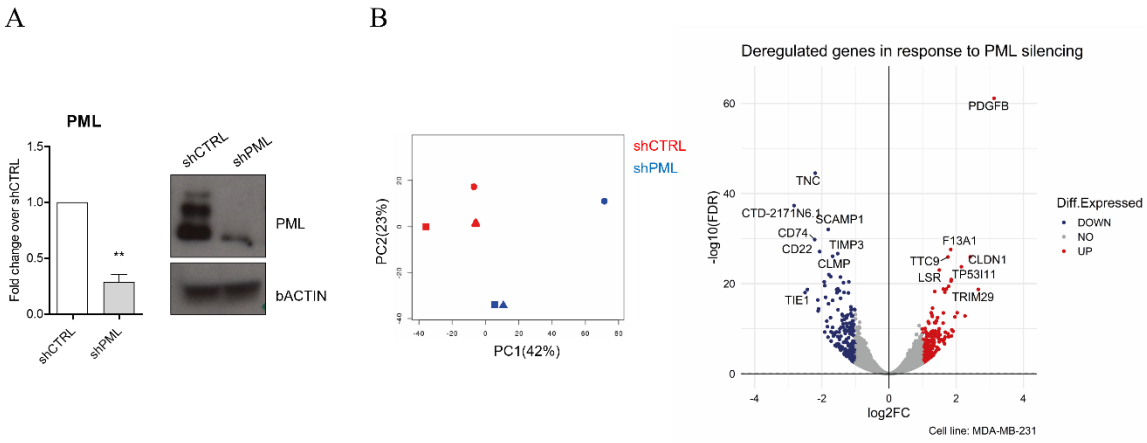

Figure 9. Transcriptomic analysis of MDA-MB-231 cells silenced for PML. *A) qRT-PCR analysis (left) on PML in control (shCTRL) and cells silenced for PML (shPML). Relative expression levels of PML were compared to control cells (shCTRL). Data represent mean values ± SD of at least three independent experiments. Statistic was calculated with paired, two-tailed, Student t-test (**=p-value<0.01). Western blot analysis (right) on endogenous PML in control*

(shCTRL) and cells silenced for PML (shPML). Beta-actin was used as loading control. B) PCA analysis (left) of RNA-seq samples showing clustering of control and PML silenced samples. Red and blue samples represent biological replicates of control (shCTRL) and PML silenced (shPML) samples respectively. Volcano plot (right) of genes deregulated in response to PML silencing. The x- and y-axis represent log2(FC) and log10(FDR) values respectively. Blue and red samples represent downregulated and upregulated genes with log2FC<-1 and log2FC>1 respectively.

Overall, silencing of PML identified a high number of differentially expressed genes (DEGs=2857, FDR 0.05, log2FC<-/>0.3, figure 9B, right panel). These are equally distributed amongst downregulated and upregulated genes (downregulated genes=1465, upregulated genes=1392). Of note however, a minor fraction of these genes shows a fold change (FC) expression difference superior to 1. These are indicated in figure 9B as 195 downregulated genes in blue and 182 upregulated genes in red (FC< - or >1 respectively, FDR 0.05).

To functionally characterize the genes activated and repressed by PML we performed gene set enrichment analysis with the EnrichR web tool (Kuleshov *et al*, 2016). Since most of the DEGs show minor changes in the FC values and our aim was to obtain a comprehensive map of gene regulation by PML in TNBC we decided to analyse all significant DEGs (FDR 0.05) with FC <-/> 0.3. Gene sets identified by EnrichR were then clustered into functional families to pinpoint the main cellular functions that are positively (figure 10) or negatively (figure 11) regulated by PML. Since we identified a large number of redundant pathways enriched among positively regulated genes, we represented only the most significant ones (figure 10).

Beginning with the genes that are positively regulated by PML, we found that they cluster in families related to the regulation of cell migration, extracellular matrix organization and EMT processes (figure 10, blue). This is in agreement with our previous findings, as we had previously demonstrated that PML is a crucial regulator of metastasis in TNBC by promoting expression of a sub-set of HIF1α-target genes involved in metastasis (Ponente *et al*, 2017). Within the metastasis genes identified by RNA-sequencing (figure 10), we found genes like *LOX* that had already been identified in our previous studies (Ponente *et al*, 2017). as well as new genes involved in breast cancer metastasis, such as *SPARC* and *TNC* (Guttlein *et al*, 2017; Oskarsson *et al*, 2011). These are two important regulators of ECM assembly and deposition, and ECM-cell interactions and their positive

regulation by PML in TNBC cells was validated by quantitative PCR (qPCR) in a set of independent experiments (figure 12).

The second cluster of gene families positively regulated by PML is related to the immune system (figure 10, orange). In this cluster, we find genes involved in cytokine signalling, inflammation and IFNγ response pathways, suggesting a possible novel function of PML in regulating immune responses in TNBC. Genes belonging to these pathways include chemokines and cytokines that regulate the production and recruitment of myeloid cells (e.g., IL8, CSF), immune checkpoint molecules that inhibit T cell activation (e.g., PDL1, CD276), and genes belonging to the INF-gamma-responsive pathway. Positive regulation of *PD-L1* by PML has not been reported before and was independently validated by qPCR (figure 12).

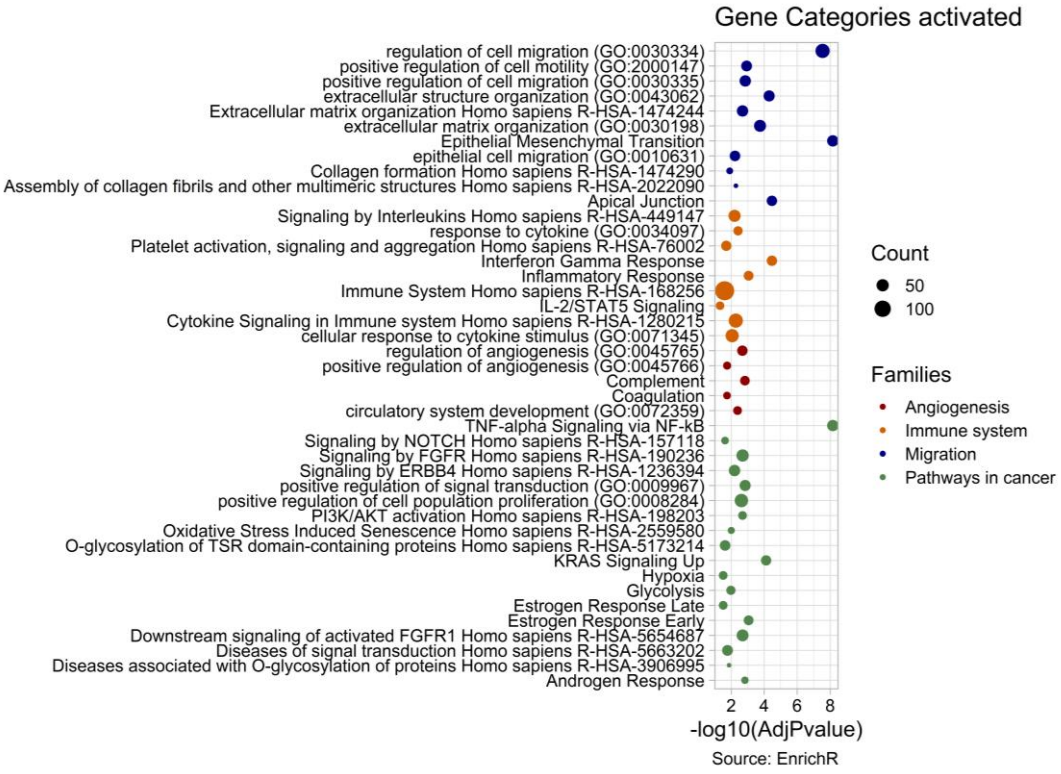

Figure 10. Gene set enrichment analysis of genes activated by PML. *Genes activated by PML (with log2FC<-0.3, FDR 0.05) were analyzed with EnrichR. Significant pathways were filtered for adjusted p.value<0.1 and clustered into functional families (blue, orange, red, green). Pathways are ordered according to their functional families and the size of the dots represents the number of PML regulated genes falling in each pathway.*

Other pathways significantly enriched in this analysis represent different tumour promoting processes, including hypoxia, glycolysis and angiogenesis that are in line with

the positive functional interaction between PML and HIF1α in TNBC (figure 10, green and red, Ponente *et al*, 2017). These pathways contain known hypoxia inducible genes, such as the metalloenzyme CA12, several metalloproteinases of the ADAMTS protein family, and the transcription factor SOX9, which had already been identified as a gene whose expression is induced by PML in TNBC (Martín-Martín *et al*, 2016).

Unlike genes activated by PML, genes whose expression is repressed by PML fall into fewer categories, which can be largely grouped into metabolism, immune system and pathways in cancer (figure 11, orange, red, blue). Among these pathways, the most recurrent term is cholesterol synthesis and metabolism, as well as metabolism in general, suggesting that silencing of PML may drive a metabolic reprogramming of cancer cells (figure 11, orange). This is in line with previously reported observations of a regulation of lipid metabolism and cell survival under metabolic stress by PML in TNBC (Carracedo *et al*, 2012), as well as a more general regulation of lipid metabolic pathways by PML in untransformed tissues like liver and fat (Cheng *et al*, 2013). More specifically, a detailed anaysis of lipid metabolic pathways in *Pml* knock-out mice revealed that while regulation of fatty acid oxidation genes by PML occurred in a tissue-specific manner, loss of Pml promoted cholesterol biosynthesis pathways in all all tissues analyzed (Cheng *et al*, 2013), in agreement with our data. In addition to metabolism, PML negatively regulates the expression of the MHC class I genes (*HLA-B, HLA-C, HLA-A, HLA-F, HLA-E*) which are comprised in gene categories like antigen processing via MHC and vacuolar and endosomal pathways (figure 11, red). These data were confirmed by independent gene expression analysis of *HLA-A, B* and *C* expression upon PML silencing (figure 12) and suggest that in TNBC PML may negatively regulate antigen presentation. Accordingly, previous findings had described PML as a factor contributing to the organization of chromatin loops within the MHC-I locus, as well as in the transcriptional regulation of the MHC-I genes in different contexts (Zheng *et al*, 1998; Liu *et al*, 2013; Kumar *et al*, 2007).

Finally, we found enrichment of few pathways generally associated with tumour progression, including p53, hypoxia and apical junction.

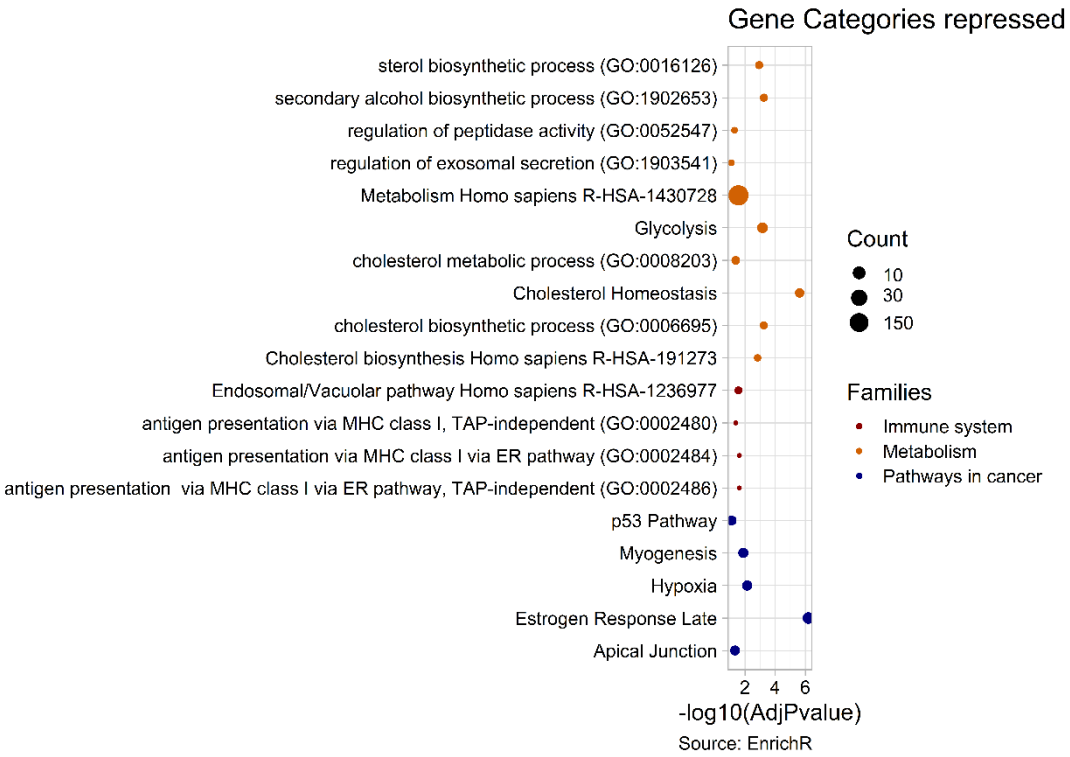

Figure 11. Gene set enrichment analysis of genes repressed by PML. *Genes repressed by PML (with log2FC>0.3, FDR 0.05) were analysed with EnrichR. Significant pathways were filtered for adjusted p.value<0.1 and clustered into functional families (blue, orange, red). Pathways are ordered according to their functional families and the size of the dots represents the number of PML regulated genes falling in each pathway.*

To confirm our RNA-sequencing data, we selected genes belonging to the two categories most significantly regulated by PML and important for cancer progression, namely metastasis and immune regulation (figure 12). Interestingly, PML displays a dual regulation of immune genes, with a positive regulation of immune factors like the cytokine CSF1, HLA class II trans activator CIITA, and a negative regulation of HLA-I genes. As illustrated in figure 12 we confirmed that PML positively regulates the expression of metastatic genes (*LOX*, *SPARC* and *TNC*), while it both positively and negatively regulate the expression of immune-related genes (*PDL1*, *CIITA*, *CSF1* and *HLA*).

In conclusion, with this analysis we confirmed that PML mainly promotes the activation of metastatic and tumour promoting pathways in TNBC. In addition, we unveiled a possible novel function of PML in regulating tumour immune responses, via complex

positive and negative regulatory mechanisms. These data open new areas of investigation into the possible ways in which PML promotes the pathogenesis of TNBC.

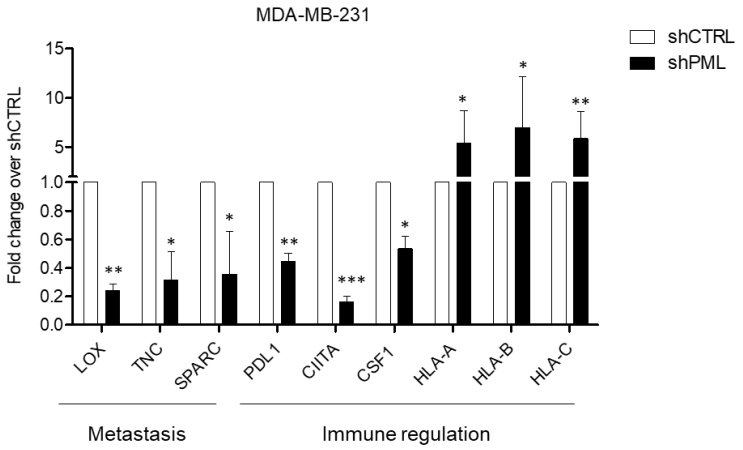

Figure 12. Evaluation of genes regulated by PML in MDA-MB-231 cells. *qRT-PCR analysis on activated genes, belonging to metastasis and immune regulation, and repressed genes, involved in immune regulation. Relative expression levels of each gene were compared to control cells (shCTRL). Data represent mean values ± SD of at least three independent experiments. Statistic was calculated with paired, two-tailed, Student t-test (*=p-value<0.05, **=p-value<0.01, ***=p-value<0.001).*

3.1.2 DNA binding profile of PML in TNBC

3.1.2.1 PML binds heterochromatin domains named PADs

Starting from our transcriptomic data, we next aimed to identify genes that may be directly regulated by PML in TNBC. For this reason, we performed ChIP-sequencing on endogenous PML in MDA-MB-231 cells. As already mentioned in the introduction, immunoprecipitation of PML is difficult because PML is a highly insoluble protein. For this reason, we planned our experiment using a validated ChIP protocol that was used to identify repressive HPTMs, heterochromatic DNA and chromatin structural proteins, and more in general for the enrichment of closed chromatin regions (Cabianca *et al*, 2012; Shastrula *et al*, 2019; Groh *et al*, 2021). In addition, since PML does not bind DNA directly, we implemented this protocol by adding a double crosslinking with disuccinimidyl glutarate (DSG), which stabilizes protein-protein interactions. Upon DNA sequencing, we called PML-bound DNA peaks with a classical peak calling algorithm used for transcription factors, MACS2, which is normally used to identify strong and punctuated binding in the promoter region of target genes. However, with this approach

we didn't succeed in identifying PML binding sites on DNA. Hence, we applied the Enriched domain detector (EDD) algorithm (Lund *et al*, 2014), a broad peak calling algorithm suitable for the discovery of genomic domains interacting with broadly distributed proteins, such as nuclear lamins. Unlike peak callers utilized for DNA binding by transcription factors, which identify enriched regions by using a sliding window of ~200bp, EDD identifies long intervals of DNA with low local variations in binding. EDD was originally created for the analysis of DNA binding by lamins (Lund *et al*, 2014), but was later utilized also for measuring PML binding to DNA. Specifically, EDD allowed the identification of large heterochromatic domains bound by PML in MEFs named PML-associated domains (PADs) (Delbarre *et al*, 2017). By applying EDD to our DNA-sequencing data, we identified 123 PADs of median length of 3Mb distributed throughout the genome and encompassing 570 mb (figure 13A, containing a representative example). Like in MEFs (Delbarre *et al*, 2017), PADs appear as large heterochromatic domains devoid of active histone marks and coding genes (figure 13B). Accordingly, alignment with maps of epigenetic marks, generated in the same cell line and downloaded from GEO, revealed that PADs are enriched with inactive chromatin marks, such as H3K9me3 which identify constitutive heterochromatin, while being devoid of active HPTMs (i.e., H3K4me3/1, figure 13C).

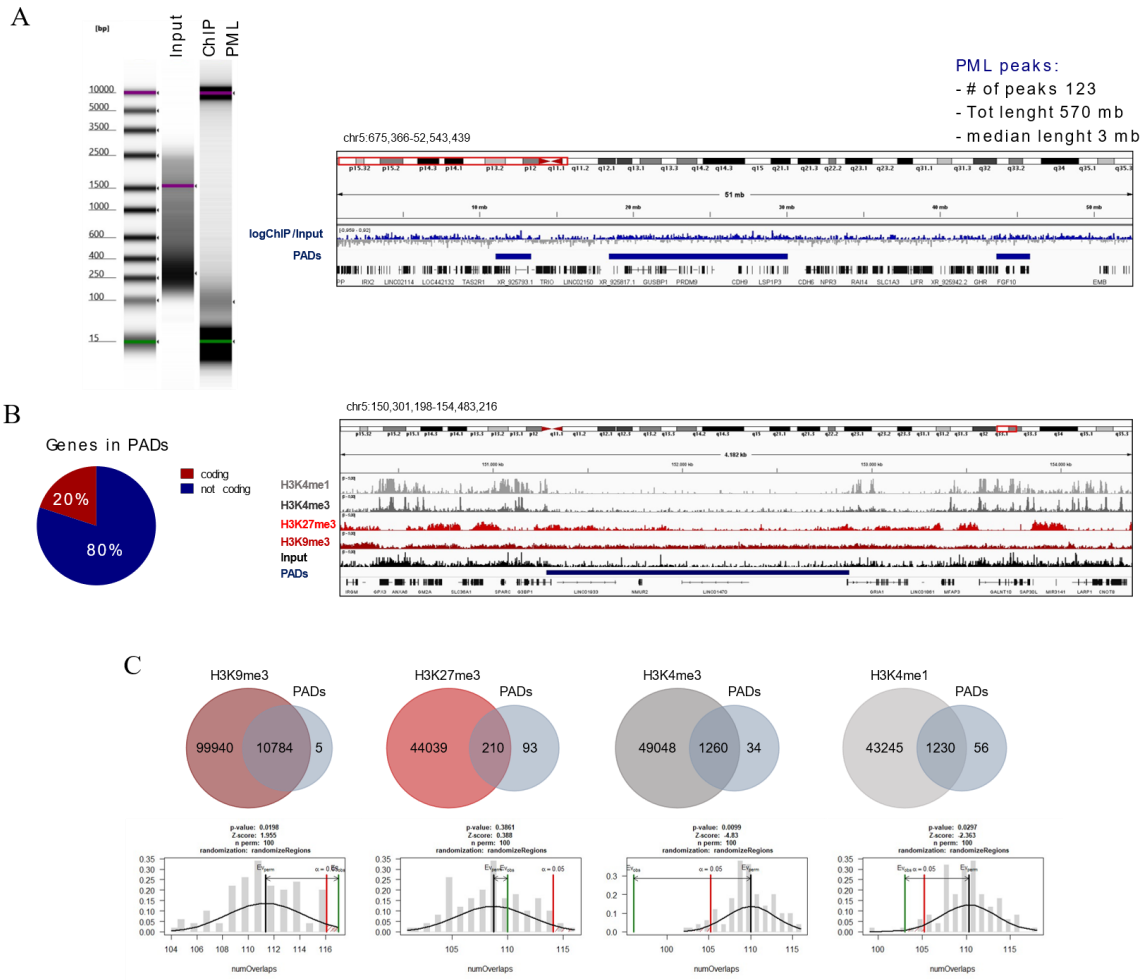

Figure 13. PML binds megabase-sized heterochromatin domains. *A) Left panel shows the DNA profile in the input sample and after PML ChIP. In the right panel, a representative genome browser view of PADs identified via EDD on chromosome 5 is shown. Data represent also the logChIP/Input values of the domains identified. B) Percentage of gene types falling in PADs (left) and representative genome browser view of PADs and profiles of H3K9me3, H3K27me3, H3K4me3 and H3K4me1 on chromosome 5 is shown. C) Number of intersecting peaks between the indicated HPTMs and PADs and results of the permutation tests assessing the association between PADs and HPTMs (number of permutations=100).*

As mentioned in the introduction, H3K9me3 and H3K27me3 mark two different types of heterochromatin. While H3K9me3 characterizes constitutive heterochromatin regions, H3K27me3 marks facultative heterochromatin and does not necessarily predict closed chromatin regions (Jiang & Mortazavi, 2018). In line with their different functional characteristics, H3K9me3 and H3K27me3 domains are often mutually exclusive and differentially distributed in the nuclear space (Ernst *et al*, 2011; Filion *et al*, 2010). However, to maintain the integrity of heterochromatin the two histone marks may

compensate each other in specific conditions (Saksouk *et al*, 2014). As such, loss of PML in MEFs led to a shift from H3K9me3 to H3K27me3 inside PADs, and an increase in incorporation of the histone variant H3.3 (Delbarre *et al*, 2017), suggesting that these regions are important to be maintained in an heterochromatic state. Interestingly, later work on PADs identified H3.3 as enriched at PADs borders in absence of PML. In particular, H3.3 deposition occurs in regions of 1.5kb outside PAD boundaries, which are often rich in gene content, active histone marks and in binding sites of the insulator protein CTCF (Spirkoski *et al*, 2019).

To delineate whether also in TNBC cells PADs are marked by these transitions in chromatin composition, we plotted the average profiles of repressive and active HPTMs signals (H3K9me3, H3K27me3, H3K4me1, H3K4me3) in a window of 1.5kb inside and upstream or downstream of all identified PADs (figure 14A).

This analysis confirmed that the repressive histone mark H3K9me3 is constantly high inside PADs, while H3K27me3 signal is depleted inside and high outside PADs (figure 14A, red graphs). Similarly, the average profiles of the active histone marks H3K4me1 (a marker of enhancer) and H3K4me3 (a marker of promoters) signals are low inside PADs, and slightly increase in regions outside PADs (figure 14A, grey graphs). Nonetheless, by widening our analysis to a window of 1mb and 3mb, we observed that the average profiles of active histone marks gradually increase moving away from PADs borders (figure 14B, C). To quantify the difference among the HPTMs signals we plotted the normalized coverage of each modification in a window of 3 mbs inside and outside our PADs which confirmed that H3K27me3, H3K4me1 and H3K4me3 are significantly depleted inside PADs when compared to H3K9me3 (figure 14D). The significance of these analyses was further confirmed by characterizing the epigenetic profile of a set of synthetic genomic regions, which instead resulted to be not enriched in any of the analysed HPTMs (data not shown). Hence, our data confirms previous findings (Spirkoski *et al*, 2019) and indicates that PADs represent constitutive heterochromatin compartments that are surrounded by opposite types of active chromatin compartments.

These features are also reminiscent of those of lamina-associated domains (LADs), which define large heterochromatin domains associated with the nuclear lamina (van Steensel & Belmont, 2017). LADs are enriched in H3K9me3 and H3K27me3, devoid of active genes and histone marks (Guelen *et al*, 2008), and play key roles in sustaining and

modulating the spatial organization of the genome and gene repression, by acting as an anchoring points for chromatin (van Steensel & Belmont, 2017). Accordingly, LADs show sharp transitions in chromatin composition at their borders, with enhanced gene density, active histone marks, CTCF and RNA polymerase II (Guelen *et al*, 2008).

In conclusion, we confirm that PML associates with large heterochromatin and gene-poor regions in TNBC cells, and we observed that PADs are similar to LADs in terms of epigenetic composition at their interior and at their borders.

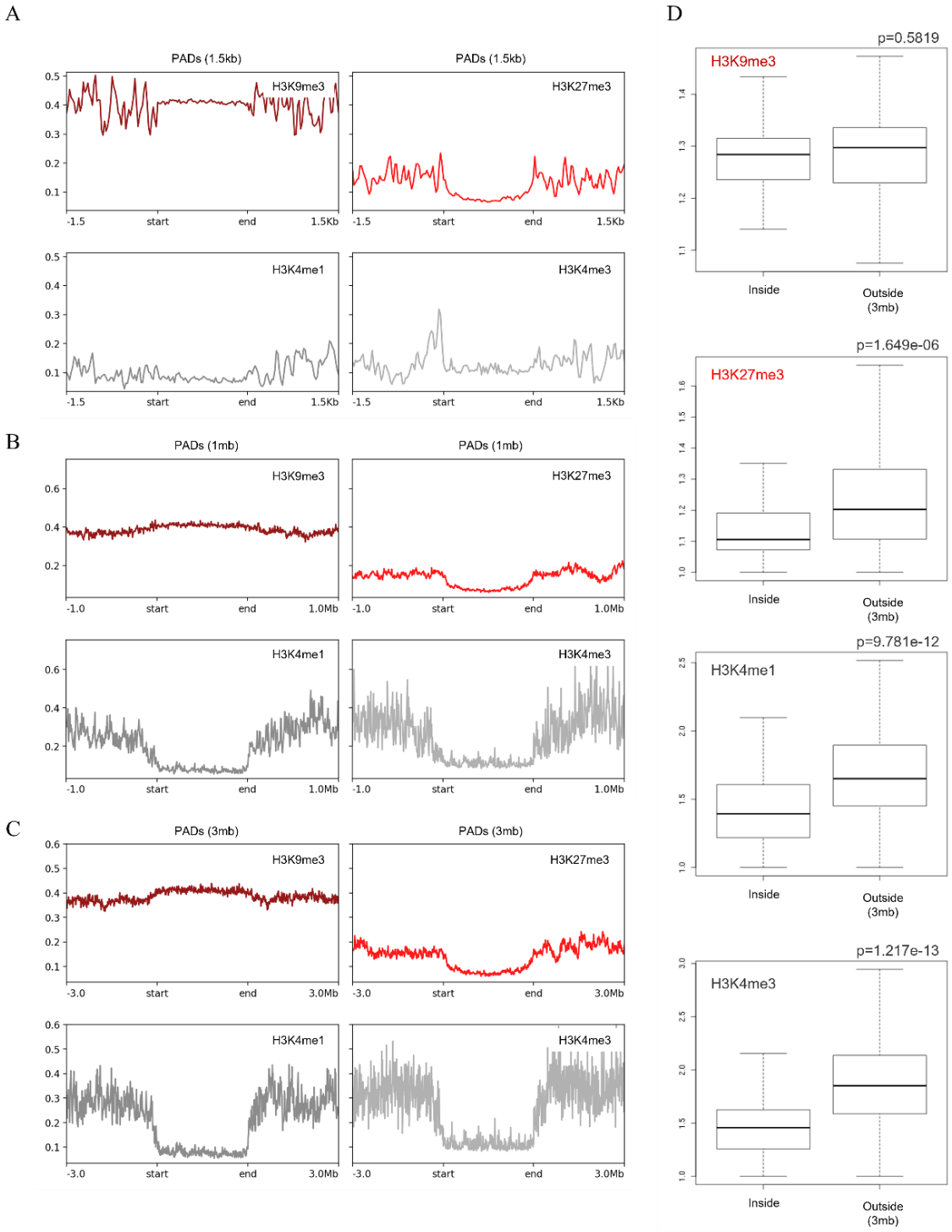

Figure 14. PADs are heterochromatin domains flanked by open chromatin regions. *Average profile of each HPTMs signal in a window of A) 1.5 kb, B) 1mb and C)3mb inside and at PADs border. D) Mean coverage of the indicated HPTMs (y-axis) in a region of 3mbs inside and outside PADs (x-axis). Statistic was calculated with the Mann-whitney test.*

3.1.2.1.1 PADs are gene poor and enriched of structural elements of chromatin

The binding of PML to large heterochromatic regions, marked by the constitutive heterochromatin mark H3K9me3, suggest that PADs may represent domains essential for the structural organization of chromatin. To test this hypothesis we characterized the genomic composition of PADs by looking at the overlap with different structural components of heterochromatin. Among them we measured the enrichment of repetitive elements, which are known components of constitutive heterochromatin (Lu *et al*, 2021, 2020). To evaluate statistically the associations between region sets we employed permutation tests, which compare the overlap of the genomic feature of interest with PADs to the distribution of the overlap generated with a group of PADs randomly shuffled on the genome. By intersecting PADs with annotated repetitive elements listed by the RepeatMasker database, we found that 50% of the PADs area is covered by repetitive elements and that this enrichment is statistically significant by permutation test (figure 15A). Among enriched classes of repetitive elements we found prevalence of repetitive elements found in heterochromatin, such as LINEs, LTRs and simple repeats (figure 15B), thus confirming that PADs are domains marked by constitutive heterochromatin. Repetitive elements partake in the assembly of chromatin compartments (Solovei *et al*, 2016; Politz *et al*, 2013) and homotypic clustering of the retrotransposon elements LINEs and SINEs support the formation of heterochromatic and euchromatic domains respectively (Lu *et al*, 2021, 2020; Cournac *et al*, 2016). Hence, we validated the binding of PML to the repetitive LINE elements *via* ChIP-qPCR, confirming enrichment of PML to these sites (figure 15C).

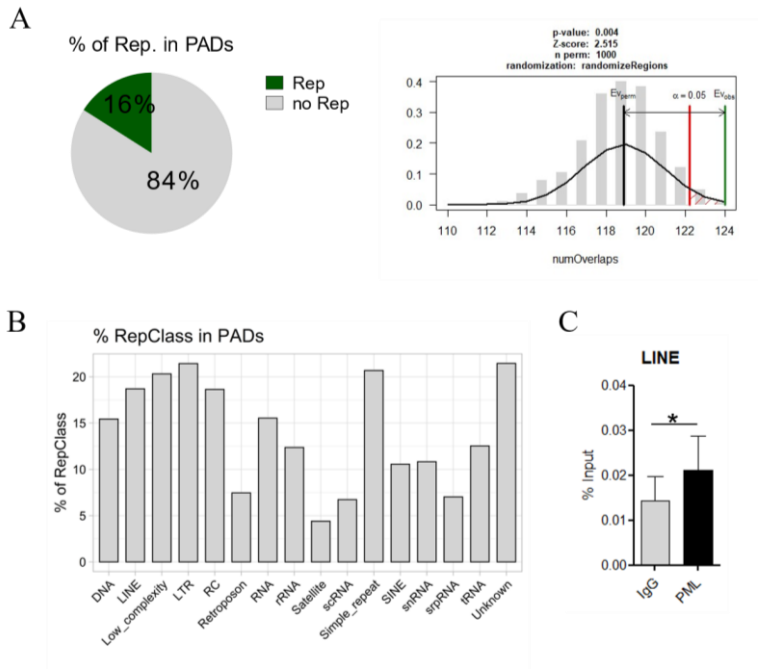

Figure 15. PADs are enriched in repetitive DNA elements. *A) Percentage of intersecting repetitive elements (from the RepeatMasker Database) with PADs (left). Results of the permutation test assessing the association between PADs and repetitive elements (right, number of permutations=1000 with p value=0.006, Z-score=2.539). B) Percentage of repetitive elements falling in PADs over the total number of repetitive elements. C) ChIP-qPCR of PML on LINE-hORF2 sequences versus control IgG. Data represent mean ± SD of three independent experiments. Statistics was calculated with paired, two-tailed, Student t-test (*=p-value<0.05).*

In line with the presence of repetitive elements, we found that PADs are enriched with other structural components of chromatin. Specifically, we took advantage of published sequencing data made in our same cell lines on matrix-associated regions (MARs) and lamina-associated domains (LADs; Dobson *et al*, 2017; Chang *et al*, 2020). MARs are DNA sequence elements characterized by the ability to bind the nuclear matrix. Although not biochemically defined, the nuclear matrix appears as a network of irregular fibres that associates with DNA to sustain chromatin lopping and compartmentalization (Razin *et al*, 2014). In this respect, PML was previously shown to bind MARs within the MHC class I locus in cooperation with the structural protein SATB1 (Kumar *et al*, 2007). In line with these findings, peak intersection reveals a significant enrichment of MARs inside PADs (figure 16A). Similarly, we found a significant overlap among PADs and LAD (figure 16B). Interestingly, we found that LADs (median length of 1.52Mb) occupy 96% of PADs area (data not shown), suggesting a possible interaction between PML and lamins in the organization of these heterochromatin domains. These data are concordant

with the strong similarity in chromatin composition between PADs and LADs that we previously described.

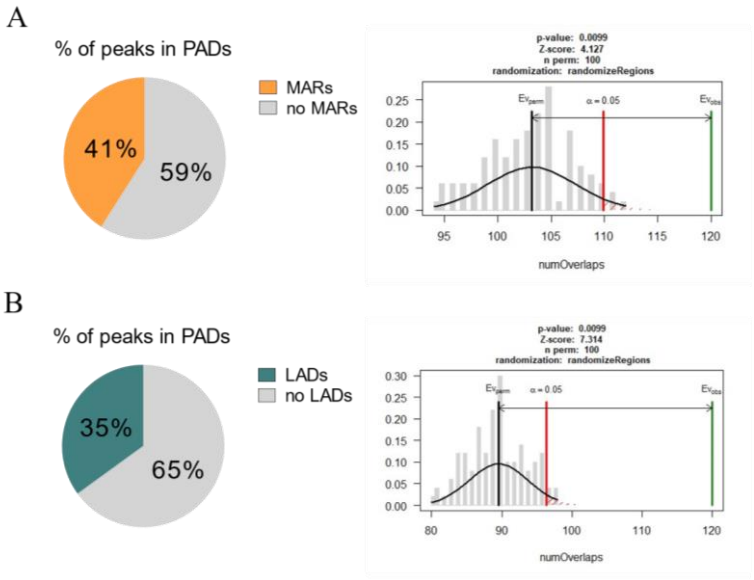

Figure 16. PADs are enriched in MARs elements and LADs. *A) Percentage of intersecting MARs with PADs (left). Results of the permutation test assessing the association between PADs and MARs (right, number of permutations=100 with p value=0.009, Z-score=4.127). B) Percentage of intersecting LADs and PADs (left). Results of the permutation test assessing the association between PADs and LADs (right, number of permutations=100 with p value=0.009, Z-score=7.314).*

In sum, our data confirm that in TNBC PML binds to large heterochromatic domains, named PADs, which are devoid of active histone marks and coding genes. Conversely, PADs are enriched in different structural elements of chromatin, which often characterize heterochromatin, such as repetitive elements, MARs and LADs. Interestingly, LADs show the highest overlap with PADs, suggesting that PML may cooperate with lamins in the assembly of heterochromatin domains.

However, although most PADs are heterochromatic and devoid of coding genes, few of them are gene rich. Specifically, they contain the olfactory, taste, the GABA receptor and the UGT gene clusters (data not shown). These data confirm published data in MEFs, where few PADs were shown to contain the same gene clusters (Delbarre *et al*, 2017), with the except of the UGT gene cluster. In addition, they demonstrate that PML binding to these clusters is conserved among species and cell types. These data might suggest that PML may promote clustering of functionally related genes (Delbarre *et al*, 2017) and

perhaps their transcriptional regulation. However, we found a minor overlap of PADs with PML regulated genes identified by RNA-sequencing (figure 17, upper Venn diagram) which are instead significantly depleted in PADs by permutation tests (figure 17, lower graphs).

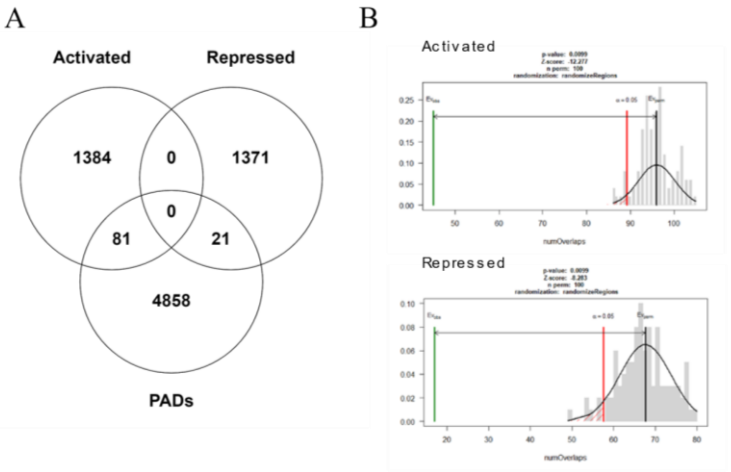

Figure 17. Overlap of PADs with PML regulated genes. *The upper Venn diagram represents the overlap of genes falling in PADs and genes activated or repressed by PML. All deregulated genes with log2FC<-/>0.3 and FDR 0.05 were considered. Fisher's exact test, two-tailed P value equals is less than 0.0001. The lower panels represent the results of a permutation test assessing the association between PADs and PML activated (left) and repressed genes (right). Both tests were made with a number of permutations=100 with p value=0.099. For activated genes the resulting Z-score=-12.277, while for repressed genes Z-score=-8.283.*

Interestingly, LADs borders have been identified as transition regions, characterized by an increase in gene density and active HPTMs, and involved in the regulation of expression of LAD-proximal genes (Harr *et al*, 2015; Peric-Hupkes *et al*, 2010; Chen *et al*, 2018). This is particular evident during differentiation when most variations in LADs structure occur at their border regions. In this context, LADs borders, which contain developmentally regulated genes, are relocated to the nuclear lamina by the deposition of H3K27me3 and the binding of both CTCF and cell-type specific TFs. Delocalization of LADs border regions to the nuclear periphery leads to the formation of a new LAD which is essential for the cell specific silencing of developmentally regulated genes, as well as for cell-specific genome organization (Harr *et al*, 2015). In addition, in mouse T lymphocyte cells one LAD has been shown essential in the recombination and expression of the mouse T cell receptor (TCR) locus. Specifically, the border of such LAD is

essential for targeting the TCR locus to the nuclear periphery and to restrain the activity of proximal enhancers, which, in absence of the LAD, would lead to the expression of the TCR linked genes. Accordingly, its deletion induces detachment of the TCR locus from the nuclear lamina, spreading of H3K27ac, transcription and recombination of the TCR genes (Chen *et al*, 2018). Given the strong overlap of PADs and LADs, and their similarities at the epigenetic level, we wondered whether also PADs borders may be functionally relevant for the expression of PML regulated genes. For this reason, we looked whether genes regulated by PML, identified by RNA-sequencing, are specifically found in regions proximal to PADs borders (figure 18B). By measuring the distance of each deregulated gene with respect to the most proximal PAD border, we found that genes whose expression is activated by PML lie more proximal to PADs that the remaining coding genes in the genome, while genes whose expression is repressed by PML are at a further distance (figure 18A, left). Genes activated by PML that lie more proximal to PADs borders include several genes involved in metastasis regulation, such as *LOX* and *SPARC*, which are among the most significantly deregulated genes upon PML silencing (figure 18A, right). This suggests that PADs are heterochromatin domains juxtaposed to active chromatin regions containing PML positively regulated genes.

In summary, we found PADs enriched in several structural components of chromatin, raising the possibility that these domains may partakes in the structural organization of the genome. In line with this hypothesis, PADs are highly similar to LADs, which are essential for the right spatio-temporal regulation of the genome structure and transcriptional status. In this concern LADs have been shown to mediate gene silencing by anchoring genes to the nuclear periphery, and to indirectly promote transcription of genes falling at LADs borders. Similarly, we found genes activated by PML proximal to PADs borders, suggesting that these sites represent transcriptionally active genomic regions.

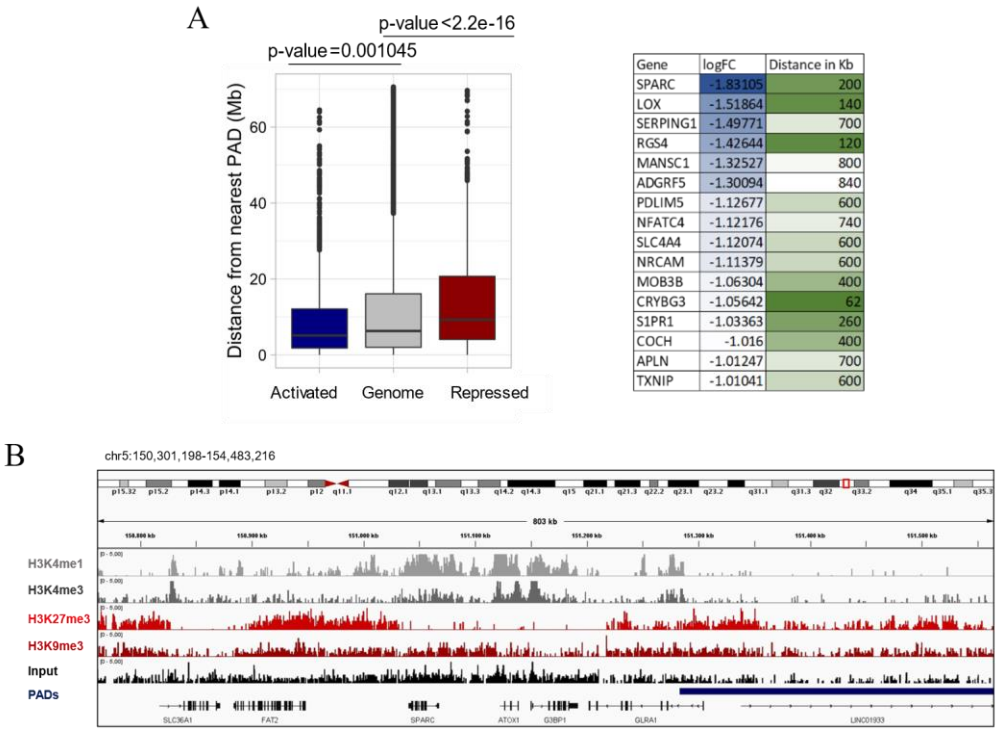

Gene	logFC	Distance in Kb
SPARC	-1.83105	200
LOX	-1.51864	140
SERPING1	-1.49771	700
RGS4	-1.42644	120
MANSC1	-1.32527	800
ADGRF5	-1.30094	840
PDLIM5	-1.12677	600
NFATC4	-1.12176	740
SLC4A4	-1.12074	600
NRCAM	-1.11379	600
MOB3B	-1.06304	400
CRYBG3	-1.05642	62
S1PR1	-1.03363	260
COCH	-1.016	400
APLN	-1.01247	700
TXNIP	-1.01041	600

Figure 18. PADs borders are enriched in PML activated *A) Distances in megabase (Mb) of each PML regulated gene (log2FC <-/>0.3, FDR 0.05) to the most proximal PAD border. Wilcoxon rank-sum test p-values are given (left). Genes activated by PML ranked by increasing log2FC values and associated distance in kilobase (Kb) from the most proximal PAD border (right). B) Representative genome browser view of one PAD border proximal to PML regulated genes, and the profiles of H3K9me3, H3K27me3, H3K4me3 and H3K4me1 on chromosome 5.*

3.1.2.2 PML binds to gene promoters

3.1.2.2.1 PML binds the promoter region of genes in non-TNBC cells

While our ChIP-sequencing data and published characterization of DNA binding in MEFs (Delbarre *et al*, 2017) describe the binding of PML to large heterochromatic domains, other ChIP-sequencing data deposited by the ENCODE project show a completely different pattern of PML binding to DNA. Peak calling of ENCODE ChIP-sequencing was performed with the MACS2 algorithm which identified PML binding to DNA in narrow peaks similar to those of TFs (figure 19A). By analysing PML ChIP-sequencing obtained in three unrelated cell lines (luminal breast cancer cells MCF7, chronic myelogenous leukaemia cells K562, and B-Lymphocyte cells GM12878), we found that PML-bound peaks are enriched in proximity to the transcription start site (TSS) and in the promoter region of coding genes (figure 19B).

Together with our ChIP-sequencing data, this analysis suggests that PML associates with different types of DNA sequences, and with a different modality: weak and constant binding to large, heterochromatic regions, and discrete binding to small euchromatin regions

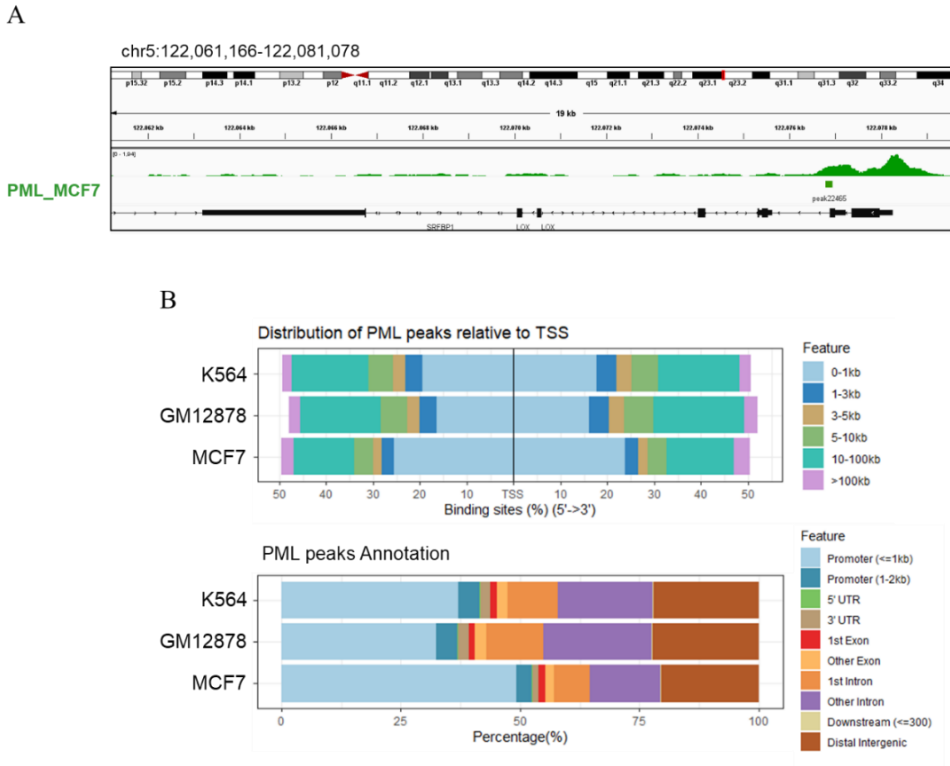

Figure 19. PML binds in narrow peaks at the promoter region of genes in DNA-sequencing data deposited by the ENCODE project. *A) Representative genome browser view of PML ChIP-sequencing in MCF7 cells on chromosome 5. B) Upper bar plots: percentage of PML peaks distributed at 0-1kb,1-3kb,3-5kb,5-10kb,10-100kb,>100kb distance to the TSS of the nearest gene. Lower bar plots percentage of PML peaks distributed on the indicated genomic annotations. The analysis was performed on PML ChIP-sequencing from three different cell lines (K562, GM12878, MCF7).*

Apart from the peak calling algorithm, another difference among our experiment and the ENCODE project data rests in the cell lines used. Therefore, the different patterns of PML binding to DNA may reflect a cell-specific activity.

However, in comparing the two experiments from a biochemical perspective we realized that ChIP-sequencing by the ENCODE project utilizes a different cell lysis protocol, based on the use of different detergents and lower salt concentrations. For this reason, we hypothesized that the different cell lysis protocol may lead to the enrichment of DNA

associated to two different PML conformations: i) PADs representing large PML aggregates, such as the PML-NBs; ii) narrow peaks representing free PML moieties in the nucleoplasm. Hence, we compared PML DNA association with the two extraction protocols in the same cell line, TNBC cells MDA-MB-231, and from now on I will refer to these experimental protocols as the PADs protocol and the narrow peaks protocol. For evaluation of DNA binding by ChIP-qPCR, we selected *LINE* elements as representative of PADs, and genes that are found bound to PML in the ENCODE ChIP-sequencing data and are regulated by PML in our MDA-MB-231 cells (*SPARC* and *LOX*) as representative of narrow PML binding to gene regulatory elements. ChIP-qPCR analysis on samples prepared with the PADs protocol revealed that PML binds to both *LINE* and the regulatory element of *SPARC* and in the promoter region of *LOX*. Conversely, with the narrow peaks protocol we observed PML enriched only at the regulatory element and promoter region of *SPARC* and *LOX*, and with a higher enrichment with respect to the PADs protocol, while no binding was detected on *LINE* elements, suggesting that this protocol may enrich PML bound to euchromatin (figure 20). We speculate that the reason why we did not detect PML binding to the regulatory regions of coding genes including *SPARC* and *LOX* when we performed DNA sequencing of the PADs protocol is that this binding may fall beyond the detection threshold.

In conclusion, these data suggest that use of different protocols of cell lysis and protein solubilization may lead to the isolation of distinct PML-chromatin complexes and prompted us to further address this issue in TNBC cells.

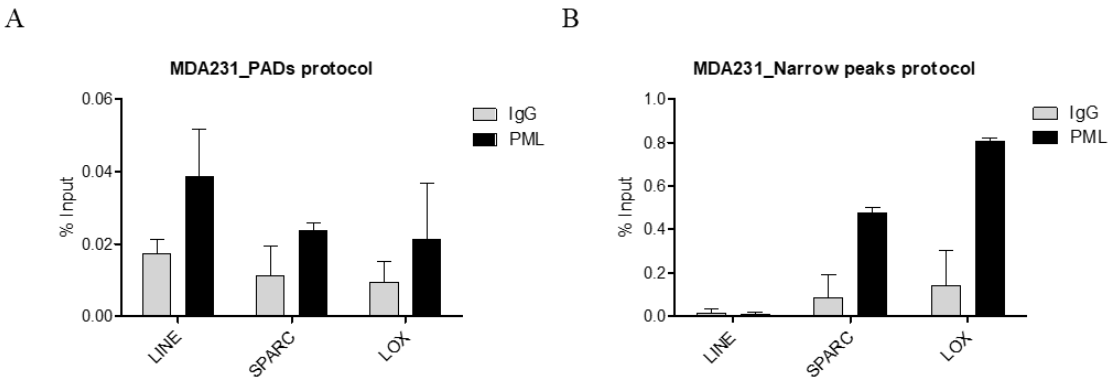

Figure 20. PML ChIP-qPCR analysis on three genomic loci using different chromatin extraction protocols. *Percentage of input values of DNA immunoprecipitated with PML in MDA-MB-231 cells A) with the PADs protocol and with B) the narrow peaks protocol. Data are representative of mean values ± SD of two independent experiments.*

3.1.2.2.2 PML binds the promoter region of genes in TNBC cells

Since we confirmed that the narrow peaks ChIP protocol utilized by ENCODE allows the enrichment of PML binding to coding genes, we aimed to characterize PML binding to gene rich regions on a genome-wide scale via sequencing. Interestingly, during library preparation, we noted that the chromatin obtained after immunoprecipitation with the narrow peaks protocol contains two pools of DNA: the canonical DNA fragments enriched around 500-100 bp that were maximally represented before chromatin IP, and a group of larger fragments enriched at ~1.5 kb (figure 21A). Similar results were already described for lamin A/C ChIP samples, and the different DNA pools were later characterized as euchromatic (low molecular weight chromatin) and heterochromatic (high molecular weight chromatin) LADs (Lund *et al*, 2014; Gesson *et al*, 2016). These studies also showed that chromatin sonication or digestion are crucial to identify differential binding of lamin A/C proteins to open or closed chromatin regions. Although lamin A/C associated LADs often overlap with heterochromatic lamin B LADs, moderate sonication conditions lead to the identification of euchromatic LADs bound by lamin A/C (Gesson *et al*, 2016). Under this condition, the lamin A/C bound DNA shows, similar to our experiment, enrichment of two groups of DNA fragments, with the canonical small fragments, around 300 kb and a set of larger fragments enriched around 1.5 kb. Large DNA fragments are usually excluded from sequencing due to size selection during library preparation, however, an increase in sonication made these regions accessible to analysis and led to the identification of heterochromatic LADs (Gesson *et al*, 2016). Since we observed the same pattern of DNA fragments from our PML ChIP, we wondered whether like lamin A/C PML bound DNA may also be enriched by these distinct types of chromatin. Specifically, we hypothesized that small fragments represented euchromatic regions bound by PML in its free conformation, like those identified by the ENCODE project, whereas large fragments may coincide with heterochromatic regions overlapping with PADs. In order to include the larger DNA fragments, we sonicated for additional cycles half of the immunoprecipitated DNA to make it available to library preparation and analysis. We thus created two different libraries: library A, containing DNA with low molecular weight (figure 21B, orange), and library B, created from large DNA fragments after additional sonication (figure 21B, green).

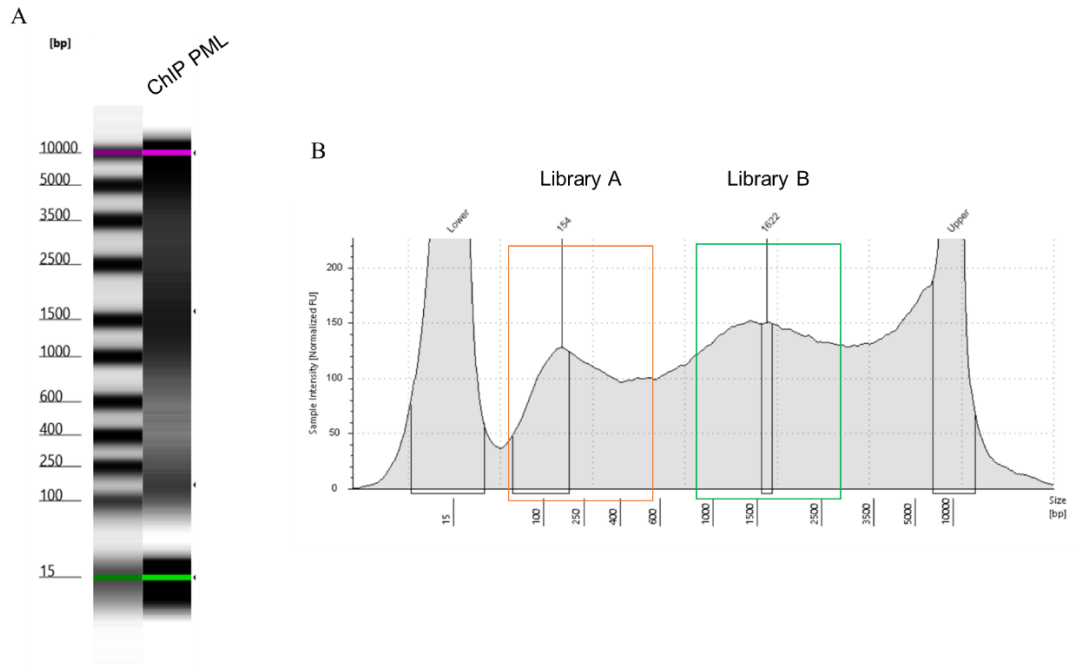

Figure 21. PML associated chromatin extracted with the narrow peaks protocol. *A) DNA profile after PML ChIP on a high-resolution agarose gel. B) Representative Bioanalyzer intensity profiles of PML ChIP sample.*

Upon sequencing, unlike with the PADs protocol, we succeeded in calling PML-associated peaks using the MACS2 peak calling algorithm (figure 22B) and observed different number of peaks in the two libraries. Specifically, we identified 1550 unique peaks from library A and 676 unique peaks from library B (figure 22A, Venn diagram, left). Notably, peaks associated with each library show a different and opposite pattern of genomic distribution: peaks from library A distribute mostly at regions proximal to the TSS of genes, whereas library B peaks are enriched at >100 kb distance from the most proximal TSS region (figure 22A, right).

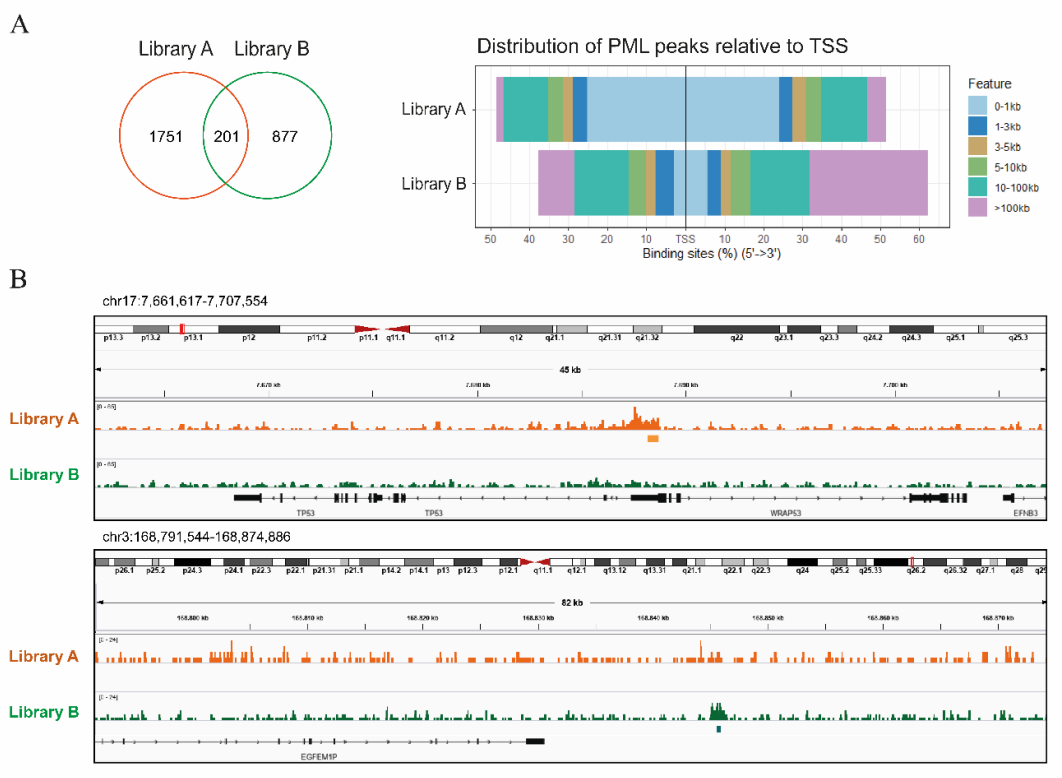

Figure 22. PML binds chromatin in narrow peaks. *A) Veen diagram of intersecting library A and B peaks (left). Percentage of library A and B peaks distributed at 0-1kb,1-3kb,3-5kb,5-10kb,10-100kb,>100kb distance to the TSS of the nearest gene (right). B) Genome browser view of two representative examples of library A (orange) and B (green) peaks on chromosomes 17 and 3 respectively.*

Other than having distinct genome distribution, peaks of library A and B are also different in terms of chromatin composition. In particular, library A peaks mostly associate with active histone modifications (figure 23A, upper bar plot, 23B, left pie chart), confirming that PML also binds open chromatin regions. On the contrary, library B peaks are enriched in intergenic regions and show a mixed pattern of active and repressive histone marks, without any enrichments of either active or repressive histone marks (figure 23A, lower bar, 23B, right pie chart).

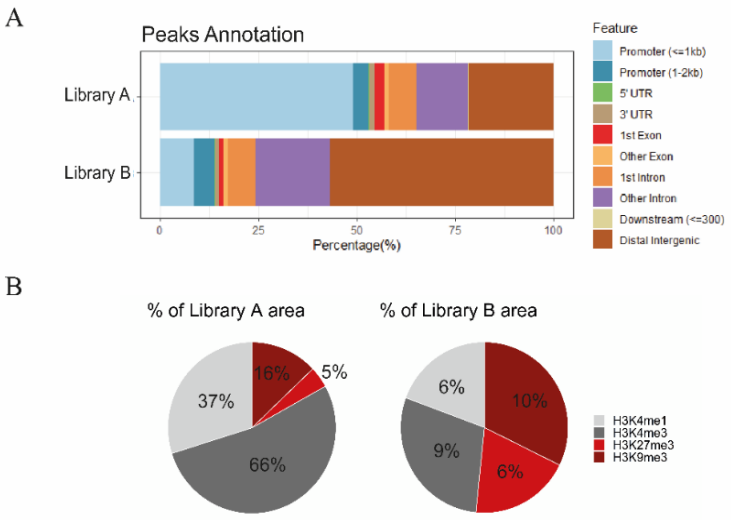

Figure 23. PML binds to promoter and intergenic regions in narrow peaks. *A) Percentage of library A and B peaks distributed on the indicated genomic annotations. B) Percentage of intersecting HPTMs signals with PML peaks.*

Since we initially hypothesized that library B may represent PADs, which are not included in the ENCODE data due to chromatin size selection during library preparation, we analysed the overlap of PADs with both library A and B generated peaks. Unexpectedly, we found that PADs minimally overlap with DNA from both libraries (figure 24A). Specifically, we found 28 peaks from library A and 12 peaks from library B intersecting with PADs. In addition, both libraries are significantly depleted inside PADs by permutation tests (figure 24B).

To exclude that the minimum overlap among PADs and DNA from library A or B may be a consequence of the different types of peak calling algorithms that were used (i.e., MACS2 and EDD), both libraries were analysed with the EDD algorithm. However, EDD did not identify PADs in library A nor in library B, which we expected to overlap with previously identified PADs. Rather, EDD identified large domains covering almost the entire genome (data not shown), suggesting that the low signal to noise ratio in ChIP-sequencing data obtained with the narrow peaks protocol makes it unsuitable for the analysis with EDD. In line with this hypothesis, we noticed a striking difference among the total amount of DNA immunoprecipitated by PML in the PADs protocol (figure 13A) compared to the narrow peaks protocol (figure 21A). Therefore, it remains to be established whether hidden within the DNA sequences of library B there are also PADs that cannot be identified due to high sequencing noise.

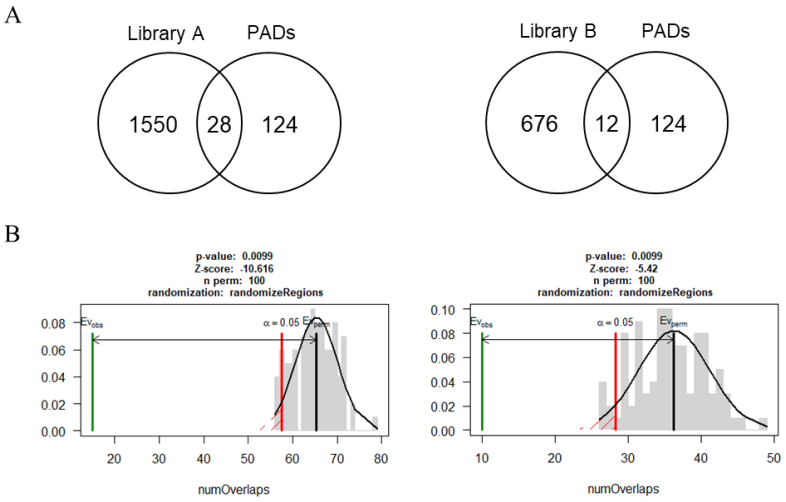

Figure 24. Overlapping of PML peaks and PADs. *A) Veen diagrams showing the intersection of library A and B peaks with PADs. B) Permutation tests assessing the association between PADs and library A (left) or library B (right) peaks. Both tests were made with a number of permutations=100 with p value=0.099. For library A (left) the resulting Z-score=-10.616, while for library B (right) Z-score=-5.42.*

In conclusion, we showed that in the same TNBC cell line PML binds not only to large heterochromatic domains but also to small chromatin regions identified by epigenetic marks of gene promoters, similar to those identified in ENCODE ChIP-sequencing data. Importantly, we provide the first evidence that different PML-associated DNA regions can be discriminated by using distinct cell lysis and chromatin immunoprecipitation protocols. Finally, by analysing all chromatin obtained with the narrow peaks protocol, including high molecular weight chromatin fragments that may be excluded from common DNA-sequencing procedures if not further fragmented, we reveal a third possible modality of PML association to DNA, which does not overlap with PADs but consists of narrow peaks enriched in intergenic DNA regions.

3.1.2.3 Tissue specific and conserved binding of PML to chromatin

Because PADs are devoid of coding and PML-regulated genes, we wondered whether PML regulated genes may fall under PML peaks obtained from the narrow peak protocol, specifically from library A. In testing this hypothesis, we also tested the overlap with library B, which we used as a possible negative control as it contains mostly peaks falling in intergenic regions. Unexpectedly, we observed only a minor overlap of PML-regulated genes and PML-bound regulatory regions of library A. Specifically, PML bound to only

95 of the genes under positive regulation by PML, as identified by RNA-sequencing, and to 109 repressed genes (figure 25A). Within the 95 and 109 genes whose regulatory regions are bound by PML and whose expression is activated or repressed by PML respectively, gene set enrichment analysis revealed enrichment of gene categories only amongst the 95 genes activated by PML (figure 25B). Notably, these genes concentrate in gene families linked to EMT, cell migration, hypoxia and inflammation (figure 25B). These data indicate that there is a subset of genes that PML appears to regulate via association to their regulatory regions that are implicated in important oncogenic pathways in TNBC, which have been in part functionally validated (i.e. the regulation of cell migration and metastasis) (Ponente *et al*, 2017). Among these genes we found the several hypoxia inducible genes, such as the serine protease inhibitor, clade E member 1 (*SERPINE1*) which is found overexpress in TNBC where it promotes epithelial-to-mesenchymal transition, migration, and drug resistance (Humphries *et al*, 2019; Zhang *et al*, 2020). In addition, these genes include several mediators of the TGF-beta signalling pathway, such as the SMAD family member 2 (*SMAD2*) and the Adenosine A2b Receptor (*ADORA2B*).

Notably, we found PML bound also to the cluster of differentiation 276 (*CD276*), an immune checkpoint protein that promotes tumour immune evasion by acting as a specific inhibitor of T-cell activity (Yang *et al*, 2020). In line with a role of PML in the regulation of immune pathways, *CD276* is also among the genes mostly deregulated in response to PML silencing, showing a log2FC value of -1 in the RNA-sequencing data.

Instead, although negatively regulated genes bound by PML do not cluster in any significant functional category (Adj.P.Value>0.1), these genes comprise several components of the lysosome and endosomal vacuolar pathways, such as the clathrin light chain A (*CLTA*) and the late endosomal/lysosomal adaptor, MAPK and MTOR activator 1 (*LAMTOR1*), which are in line with previously enriched pathways among genes suppressed by PML (figure 11, orange).

Similar to library A, genes annotated in library B show a small overlap with genes regulated by PML, with 56 genes bound and regulated by PML. These genes do not cluster in any functional category.

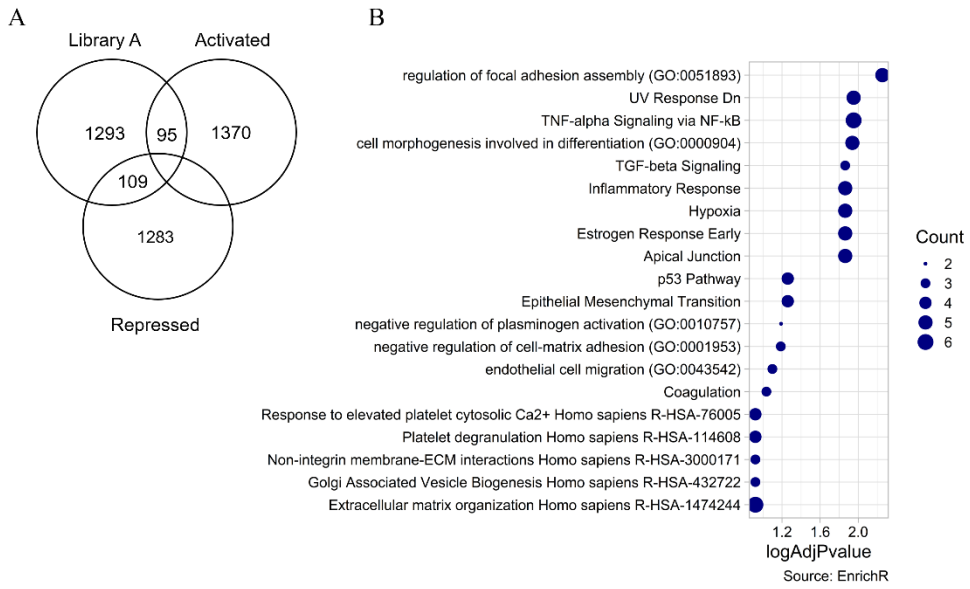

Figure 25. Gene set enrichment analysis of genes bound and activated by PML. *A) Venn diagram showing the overlap of genes regulated by PML identified by RNA-sequencing and bound by PML in library A (with log2FC<-/>0.3, FDR 0.05). Fisher's exact test, two-tailed P value equals 0.9402 for activated genes and 0.5729 for repressed genes. B) Gene set enrichment analysis performed with EnrichR on genes bound and activated by PML (with log2FC<-0.3, FDR 0.05). Significant pathways were filtered for adjusted for p value<0.1. Pathways are ordered according to their adjusted p-value (-log10AdjPvalue) and the size of the dots represents the number of PML bound and activated genes falling in each pathway.*

Since only a subset of genes bound by PML is regulated upon PML silencing, we investigated the nature of genes that associate with PML but are not regulated. For library A we found 1293 genes that are bound and not regulated by PML (figure 26A). These are enriched in three main functional categories that may be aggregated in stress response mechanisms, regulation of translation and regulation of splicing/transcription (figure 26B, orange, blue, green). Among the stress-related pathways we found enrichment of p53, hypoxia, cell cycle and viral infection terms. Genes falling in these pathways include the JUN transcription factor, known to be involved in hypoxia and p53-mediated responses, ribonucleoproteins and nucleoporins (i.e., *NUP155* and *UBA52*), often upregulated during viral infections, and proteins involved in microtubule formation and cell division, like dyneins and septins. In addition, we see enrichment of pathways involved in translation and transcription which include genes involved in basic biological processes, such as the eukaryotic translation initiation factor 4A1 (*EIF4A1*), several ribosomal proteins, the large subunit of RNA polymerase II (*POLR2A*) and serine and

arginine-rich splicing factors (*SRSF*). On the contrary, we see no enrichment of functional categories among the 427 genes of library B bound and not regulated by PML.

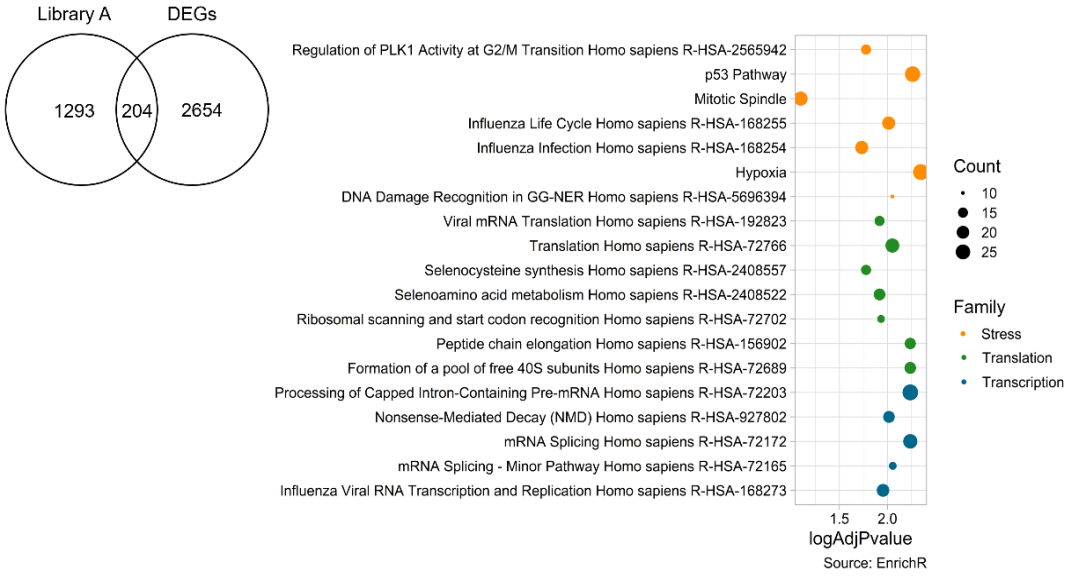

Figure 26. Gene set enrichment analysis of genes bound and not regulated by PML. *On the left, Venn diagram showing the overlap of genes regulated and bound by PML in library A. On the right, gene set enrichment analysis performed with EnrichR on genes bound and not regulated by PML. Significant pathways were filtered for adjusted p value<0.1 and clustered into functional families (blue, orange, green). Pathways are ordered according to their functional families and the size of the dots represents the number of PML bound genes falling in each pathway.*

The pathways enriched in the genes bound by PML in library A recall the constitutive and stress induced functions of PML. As mentioned in the introduction, it is broadly accepted that PML acts as an antiviral agent by restricting viral proteins and nucleic acid inside the PML-NBs. Interestingly, during viral infections, the endogenous transcriptional and translational machineries are often deregulated and usurped by viral particles to promote viral replication (Li, 2019). In addition, in order to migrate from the cytoplasm to the nucleus, viruses exploit the active transport of the endogenous cytoskeletal system (i.e., microtubules) to reach their site of replication (Merino-Gracia *et al*, 2011), suggesting that binding of PML to these sets of genes may reflect the viral and perhaps ancestral functions of PML. With this in mind, we asked whether these genes may be bound by PML in a conserved manner among different cell lines and we compared our library A ChIP-sequencing and the ENCODE PML ChIP-sequencing data, as these data were obtained with the same protocol. By overlapping genes bound by PML among the 4 different cell lines (figure 27A, right) we found a recurrence of stress, transcription

and translation pathways, which include the genes mentioned before (figure 27B, left, orange, blue, green). On the contrary, we observed no overlap among ENCODE ChIP-sequencing data and library B, possibly due to the exclusion of these DNA fragments after size selection during library preparation.

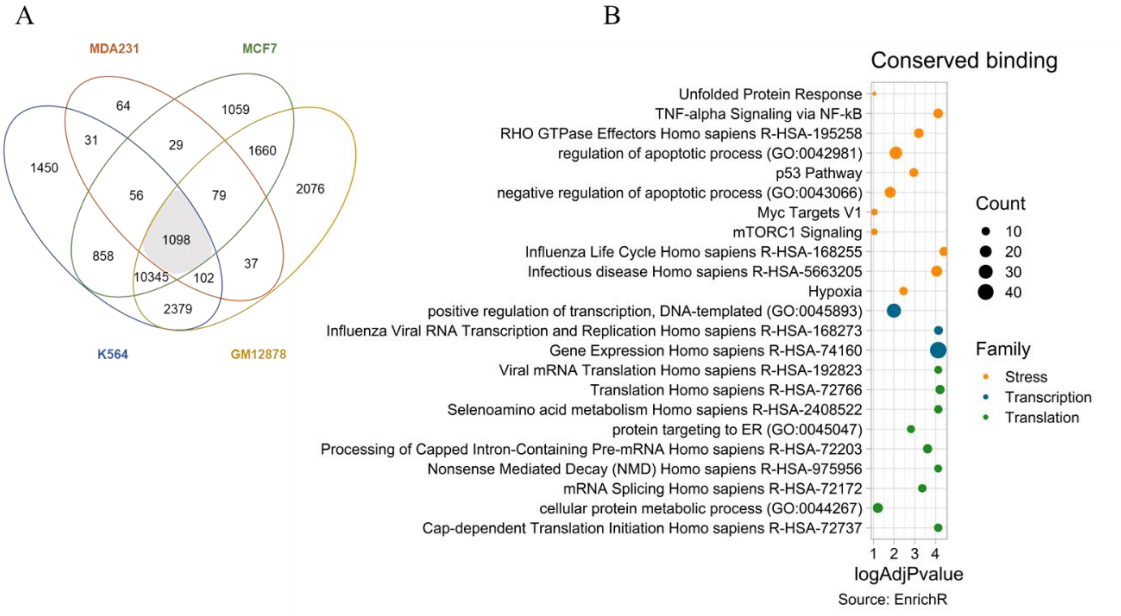

Figure 27. Gene set enrichment analysis of genes bound by PML across different cell lines. *On the left, Venn diagram showing the overlap of genes commonly bound by PML in MDA-MB-231, MCF7, K564 and GM12878 cell lines. On the right, gene set enrichment analysis performed with EnrichR on genes commonly bound by PML in the indicated cell lines. Significant pathways were filtered for adjusted p value<0.1 and clustered into functional families (blue, orange, green). Pathways are ordered according to their functional families and the size of the dots represents the number of PML bound genes falling in each pathway*

We next investigated the epigenetic and genomic composition of tissue specific and conserved PML binding sites obtained from library A. PML peaks unique to MDA-MB-231 TNBC cells were enriched on gene promoters and enhancer sequences, marked by H3K4me3 and H3K4me1 (figure 28A, right). In addition, motif calling analysis showed a recurrence of the AP-1 TFs binding motif, which represent a large family of dimeric TFs made up of members of the Jun (c-Jun, JunB and JunD), and Fos (c-Fos, FosB, Fra-1/Fosl1 and Fra- 2/Fosl2) gene families (Shaulian & Karin, 2002). The AP-1 TFs are involved in the transcriptional regulation of a variety of pathways, including cell proliferation, differentiation, apoptosis and oncogenesis, and act as downstream activators of many stimuli, such as growth factors, cytokines, neurotransmitters, cell–

matrix interactions, bacterial and viral infections, and physical and chemical stresses (Shaulian & Karin, 2002). In TNBC, the Fos family protein Fra-1 is overexpressed and promotes the expression of metastatic genes by mediating enhancer-promoter interactions (Bejjani *et al*, 2021) and is thus in line with the pro-metastatic tissue specific activity of PML in TNBC cells (Ponente *et al*, 2017). Conversely, among the PML peaks conserved amongst the 4 cell lines, we found enrichment of peaks on promoter regions, marked by H3K4me3, and with a ETS proteins binding motif (figure 28B). ETS proteins have been widely involved in the regulation of the innate immunity immune system and in its development (Seifert *et al*, 2019; Panagoulias *et al*, 2018; Gallant & Gilkeson, 2006). Interestingly, we found enrichment of the ternary complex factor (TCF) subfamily of ETS proteins (Elk1/4), which is found in complex with serum response factor (SRF) to regulate the expression of a class of cellular genes known as immediate-early genes (IEGs). IEGs are genes whose expression is quick and transient to provide a rapid response after different extracellular signals, such as growth factors, mitogens, developmental, and stress (Bahrami & Drabløs, 2016). Accordingly, TCFs are direct targets of MAPK pathways that respond to growth (ERK) and stress (JNK and p38) stimuli (Sharrocks, 2001), supporting a general stress-responsive role the genes bound by PML across different cell lines.

In summary, we found that within the PML bound regulatory regions identified in library A, a minority of associated genes are regulated upon PML silencing in TNBC cells. These are involved mainly in metastasis regulation, hypoxia and inflammation. Genes that are bond by but not regulated by PML in TNBC cells can be divided in two categories, those that are specifically associated to PML in TNBC cells, and those that are PML-bound across different cell lines. Interestingly, this last category identifies genes that are involved in stress and anti-viral responses. We speculate that PML binding may mark these DNA sequences for activation upon viral infection of cellular stresses. In addition, we see no commonality amongst genes bound by and repressed by PML, suggesting that this may be an indirect effect of PML silencing.

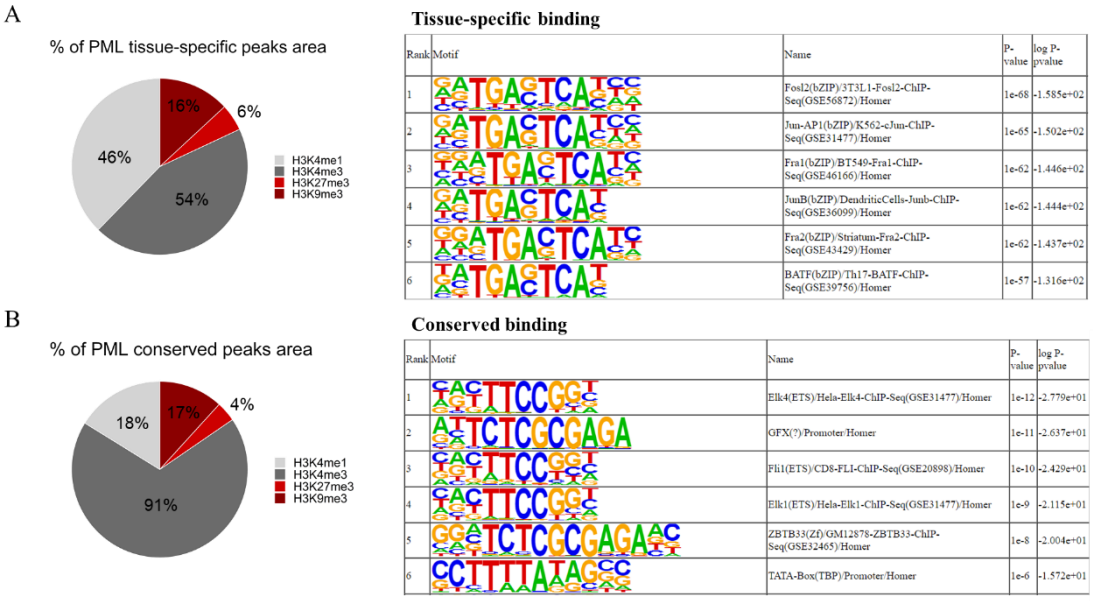

Tissue-specific binding

Rank	Motif	Name	P-value	log P-pvalue
1		Fosl2(bZIP)/3T3L1-Fosl2-ChIP-Seq(GSE56872)/Homer	1e-68	-1.585e+02
2		Jun-AP1(bZIP)/K562-cJun-ChIP-Seq(GSE31477)/Homer	1e-65	-1.502e+02
3		Fra1(bZIP)/BT549-Fra1-ChIP-Seq(GSE46166)/Homer	1e-62	-1.446e+02
4		JunB(bZIP)/DendriticCells-Junb-ChIP-Seq(GSE36099)/Homer	1e-62	-1.444e+02
5		Fra2(bZIP)/Striatum-Fra2-ChIP-Seq(GSE43429)/Homer	1e-62	-1.437e+02
6		BATF(bZIP)/Th17-BATF-ChIP-Seq(GSE39756)/Homer	1e-57	-1.316e+02

Conserved binding

Rank	Motif	Name	P-value	log P-pvalue
1		Elk4(ETS)/Hela-Elk4-ChIP-Seq(GSE31477)/Homer	1e-12	-2.779e+01
2		GFX(?)/Promoter/Homer	1e-11	-2.637e+01
3		Fli1(ETS)/CD8-FLI-ChIP-Seq(GSE20898)/Homer	1e-10	-2.429e+01
4		Elk1(ETS)/Hela-Elk1-ChIP-Seq(GSE31477)/Homer	1e-9	-2.115e+01
5		ZBTB33(Zf)/GM12878-ZBTB33-ChIP-Seq(GSE32465)/Homer	1e-8	-2.004e+01
6		TATA-Box(TBP)/Promoter/Homer	1e-6	-1.572e+01

Figure 28. Genomic characterization of tissue specific and conserved PML peaks. *PML peaks identified in library A were divided in those specific to MDA-MB-231 TNBC cells A) and those common to the 4 cell lines analysed by us and the ENCODE project B). The pie charts on the left describes the percentage of intersecting HPTMs signals with PML peaks. The tables on the right describe the most significant TF binding sites identified by motif calling in tissue specific or conserved PML peaks.*

3.1.3 Silencing of PML induces global changes in chromatin accessibility

Using two chromatin extraction protocols, we have identified PML in association with different chromatin environments via distinct DNA binding profiles. However, we found that only a small fraction of PML bound genes identified in both conditions are regulated upon PML silencing. Hence, to fully characterize how PML regulates transcription we performed ATAC-sequencing in MDA-MB-231 cells silenced for PML (figure 29A). By comparing ATAC peaks in PML-silenced versus control samples, we identified 7963 differential peaks (FDR<0.05), corresponding to open (logFC>1) or close (logFC<-1) chromatin regions in absence of PML (figure 29B).

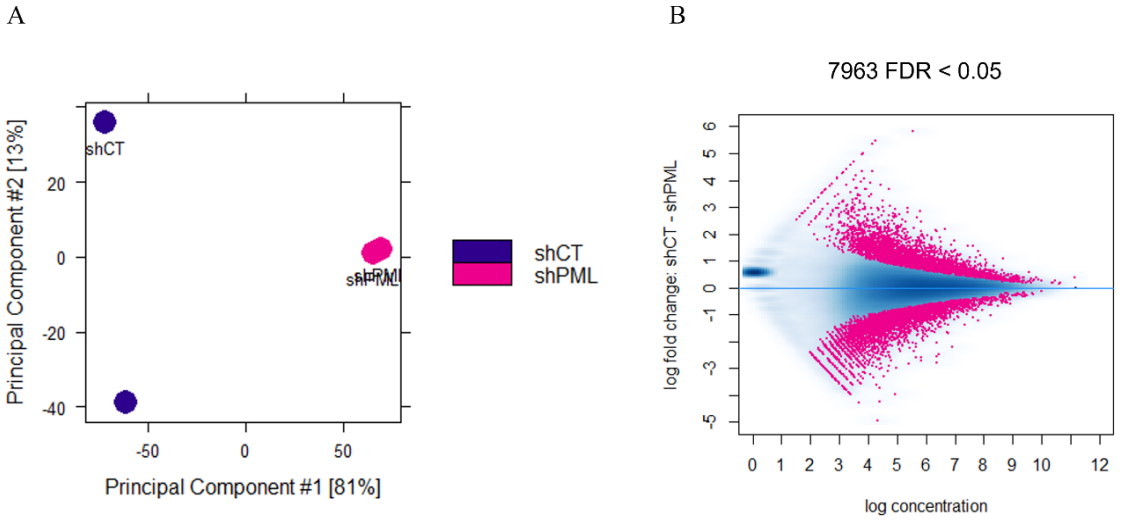

Figure 29. Differential analysis of ATAC-sequencing peaks in MDA-MB-231 cells silenced for PML. *A) PCA analysis of ATAC-sequencing data shows clustering of PML-silenced samples. Blue dots represent technical replicates of control samples (shCTRL), pink dots represent technical replicates of PML-silenced samples (shPML). B) MA plot of shCTRL-shPML contrast, with sites identified as significantly differentially open or closed chromatin regions shown in pink with FDR <0.05.*

We characterized the genomic distribution of all differential peaks by discriminating between peaks that marks chromatin regions whose structure is close or open in absence of PML (figure 29B, pink). This analysis revealed that both sets of peaks distribute similarly among different genomic regions (figure 30A), but close peaks appear more enriched at the promoter region of genes and near the TSS, compared to open peaks (figure 30A, upper bar plots). On the contrary, open peaks appear more enriched in intergenic regions and far from the TSS, compared to close peaks (figure 30A, lower bar plots). Consistently, close peaks are more enriched in active histone marks, identified by H3K4me1/3, whereas open peaks show an increase in the repressive histone marks H3K9/27me3.

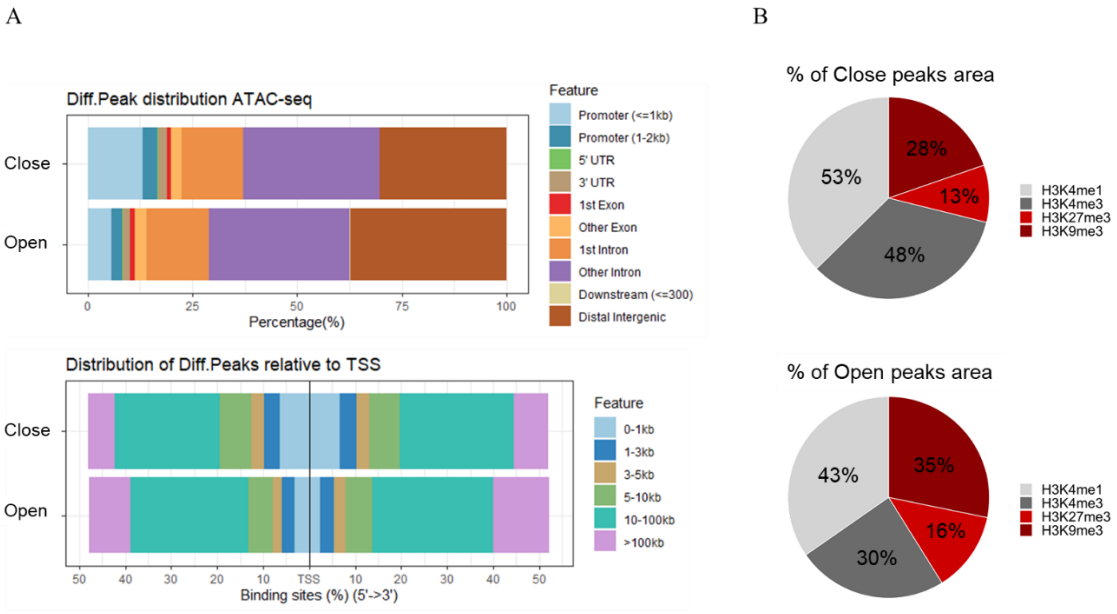

Figure 30. Characterization of differential ATAC-sequencing peaks. *A) Upper bar plots percentage of close and open ATAC-sequencing peaks distributed on the indicated genomic annotation. Lower bar plot: percentage of close and open ATAC-sequencing peaks distributed at 0-1kb,1-3kb,3-5kb,5-10kb,10-100kb,>100kb distance to the TSS of the nearest gene. B) Percentage of intersecting HPTMs signals with close and open ATAC-sequencing peaks.*

To understand if genes differentially expressed upon PML silencing have a different state of chromatin accessibility we overlapped RNA-sequencing and ATAC-sequencing data. Specifically, we compared all differential ATAC-sequencing peaks (logFC<-/>1, FDR<0.05) with genes activated or repressed by PML (logFC<-/>0.3, FDR<0.05). Among genes activated by PML we found 445 genes containing a differential chromatin accessibility in absence of PML (figure 31A). By performing gene set enrichment analysis, we found that these genes cluster in tumour promoting pathways such as cell migration, metastasis, hypoxia and inflammation, which are in line with PML functions in this tumour context (Ponente *et al*, 2017, figure 31A). In addition, these include the genes that are more regulated by PML (logFC<-1), like *SPARC*, *TNC* and *CD276*. Instead, among genes repressed by PML we found 205 genes with a differential chromatin accessibility (figure 31A). Strikingly, we observed that these genes cluster in few functional categories, which contain few genes (figure 31B). Although these genes cluster in pathways involved in estrogen response, TGF-beta and hypoxia signalling pathways, most of them are involved in lysosome assembly (i.e. *TFEB* and *LMBRD1*) and include

several molecules involved in cell junction organization, like cadherins and claudins (i.e. CDH1 and CLDN4).

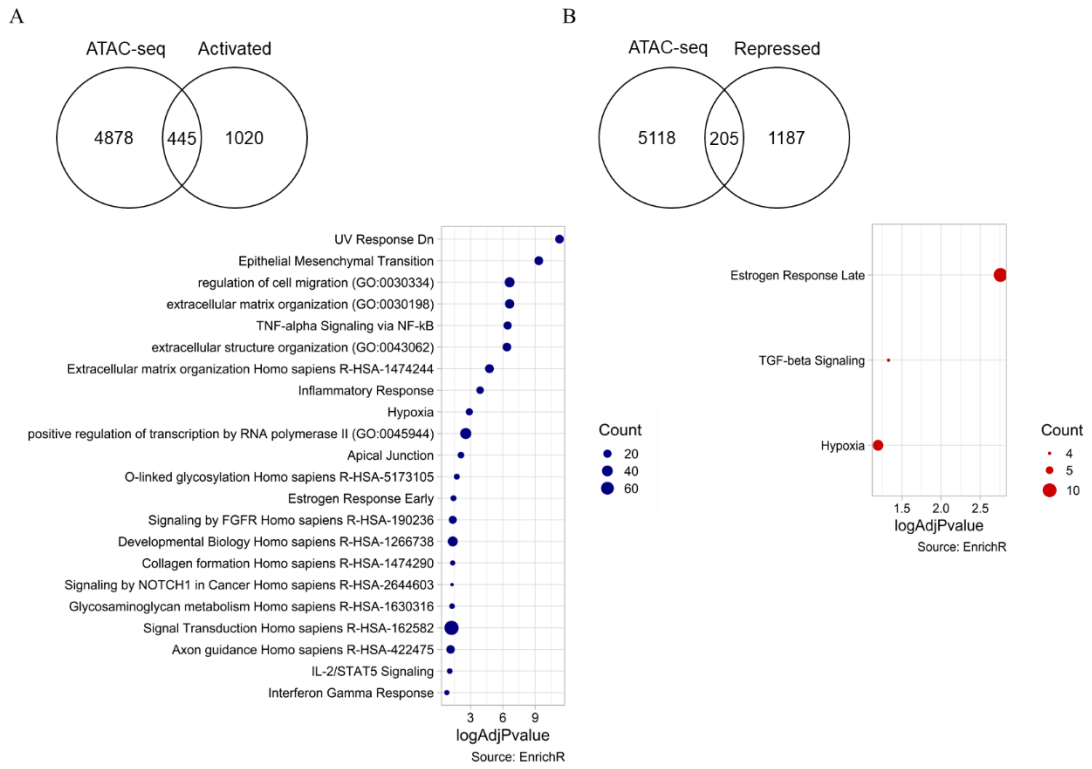

Figure 31. Gene set enrichment analysis of genes regulated by PML and containing differential ATAC-sequencing peaks upon PML silencing. *A) Upper panel: venn diagram showing the overlap of genes activated by PML (RNA-seq) and found in ATAC-sequencing peaks. Fisher's exact test, two-tailed P value equals is less than 0.0001. Lower panel: Genes activated PML overlapping with ATAC-sequencing peaks were analysed with EnrichR. B) Upper panel: venn diagram showing the overlap of genes repressed by PML (RNA-seq) and found in ATAC-sequencing peaks. Fisher's exact test, two-tailed P value equals is less than 0.0001. Lower panel: Genes activated PML overlapping with ATAC-sequencing peaks were analysed with EnrichR. Significant pathways were filtered for adjusted p value<0.1. Pathways are ordered according to their adjusted p-value (-log10AdjPvalue) and the size of the dots represents the number of genes falling in each pathway*

In line with the transcriptomic data, silencing of PML induces a decrease of chromatin accessibility in genes positively regulated by PML, involved in metastatic and tumor promoting pathways (i.e *SPARC* in figure 32A, upper panel). Conversely, genes negatively regulated by PML express an opening of chromatin structure (i.e *LMBRD1* in figure 32A, lower panel). However, in integrating ATAC-sequencing and RNA-sequencing data we realized that the opening or closing of chromatin as a result of PML silencing does not always correlate with increased or decreased expression of PML-

regulated genes. For instance, some genes activated by PML like *SERPINE1* (whose expression thus diminishes upon PML silencing) are marked by regions of open chromatin in absence of PML (figure 32B, upper panel). Conversely, genes repressed by PML, such as *RALGPS1*, show closing of chromatin in absence of PML (figure 32B, lower panel).

Therefore, these data indicate that there is some discordancy between PML transcriptional regulation and chromatin opening or closing.

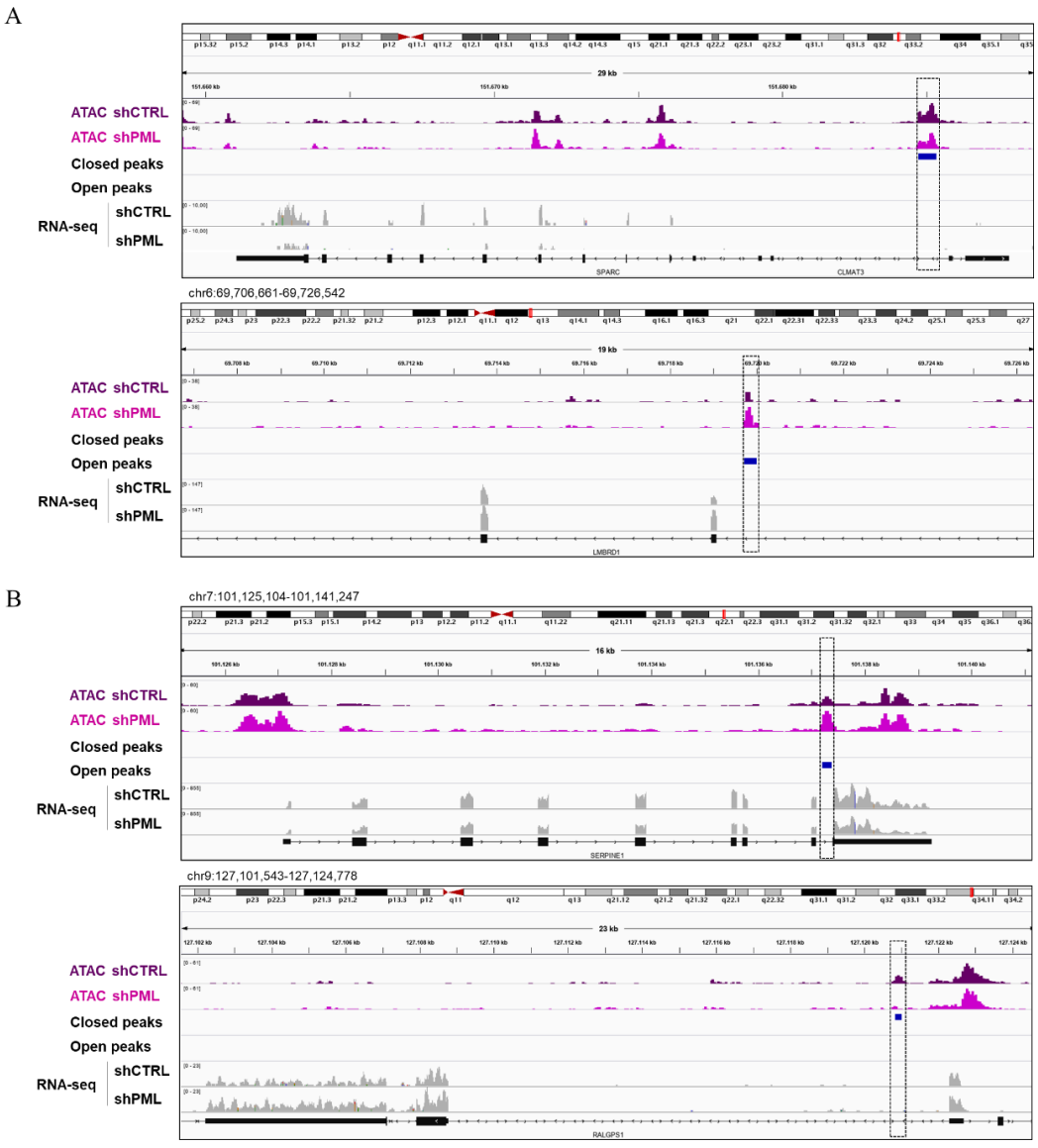

Figure 32. Alignment of ATAC-sequencing peaks and RNA-sequencing expression profiles. *Genome browser view of ATAC-sequencing peaks and RNA-sequencing expression data on the A) SPARC and LMBRD1 genes and on the B) SERPINE1 and RALGPS1 genes.*

Finally, to understand whether PML regulates chromatin accessibility via association to DNA, we compared the ATAC-sequencing and ChIP-sequencing data. We first looked at the overlap of genes falling in PADs and genes showing a differential chromatin accessibility in absence of PML (figure 33A, Veen diagram, blue). We found 382 genes common to both gene sets, enriched in functional categories belonging to the nervous systems and cell-cell adhesion pathways, which are among the few coding genes found in PADs (figure 33B). In addition, in line with the heterochromatic state of PADs, few of these genes are regulated by PML (figure 33A, Venn diagram). Nonetheless, ATAC peaks appear significantly depleted in PADs by permutation test (figure 33A, lower panel), suggesting that PML regulates chromatin accessibility in genomic regions outside PADs (figure 33C).

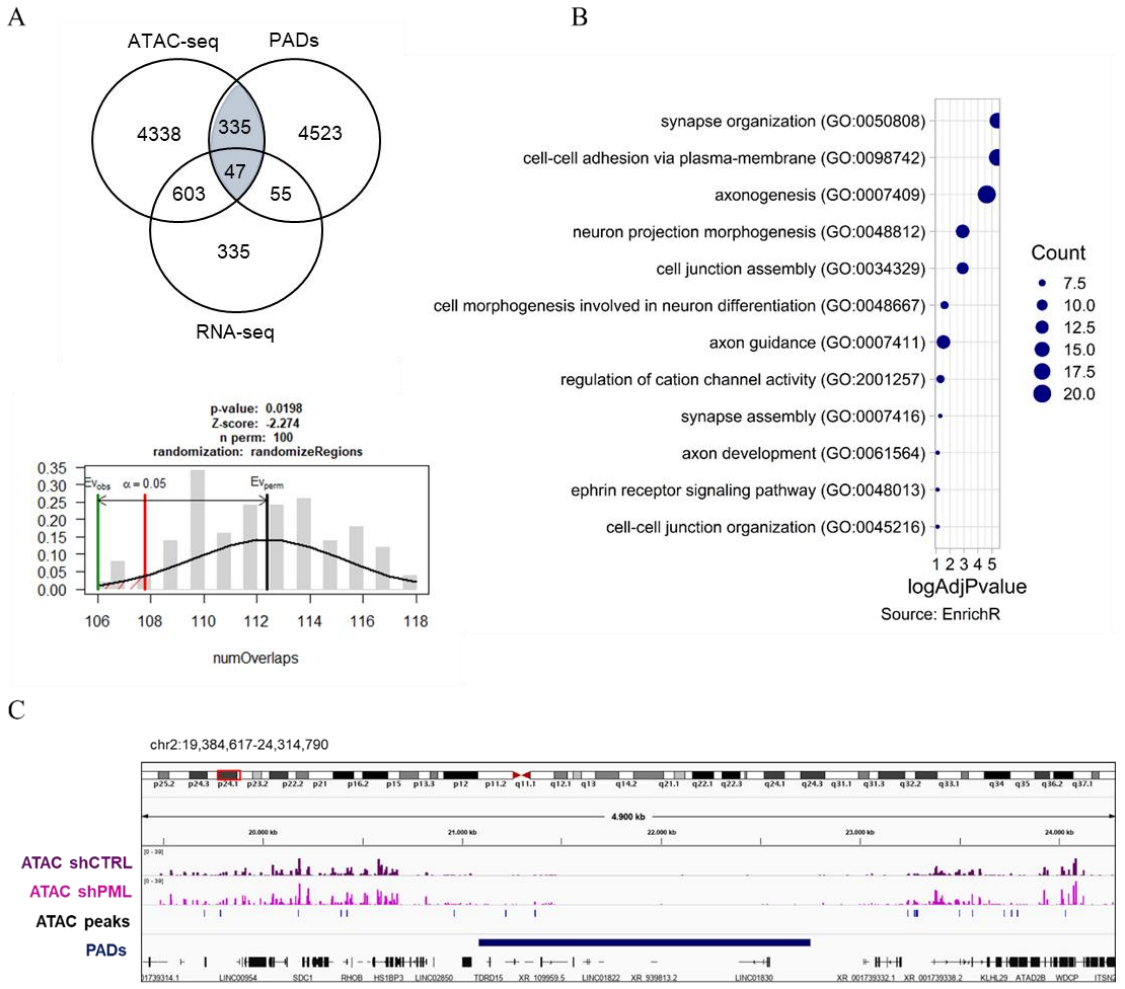

Figure 33. Overlap of ATAC-sequencing, ChIP-sequencing with PADs protocol and RNA-sequencing data. *A) Upper panel: venn diagram showing the overlap of genes regulated by PML (RNA-seq) and found in ATAC-sequencing peaks and PADs. Fisher's exact test, two-tailed P value*

equals 0.2744. Lower panel: results of the permutation test assessing the association between ATAC peaks and PADs (umber of. permutations=100 with p value=0.0198, Z-score=-2.274. B) Gene set enrichment analysis of genes overlapping with ATAC-sequencing peaks and PADs. Significant pathways were filtered for adjusted p value<0.1. Pathways are ordered according to their adjusted p-value (-log10AdjPvalue) and the size of the dots represents the number of genes falling in each pathway. C) Genome browser view of ATAC-sequencing peaks and representative PAD on chromosome 2.

We next overlapped the ATAC-sequencing data with genes bound by PML in library A (figure 34A, Venn diagram, orange). We found 407 genes bound by PML showing a change in chromatin accessibility, with this overlap being statistically significant (figure 34A). These genes fall in few functional categories, such as hypoxia and the TGF-beta signalling pathway (figure 34B). Accordingly, these pathways comprise SMAD2, which mediates the signal of the transforming growth factor TGF-beta, and several hypoxia inducible genes, like the N-myc downstream regulated gene 1 (*NDRG1*), the solute carrier family 6 member 6 (*SLC6A6*), and *ADORA2B*.

Interestingly, among the genes bound by PML and showing differential chromatin accessibility in absence of PML, 62 are also regulated (figure 34A, Veen diagram). These genes include *SMAD2* and *ADORA2B*, as well as *CD276* (figure 34C) and other pro-tumorigenic genes such as, the metastasis associated lung adenocarcinoma transcript 1 (*MALAT1*) and the metallopeptidase *ADAMTS15*, which are positively regulated by PML.

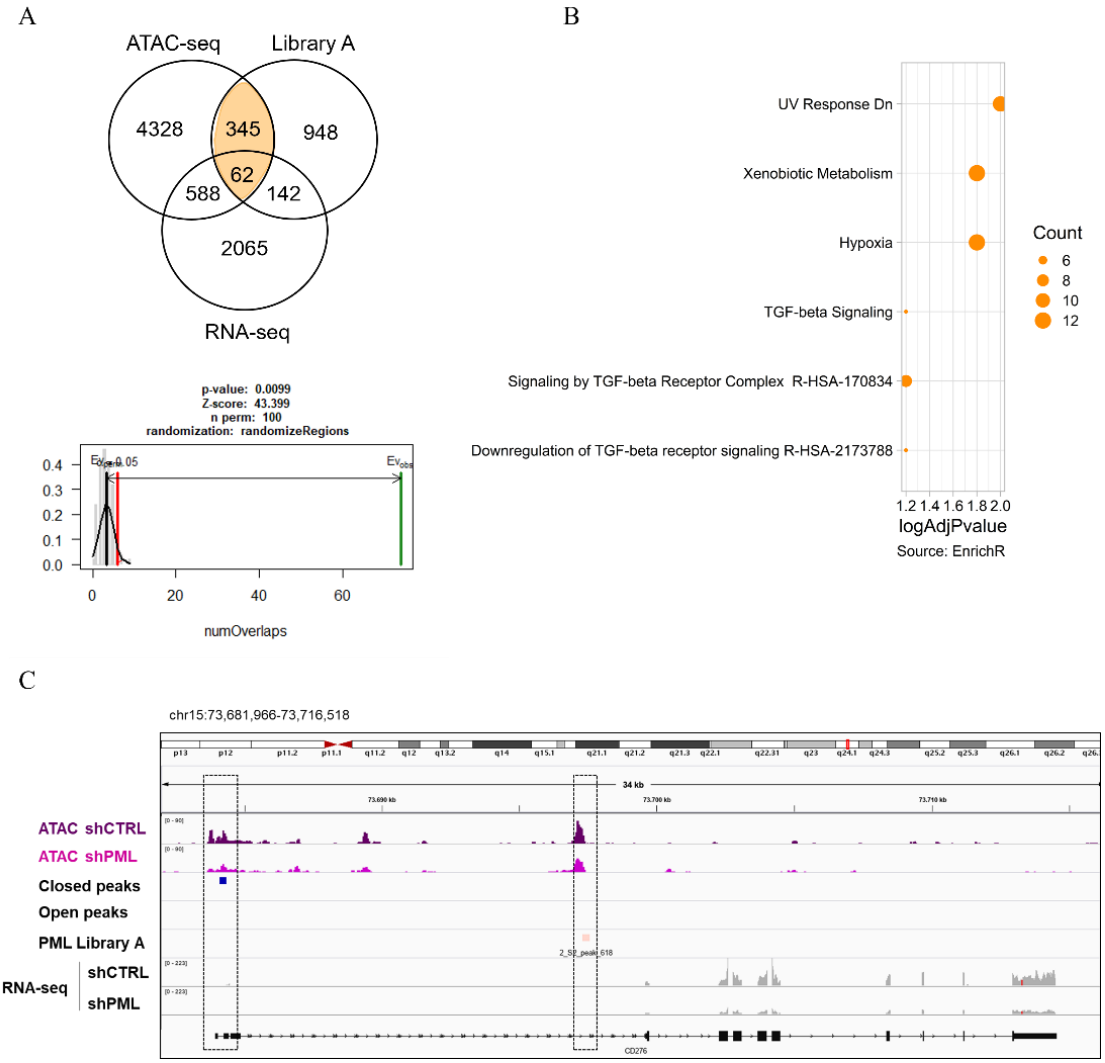

Figure 34. Overlap of ATAC-sequencing, ChIP-sequencing with narrow peaks protocol and RNA-sequencing data. *A) Upper panel: venn diagram showing the overlap of genes regulated by PML (RNA-seq) and found in ATAC-sequencing and library A peaks. Fisher's exact test, two-tailed P value is less than 0.0001. Lower panel: results of the permutation test assessing the association between ATAC-sequencing and library A peaks (number of permutations=100 with p value=0.0198, Z-score=-2.274. B) Gene set enrichment analysis of genes overlapping with ATAC-sequencing and library A peaks. Significant pathways were filtered for adjusted p value<0.1. Pathways are ordered according to their adjusted p-value (-log10AdjPvalue) and the size of the dots represents the number of genes falling in each pathway. C) Genome browser view of ATAC-sequencing peaks, RNA-sequencing expression and ChIP-seq data on the CD276 gene.*

In summary, ATAC-sequencing showed that silencing of PML induces global changes in chromatin accessibility, both at promoters and intergenic regions. Peaks corresponding to regions of changes in chromatin accessibility were found both on genes positively and negatively regulated by PML. However, only positively regulated genes with changes in

chromatin accessibility appear to cluster in significant functional categories belonging to pathways functionally regulated by PML in TNBC, such as cell migration and inflammation. In line with the transcriptomic data genes positively regulated by PML show a close chromatin state in absence of PML, whereas negatively regulated genes have a more open chromatin structure. However, ATAC-sequencing peaks in some instances show a discordant distribution when compared to transcriptomic data, with some positively regulated genes showing closure of chromatin and negatively regulated genes having a more open chromatin structure.

Also, by integrating ATAC-sequencing and ChIP-sequencing data, we found that changes in chromatin accessibility were significantly depleted inside PADs, while ATAC-sequencing peaks significantly overlap with library A PML-bound peaks. These peaks identify genes that cluster in few functional categories and contain few PML regulated genes, suggesting that PML mostly regulates the accessibility of chromatin indirectly and conversely, that PML association to DNA often does not result in changes in chromatin accessibility. Nonetheless, PML regulates gene expression and chromatin accessibility by directly binding to a small subset of genes involved in tumour promoting process. Among them the TGF-beta signalling pathway is known to be involved in breast cancer development and metastasis (Kang *et al*, 2003). Interestingly, cytoplasmic PML has been shown to regulate the activation of the TGF-beta signaling pathway promoting EMT and invasion in prostate cancer (Buczek *et al*, 2016). This and our data suggest that PML might promote cancer metastasis by regulating the TGF-beta pathways at multiple levels, via protein interactions and at the transcriptional level.

3.1.4 PML and the PML-NBs localize with markers of heterochromatin

By performing ChIP-sequencing on PML using a validated ChIP protocol used to identify repressive HPTMs we identified PML bound to large heterochromatic domains (PADs), while a milder chromatin extraction procedure allowed us to identify PML bound to discrete peaks, similar to those of TFs, localized within euchromatic regions. We hypothesized that because of their extension and the lower solubility of PML, PADs may represent large PML aggregates like the PML-NBs, while PML narrow peaks may represent PML moieties found in the nucleoplasm. To characterize the spatial association

between heterochromatin and the PML-NBs and PML proteins we performed colocalization studies via indirect immunofluorescence and proximity ligation assay (PLA) of PML and several heterochromatin marks. All experiments were performed in control and MDA-MB-231 cells where PML had been silenced as a negative control. As constitutive heterochromatin mark we choose H3K9me3, which is enriched inside PADs. LaminB1 (LMNB1) antibody was used to identify heterochromatin LADs (Briand & Collas, 2020), given the highly significant overlap of heterochromatic LADs with PADs in TNBC cells. Finally, H3K27me3 was used to detect facultative heterochromatin, which is found depleted inside PADs. By performing indirect immunofluorescence with specific antibodies, we found that on average 2 out of 5 PML-NBs in TNBC cells MDA-MB-231 are found in close proximity of all three markers (figure 35).

Of note, both markers of heterochromatin display a dotted distribution inside the nucleus and some accumulation at the nuclear membrane, while laminB1 is mostly concentrated at the nuclear membrane or in laminar structures that protrude inside the nucleus, as expected (Moir *et al*, 2000; Pascual-Reguant *et al*, 2018). Interestingly, as we were performing these experiments, we noticed that the nuclear distribution of H3K9me3 and LMNB1 changed qualitatively in cells where PML had been silenced, as described later in further detail.

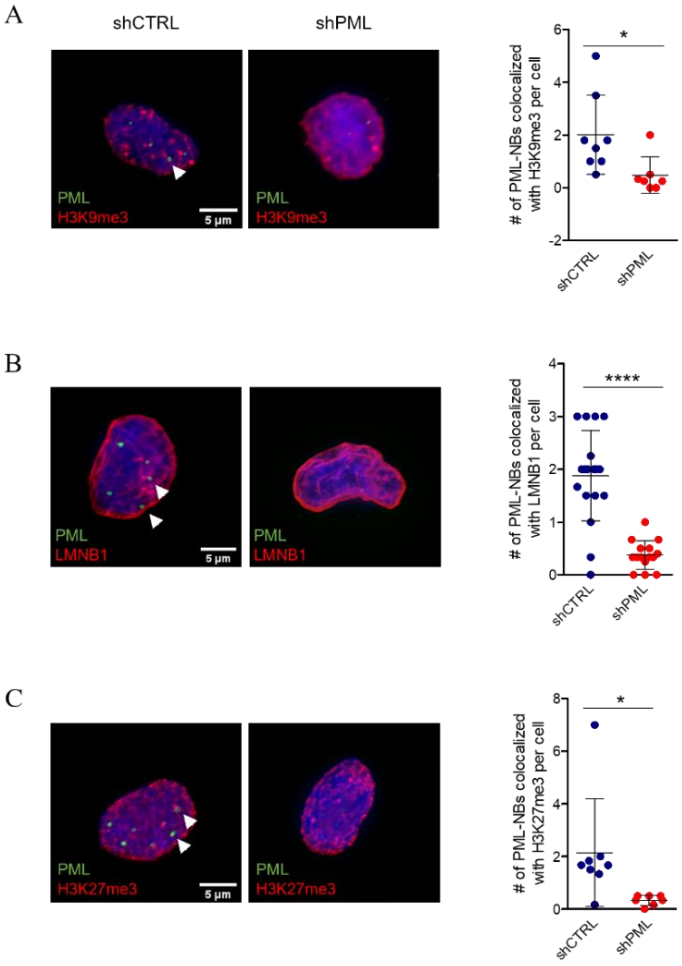

Figure 35. Coimmunofluorence of PML with H3K9me3, LMNB1 or H3K27me3. *Colocalization analysis between PML (green) and A) H3K9me3 B) LMNB1 C) H3K27me3 (red) in control (shCTRL) and PML-silenced (shPML) MDA-MB-231 cells. DNA was stained with DAPI (blue). Bar, 5 µm. Images shown are compressed z-stacks. Scattered plots represent the number of PML-NBs colocalizing with each marker in control (shCTRL) and PML-silenced (shPML) cells. Data represent mean values ± SD of at least three independent experiments. On average, a total of 40 nuclei/condition were analysed. Statistics was calculated with unpaired, two-tailed, Student t-test (*=p-value<0.05, **=p-value<0.01, ***=p-value<0.001, ****=p-value<0.0001).*

Immunofluorescence staining of PML allows a clear definition of the PML-NBs, big protein aggregates that contain many moieties of PML, but do not allow detection of free PML moieties in the nucleoplasm due to limiting signal resolution. For this reason, we also performed PLA to obtain a complete *in-situ* characterization of protein complexes between PML and H3K9me3, LMNB1 or H3K27me3 regardless of PML localization to the PML-NBs. Interestingly, PLA identified a higher number of PML interactions with H3K9me3 and LMNB1 compared to the immunofluorescence signals, with a mean value

of 15 and 20 dots of colocalization per nucleus, respectively (figure 36A, B; compared to figure 35A, B). Of note, many PML- LMNB1 PLA dots localized at the nuclear periphery (figure 36B). Conversely, fewer PLA dots were observed between PML and H3K27me3 (on average 0.3 dots per cell, figure 36C) with respect to their proximity measured by indirect immunofluorescence (figure 35C). The PLA dots were significantly decreased in control cells where PML had been silenced, but not abolished. This is in line with PML silencing abating PML expression of about 0.3-0.5 folds and demonstrate the specificity of these interactions.

Taken together, these data indicated that PML has a high number of interactions with H3K9me3 and LMNB1, but these interactions occur predominantly outside the PML-NBs, where they presumably involve soluble PML moieties in the nucleoplasm.

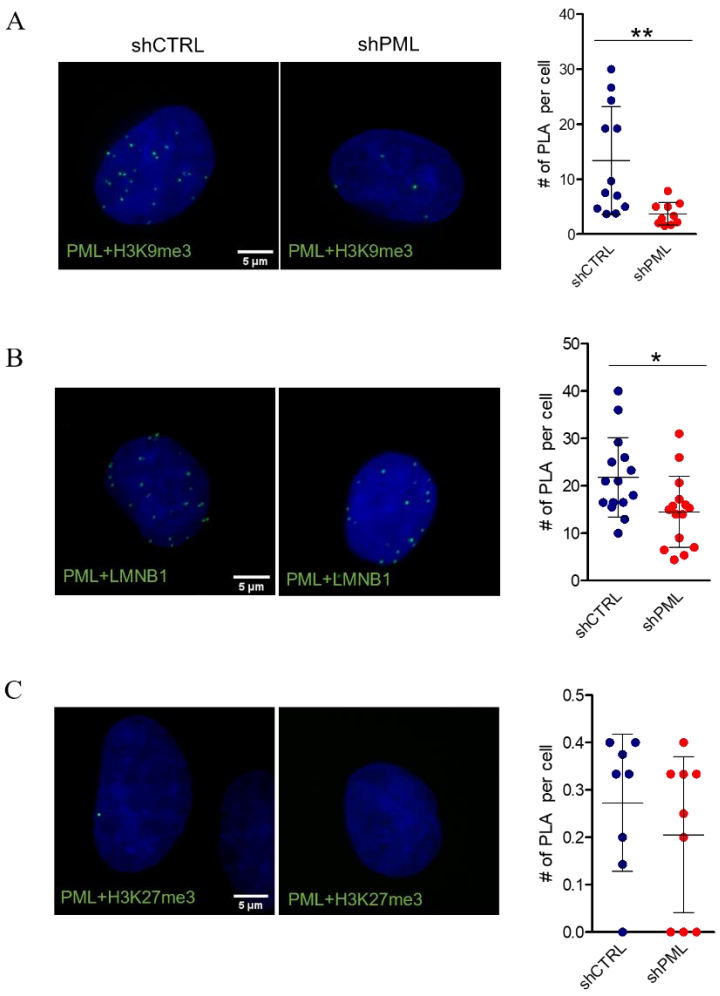

Figure 36. PLA between PML and H3K9me3, H3K27me3 or LMNB1. *PLA analysis between PML and A) H3K9me3 B) LMNB1 C) H3K27me3 in control (shCTRL) and PML-silenced (shPML) MDA-MB-231 cells. DNA was stained with DAPI (blue). Bar, 5 µm. Images shown are*

compressed z-stacks. Scattered plots represent the number of PLA dots per cell in control (shCTRL) and PML-silenced (shPML) MDA-MB-231 cells. Data represent mean values ± SD of at least three independent experiments. On average, a total of 40 nuclei/condition were analysed. Statistics was calculated with unpaired, two-tailed, Student t-test (=p-value<0.05, **=p-value<0.01).*

To further characterize the spatial relation among the complexes that PML forms with H3K9me3 and LMNB1 and the PML-NBs we combined PLA with PML immunofluorescence. Colocalization analysis confirmed that PML and H3K9me3 complexes are mostly found outside the PML-NBs, with cells showing an average of 1 dot of proximal localization per nuclei (figure 37A). Similar results were obtained on the association of PML and LMNB1, as on average only 1 out of 20 PLA dots is found in proximity to a PML-NB (figure 37B).

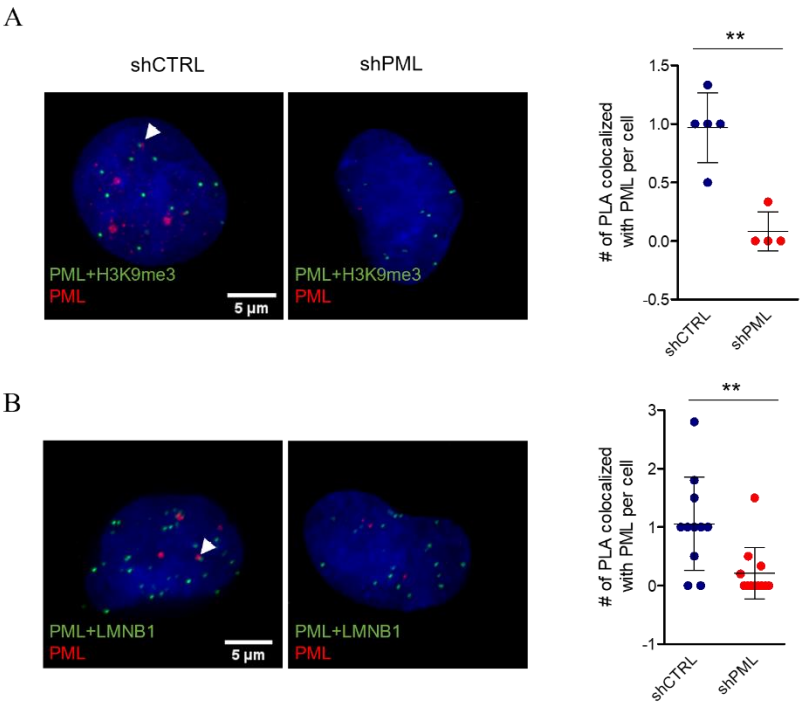

Figure 37. Colocalization of PML/H3k9me3 and PML/LMNB1 complexes and the PML-NBs. *Combined immunofluorescence against PML (red) and PLA (green). between PML and A) H3K9me3 or B) LMNB1 in control (shCTRL) and PML silenced (shPML) MDA-MB-231 cells. DNA stained with DAPI (blue). Bar, 5 µm. Images shown are compressed z-stacks. Scattered plots represent the number of PLA dots colocalizing with the PML-NBs per cell. Data represent mean values ± SD of at least two independent experiments. On average, a total of 30 nuclei/condition were analysed. Statistic was calculated with unpaired, two-tailed, Student t-test (**=p-value<0.01).*

Next, because PML-LMNB1 PLA complexes appeared to accumulate in proximity of the nuclear membrane (figure 36B), and because LADs significantly overlap with PADs, we performed PLA of PML and H3K9me3 or LMNB1 along with LMNB1 immunofluorescence. While on average 2 dots of PML and H3K9me3 PLA complexes localized in proximity of LMNB1 (figure 38A), comparably to their proximity to the PML-NBs, on average half of the PML and LMNB1 complexes highly colocalized with LMNB1 (figure 38B), thus further demonstrating that there PML associates more significantly to LMNB1and to a lesser extent to H3K9me3.

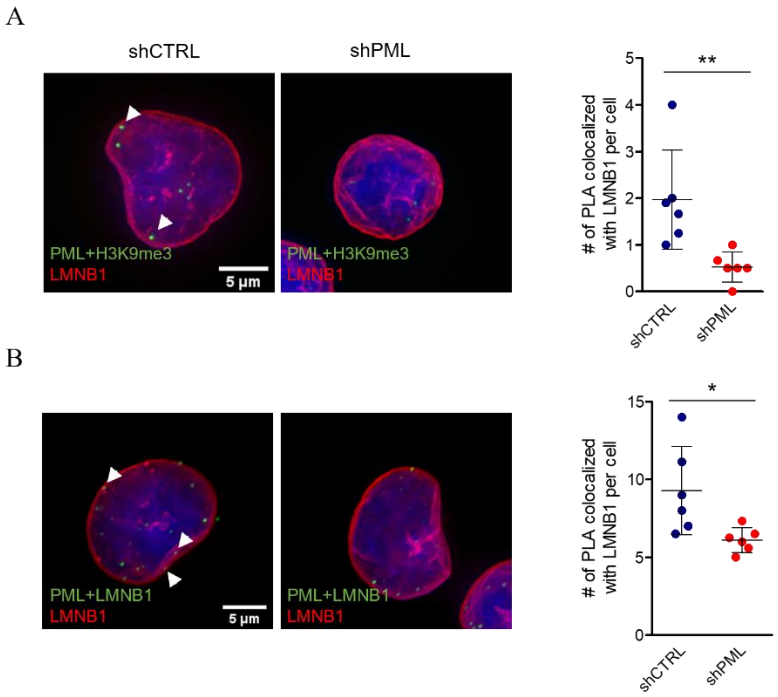

Figure 38. Colocalization of PML/H3K9me3 and PML/LMNB1 PLA complexes and LMNB1. *Combined LMNB1 immunofluorescence (red) and PLA (green) between PML and A) H3K9me3 or B) LMNB1 in control (shCTRL) and PML-silenced (shPML) MDA-MB-231 cells. DNA was stained with DAPI (blue). Bar, 5 µm. Images shown are compressed z-stacks. Scattered plots represent the number of PLA dots colocalizing with LMNB1 per cell. Data represent mean values ± SD of at least two independent experiments. On average, a total of 30 nuclei/condition were analysed. Statistics was calculated with unpaired, two-tailed, Student t-test (*=p-value<0.05, **=p-value<0.01).*

Taken together, these colocalization experiments demonstrate that PML interacts with the histone mark of constitutive heterochromatic H3K9me3 and, more pronouncedly, with the organizer of heterochromatic regions LMNB1 but not with the histone mark of facultative heterochromatin H3K27me3. Intriguingly, these interactions occur outside of

the PML-NBs and thus presumably involve soluble PML moieties within the nucleoplasm and at the nuclear periphery.

3.1.4.1 The association of PML and PML-NBs with constitutive heterochromatin is cell cycle-dependent

As discussed in the introduction, the structural integrity of the PML-NBs is linked to chromatin organization. This intimate relation is particularly evident during cell cycle progression, which is accompanied by changes in chromatin structure and in the morphology and number of PML-NBs. In particular, during DNA replication the PML-NBs disassemble by fission mechanisms into numerous micro-bodies spread throughout chromatin fibres (Dellaire *et al*, 2006). Interestingly, during S-phase PML has been shown to regulate H3.3 and H3K9me3 deposition to an exogenous transgene array suggesting that its localization to chromatin may promotes the assembly of heterochromatin domains (Shastrula *et al*, 2019). Since we observed that PML associates with H3K9me3 and LMNB1 mostly in a non-NB bound form we wondered whether these associations may be temporally regulated during the cell cycle. To this aim, we synchronized MDA-MB-231 cells with nocodazole, an anti-mitotic agent able to block cells in the G2/M phase. By performing FACS analysis at different times upon release from nocodazole we identified three time points that allowed us to enrich cells in the G1, S and G2 phases of the cell cycle (figure 39A, 8h, 20h, 24h). In line with published literature, we observed an increase in the number of PML-NBs after 20 and 24h from the release of nocodazole when compared to 8h, as representative of the S and G2 phases of the cell cycle (figure 39B). Hence, we performed PLA between PML and H3K9me3 or LMNB1 under these experimental conditions.

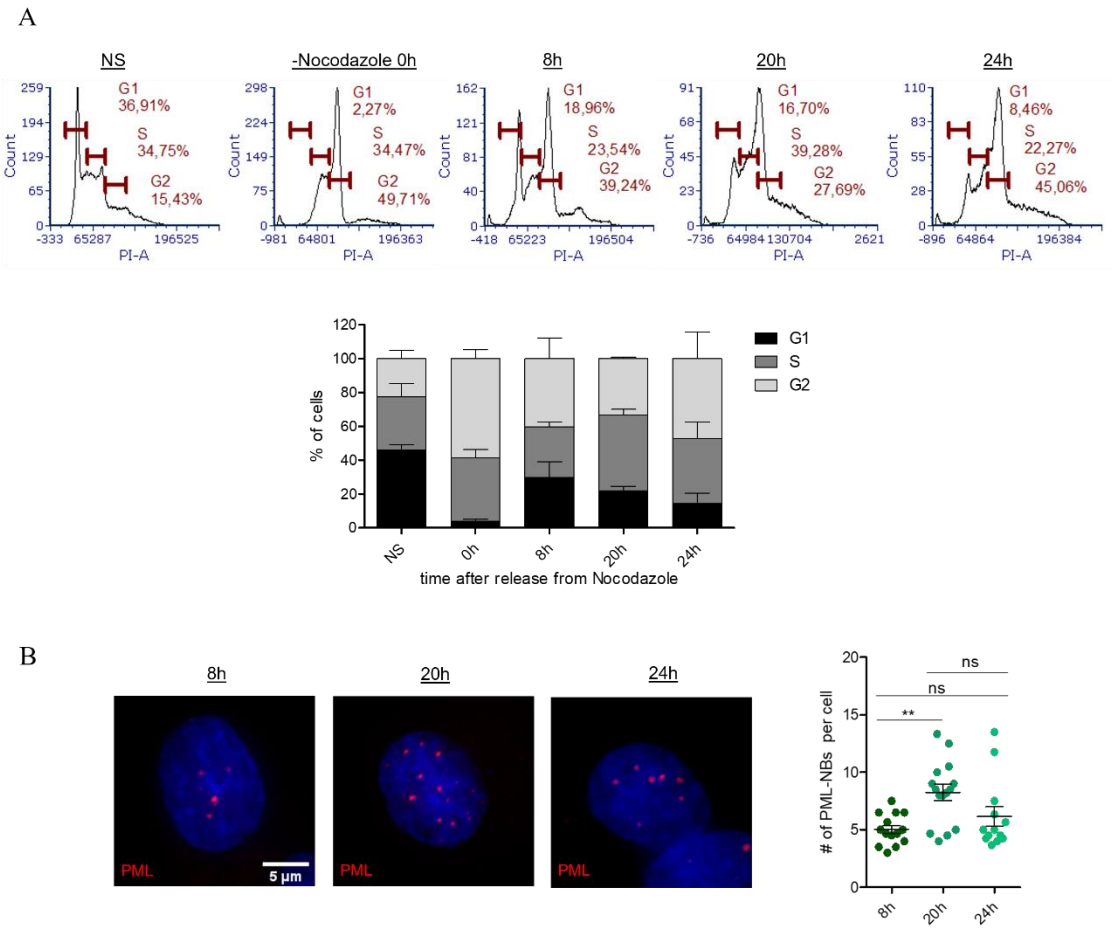

Figure 39. Cell cycle synchronization of MDA-MB-231 cells. *A) The upper panel shows the flow cytometry with PI staining for cell cycle analysis of control (NS) and synchronized cells at the indicated time point after release from nocodazole treatment (-Nocodazole, 0h.) The lower panel shows the bar plot with the % of cells in each phase of the cell cycle. B) On the left, immunofluorescent of PML (red) in synchronized cells at the time points indicated after release from nocodazole. DNA was stained with DAPI (blue). Bar, 5 µm. Images shown are compressed z-stacks. On the right, scattered plots representing the number of PML-NBs in the nucleus of cells at 8, 20, 24h after release from nocodazole. Data represent mean values ± SD of at least three independent experiments. On average, a total of 30 nuclei/condition were analysed. Statistics was calculated with One-way analysis of variance, Tukey's Multiple Comparison test (**=p-value<0.01).*

Upon release from cell cycle synchronization, we found a gradual increase in the number of PML-H3K9me3 complexes, reaching an average of 30 dots per cell 24h after nocodazole release (figure 40A). PML-LMNB1 complexes also increase during cell cycle progression but only 20h after nocodazole release, when cells express on average 25 dots per nuclei (figure 40B). These data indicate that PML associates dynamically with H3K9me3 and LMNB1 throughout the cell cycle, with a predominance of PML-LMNB1

associations in S phase, and PML-H3K9me3 complexes gradually accumulating through S and maximally in G2.

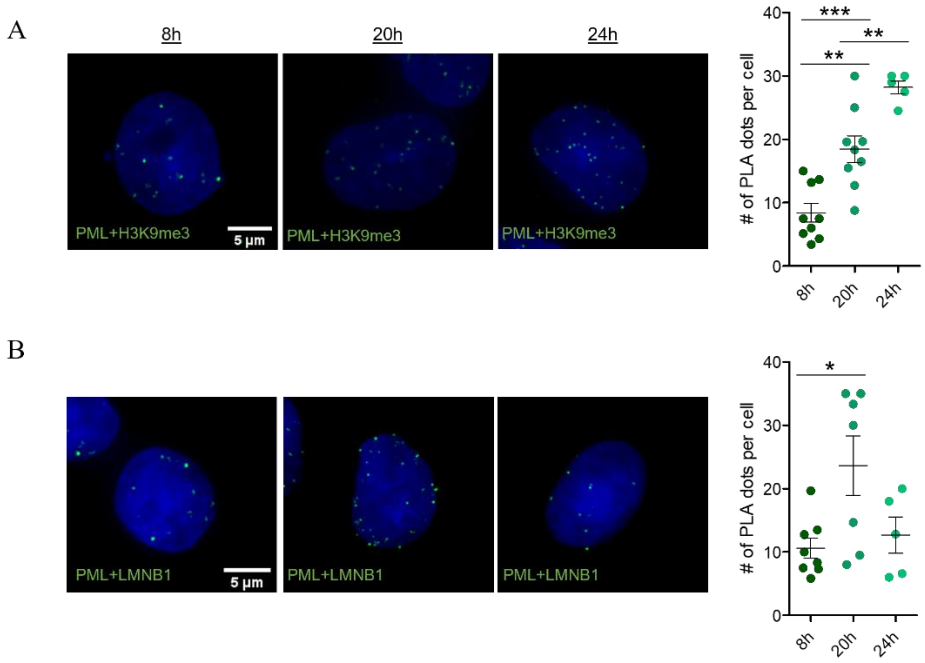

Figure 40. PLA between PML and H3K9me3 or LMNB1 in synchronized cells. *PLA analysis between PML and A) H3K9me3 or B) LMNB1 in the nucleus in cells at 8, 20, 24h after release from nocodazole. DNA was stained with DAPI (blue). Bar, 5 µm. Images shown are compressed z-stacks. Scattered plots represent the number of PLA dots per cell at 8, 20, 24h after release from nocodazole. Data represent mean values ± SD of at least two independent experiments. On average, a total of 30 nuclei/condition were analysed. Statistic was calculated with One-way analysis of variance, Tukey's Multiple Comparison test (*=p-value<0.05, **=p-value<0.01, ***=p-value<0.001).*

Because in unsynchronized cells we found that most of PML-H3K9me3 and PML-LMNB1 complexes localize outside of the PML-NBs, we analysed the association of PML complexes with PML-NBs throughout the cell cycle. By combining PLA and immunofluorescence we found increased colocalization between PML-H3K9me3 and PML-LMNB1 complexes and the PML-NBs (figure 41A, B), but this occurred at time points where PLA signals significantly increased (S phase for LMNB1 and G2 phase for H3K9me3) and the number of PML-NBs doubled (S phase). Because the increase in colocalizing dots is about double of that occurring in unsynchronized cells, this may be caused by the general increase in PLA signals and PML-NBs.

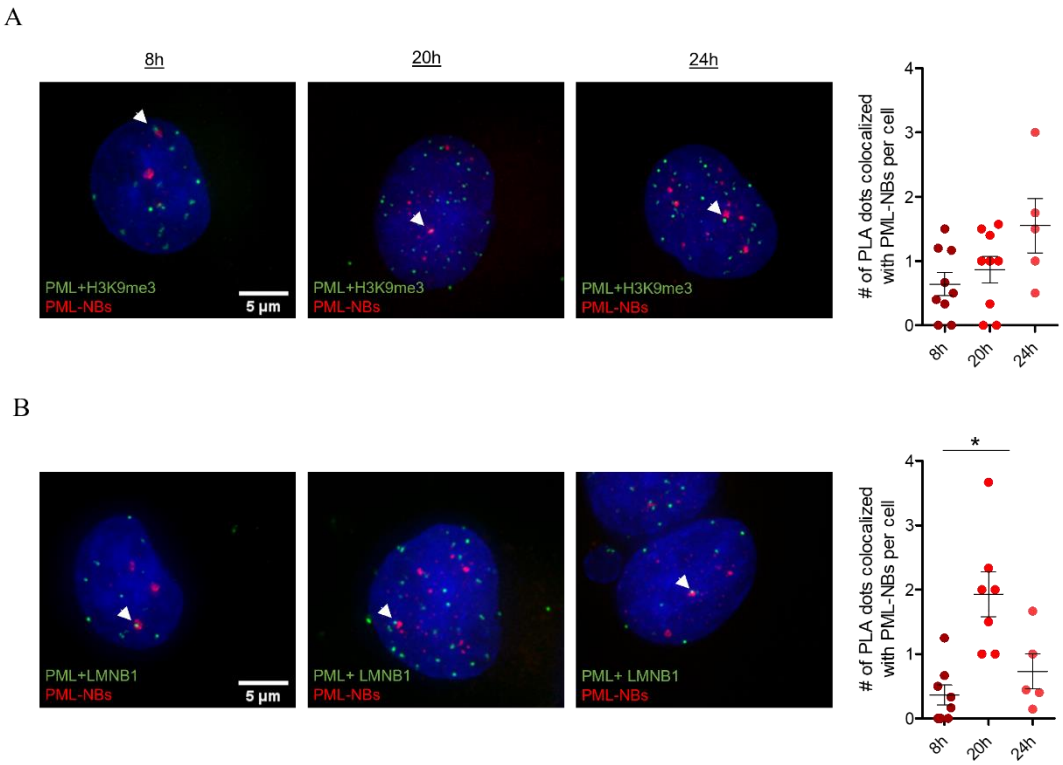

Figure 41. Colocalization of PML-H3k9me3 and PML-LMNB1 complexes with the PML-NBs. *Combined immunofluorescence against PML (red) and PLA (green) between PML and A) H3K9me3 or B) LMNB1 in synchronized cells at 8, 20, 24h after release from nocodazole. DNA was stained with DAPI (blue). Bar, 5 µm. Images shown are compressed z-stacks. Scattered plots represent the number of PLA dots colocalizing with the PML-NBs per cell at 8, 20, 24h after release from nocodazole. Data represent mean values ± SD of at least two independent experiments. On average, a total of 30 nuclei/condition were analysed. Statistics was calculated with One-way analysis of variance, Tukey's Multiple Comparison test (*=p-value<0.05).*

In sum, our data shows that PML binds heterochromatin in a cell cycle dependent manner and that PML-H3K9me3 and PML-LMNB1 represent two different protein complexes, which are differentially distributed and temporally regulated in the nuclear space. In addition, like in unsynchronized cells, both PML-H3K9me3 and PML-LMNB1 complexes localize outside the PML-NBs, thus confirming that PML associates with heterochromatin mostly in its free conformation. These data also raise the possibility that the PML-NBs do not represent PML binding to PADs. However, this hypothesis needs to be addressed with specific colocalization studies between PML and DNA-FISH probes designed within and outside PADs (in progress). In this respect, during the S phase we found an increase also in the colocalization of the PML-NBs with H3K9me3 (figure 42). These interactions involve both spatial proximities between H3K9me3 foci and large

PML-NBs or colocalization with smaller PML aggregates (figure 42). The heterogeneity of such associations may represent an indirect or casual interaction occurring between the PML-NBs and H3K9me3 due to the increased number of PML-NBs during S phase. However, we cannot exclude that PML binds heterochromatin in two different conformations, as nucleoplasmic PML moieties that accumulate in G2, and as small PML-NBs enriched in S phase.

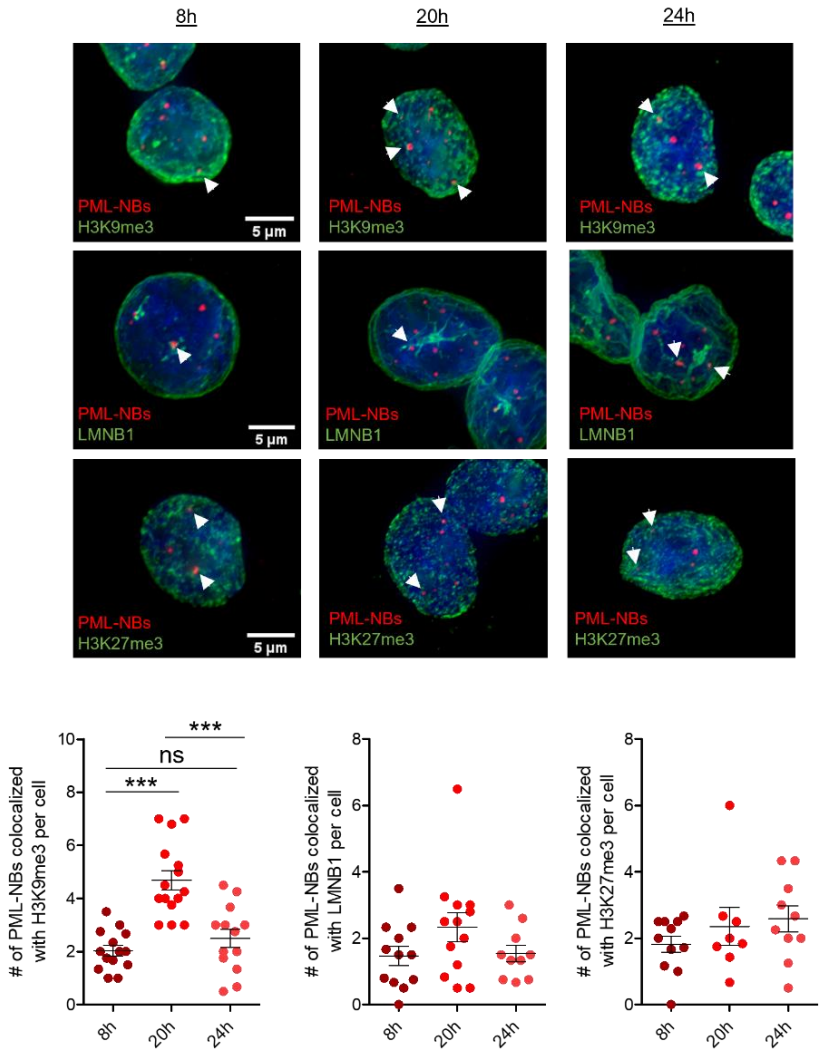

Figure 42. Immunofluorescence of PML and H3K9me3, LMNB1and H3K27me3. *Colocalization analysis between PML (red) and A) H3K9me3 B) LMNB1 C) H3K27me3 (green) in synchronized cells at 8, 20, 24h after release from nocodazole. DNA was stained with DAPI (blue). Bar, 5 µm. Images shown are compressed z-stacks. Scattered plots represent the number of PML-NBs colocalizing with each protein per cell at 8, 20, 24h after release from nocodazole. Data represent mean values ± SD of at least three independent experiments. On average, a total of 40 nuclei/condition were analysed. Statistics was calculated with One-way analysis of variance, Tukey's Multiple Comparison test (*=p-value<0.05, **=p-value<0.01, ***=p-value<0.001).*

3.1.4.2 Silencing of PML induces changes in the nuclear distribution of constitutive heterochromatin regions

Interestingly, as mentioned above, while we were performing colocalization experiments we detected a change in the nuclear distribution of H3K9me3 and LMNB1 in cells silenced for PML. More specifically, in control cells H3K9me3 distributes both at the nuclear periphery and inside the nucleus, where it forms well defined domains (or foci, figure 43A, B). However, by plotting the average signal intensity of H3K9me3 along a defined line across the nucleus, we observed that cells silenced for PML show a more dispersed H3K9me3 signal in the nucleus when compared to control cells (figure 43A, right line plot). In addition, by measuring the surface intensities of each pixel in cell nuclei, we found that in control cells H3K9me3 display a well-defined signal with peaks of intensity scattered throughout the nucleus and at the periphery (figure 43B, left), while upon silencing of PML H3K9me3 foci appear less defined (figure 43B, right). Consistently, quantitative analysis of H3K9me3 foci per nucleus shows a decrease in the number of H3K9me3 foci in absence of PML (figure 43C).

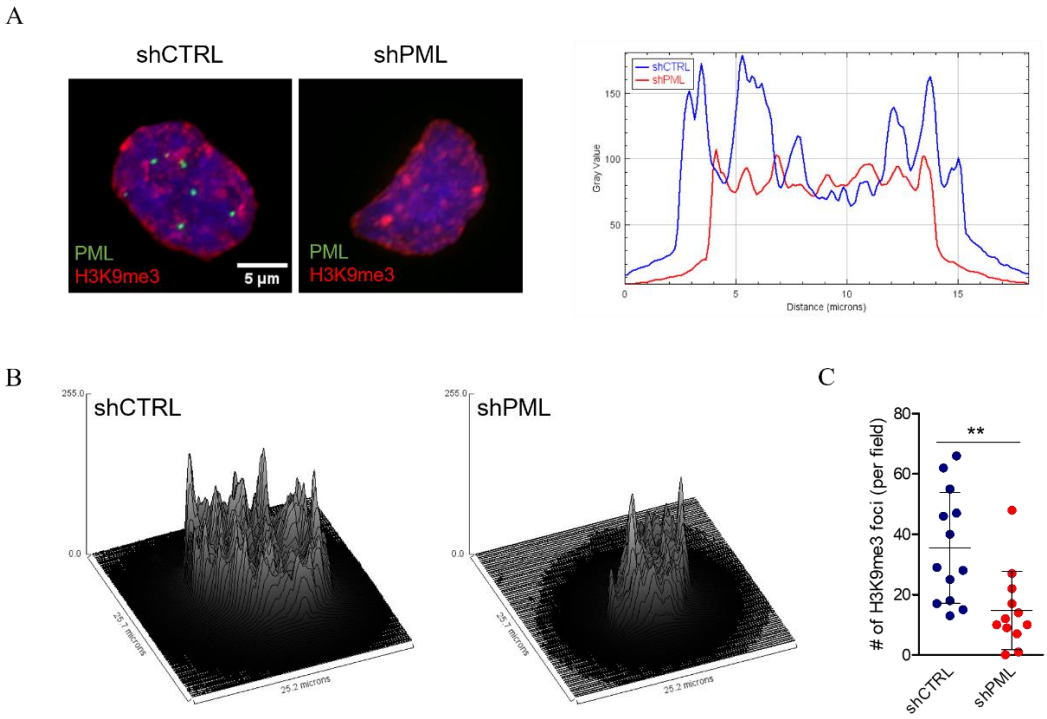

Figure 43. Nuclear distribution of H3K9me3 upon PML silencing. *A) Immunofluorescence of PML (green) and H3K9me3 (red) in control (shCTRL) and PML-silenced (shPML) MDA-MB-231 cells. DNA was stained with DAPI (blue). Bar, 5 µm (left panel). Images shown are compressed z-stacks. Line plot profile of H3K9me3 signal in control (shCTRL, blue) and cells*

*silenced for PML (shPML, red, right panel). B) Surface plot of H3K9me3 signal in control (shCTRL, left) and cells silenced for PML (shPML, right). C) Scattered plots representing the number of H3K9me3 foci present in the nucleus of control (shCTRL) and PML-silenced (shPML) cells. Data represent mean values ± SD of at least three independent experiments. On average, a total of 40 nuclei/condition were analysed. Statistics was calculated with unpaired, two-tailed, Student t-test (**=p-value<0.01).*

In the case of LMNB1, the nuclear delocalization appears even more dramatic in the absence of PML. Although LMNB1 mostly localizes at the nuclear periphery, control cells also show LMNB1 staining as lamellae protruding towards the internal space of the nucleus (figure 44A), which is in line with previous evidence showing LMNB1 localization within the nucleus (Moir *et al*, 2000; Pascual-Reguant *et al*, 2018). In cells silenced for PML we observed a reduction in the inner nuclear distribution of LMNB1 and an increase in its signal at the nuclear periphery (figure 44A). This is particularly evident in the surface plots, which display different LMNB1 nuclear topologies in control and PML-silenced cells and demonstrate that upon PML silencing LMNB1 is almost uniquely localized at the nuclear periphery (figure 44B).

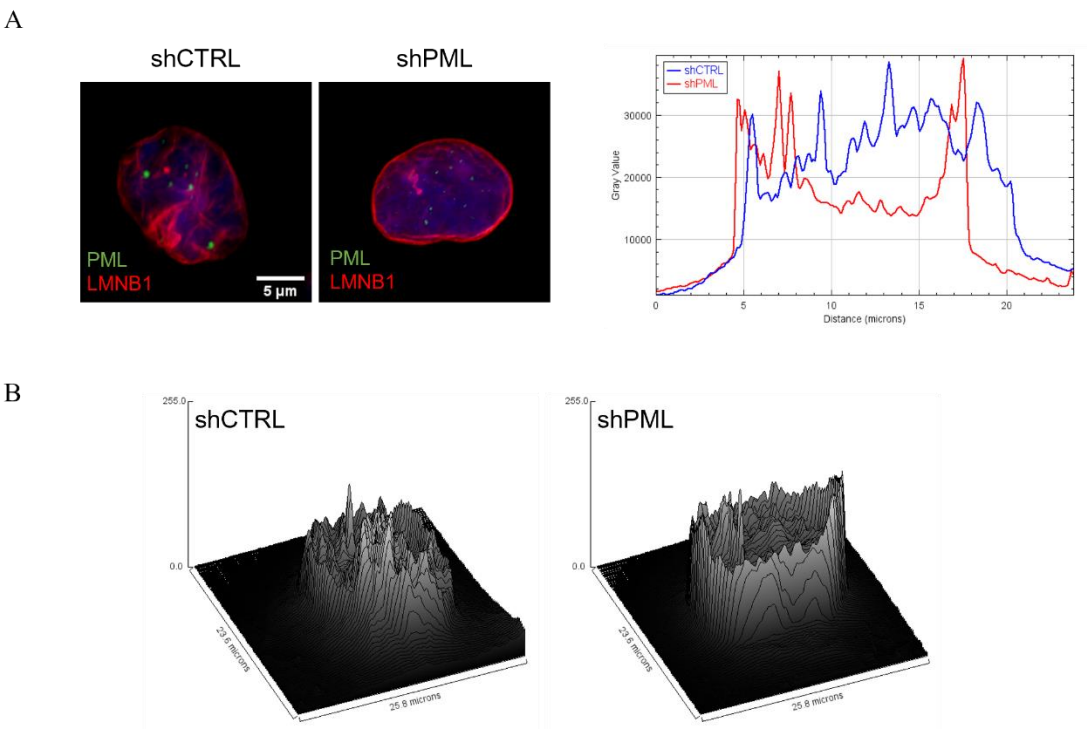

Figure 44. Nuclear distribution of LMNB1 in cell silenced for PML. *A) Immunofluorescence of PML (green) and LMNB1(red) in control (shCTRL) and PML-silenced (shPML) MDA-MB-231 cells. DNA was stained with DAPI (blue). Bar, 5 µm (left panel). Images shown are compressed z-stacks. Line plot profile of LMNB1 signal in control (shCTRL, blue) and cells silenced for PML*

(shPML, red, right panel). B) Surface plot of LMNB1 signal in control (shCTRL, left) and cells silenced for PML (shPML, right).

Because the different nuclear distribution of H3K9me3 and LMNB1 upon PML silencing may be influenced by their relative abundance, we analysed H3K9me3 and LMNB1 total protein levels. To visualize histone proteins and efficiently solubilize the nuclear lamina, proteins were extracted in RIPA buffer followed by a mild sonication. Interestingly, by western blot analysis we observed that silencing of PML induces a slight downregulation of H3K9me3, suggesting that the decrease in the number of H3K9me3 nuclear foci may be influenced by the reduced protein levels. On the contrary, in absence of PML, LMNB1 is upregulated at the protein level indicating that the reduced localization of LMNB1 at the nuclear interior is not caused by decreased LMNB1 levels (figure 45).

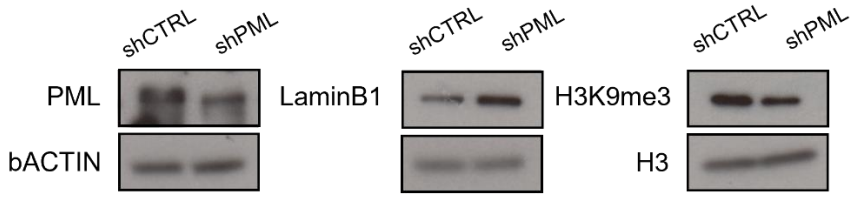

Figure 45. Protein levels of PML, LMNB1 and H3K9me3 upon PML silencing. *Western blot analysis on endogenous PML (left panel,) LMNB1 (middle panel) and H3K9me3 (right panel) in control (shCTRL) and cells silenced for PML (shPML). Beta-actin was used as loading control for PML and LMNB1 and total H3 was used to normalize H3K9me3.*

In summary, these data describe the spatial relation of PML, in its free or NB-bound conformation, to different marks of heterochromatin and the topological consequences of PML silencing on their nuclear distribution. By immunofluorescence we observed that few PML-NBs per nucleus are proximal to H3K9me3 and LMNB1, which mark regions of constitutive heterochromatin, and H3K27me3, present at facultative heterochromatin. However, proximity ligation assays revealed a higher number of interactions among PML and H3K9me3 and LMNB1, when compared to proximity of nuclear aggregates. On the contrary, we detected few interactions between PML and H3K27me3, which is in line with our genomic data showing depletion of H3K27me3 inside PADs. In addition, by performing proximity ligation studies coupled to immunofluorescence we found that PML-H3K9me3 complexes mostly localize in the nuclear space outside the PML-NBs. Similarly, PML-LMNB1 complexes show few colocalizations with the PML-NBs, but

concentrate at the nuclear lamina. These data suggests that PML interact with heterochromatin mostly in its soluble, non-NB-bound conformation and this may occur at distinct nuclear spaces. Finally, silencing of PML induces a decrease of H3K9me3 at the protein level and in the number H3K9me3 nuclear foci. Furthermore, in absence of PML, LMNB1 is upregulated and localize at the nuclear periphery. These data suggest that PML not only physically associates with heterochromatin regions, but it also regulates their nuclear distribution.

3.2 Aim 2. Characterize the functional interaction of PML and HIF1α in TNBC

3.2.1 Gene regulation by HIF1α in TNBC

Although highly heterogenous at the genetic level, TNBC display deregulation of few transcriptional networks, which include the HIF1α transcriptional program (Curtis, C., 2012). In breast cancer, HIF1α is overexpressed and correlates with advanced disease and poor clinical outcome, suggesting that it may regulate tumor promoting pathways (Gilkes & Semenza, 2013). Accordingly, several molecular studies have indicated that HIF1α promotes breast cancer metastasis by influencing at multiple level the metastatic cascade (Gilkes & Semenza, 2013). Along this works, our group has recently demonstrated that PML acts as an oncogene in TNBC, by promoting the expression of a specific subset of HIF1α metastatic target genes. In particular, we found that PML and HIF1α directly bind and induce the expression of these genes specifically in TNBC cells and not in other breast cancer cell lines, thus revealing cell type-specific transcriptional regulation by PML and HIF1α in the breast cancer context (Ponente *et al*, 2017).

To have a comprehensive view of all the possible functions exerted by HIF1α in TNBC, we characterized all the genes regulated by HIF1α in TNBC by evaluating the transcriptomic profile of MDA-MB-231 cells silenced for HIF1α *via* lentiviral shRNA (figure 46). As mentioned in the introduction, HIF1α is stabilized by several oxygen-independent mechanisms in TNBC and hypoxia metagenes are constitutively expressed in normoxic conditions (Lin *et al*, 2016, Briggs *et al*, 2016, Kim *et al*, 2021). For these reasons, we performed our experiments in cells cultured at 21% O_2. Silencing of HIF1α led to the deregulation of two sets of genes compared to control cells (shCTRL, figure 46A, red): downregulated genes, which are genes positively regulated by HIF1α, and upregulated genes, which are repressed in the presence of HIF1α. Overall, silencing of HIF1α resulted in significant deregulation of 849 genes (FDR 0.05, log2FC<-/>0.3, figure 46B) with a prevalence of activated genes compared to repressed (downregulated=323, upregulated=234, figure 46B), which is in line with HIF1α being mostly a transcriptional activator.

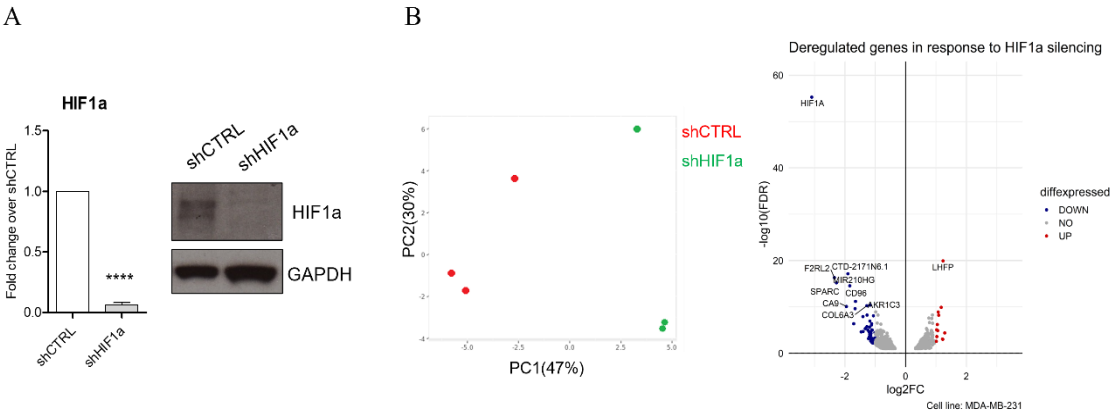

Figure 46. Transcriptomic analysis of MDA-MB-231 cells silenced for HIF1α. *A) qRT-PCR analysis (left) on HIF1α in control (shCTRL) and cells silenced for HIF1α (shHIF1α). Relative expression levels of HIF1α were compared to control cells (shCTRL). Data represent mean values ± SD of at least three independent experiments. Statistic was calculated with paired, two-tailed, Student t-test (****=p-value<0.0001). Western blot analysis (right) on endogenous HIF1α in control (shCTRL) and cells silenced for HIF1α (shHIF1α). GAPDH was used as loading control. B) PCA analysis of RNA-sequencing data showing clustering of control and HIF1α silenced samples. Red samples represent biological replicates of control samples (shCTRL), green samples represent biological replicates of HIF1α silenced samples (shHIF1α). B) Volcano plot of genes deregulated in response to HIF1α silencing. The x- and y-axis in the volcano plot represent log2(FC) and log10(FDR) values, respectively. Blue samples represent downregulated genes with log2FC<-1, whereas red samples represent upregulated genes with log2FC>1.*

We characterized genes activated and repressed by HIF1α by performing gene set enrichment analysis with the EnrichR webtool. Similar to PML transcriptomic data, we analysed all significant (FDR 0.05) DEGs resulting from HIF1α silencing with FC <-/> 0.3. In line with our previous findings (Ponente *et al*, 2017), we found HIF1α activated genes involved in extracellular matrix organization and EMT process (figure 47, blue). Among genes belonging to these pathways, we found known HIF1α target genes, such as *MMP9*, *LOX* and several *ADAMTS* protein family members, which have been involved in promoting breast cancer aggressiveness (Mehner *et al*, 2014; Saatci *et al*, 2020). Interestingly, these categories include also PML regulated genes like *TNC*, *SPARC* and *LOX*, supporting the functional interaction of PML and HIF1α in TNBC (Ponente *et al*, 2017). Along with known HIF1α pro-oncogenic functions, activated genes clusters included hypoxia, glycolysis and mTORC1 pathway (figure 47, green and red). These pathways contain know HIF1α target genes, such as Pyruvate dehydrogenase (*PDK1*), and several glycolytic enzymes. Moreover, we found the enrichment of a category of genes related to immune and inflammatory responses (figure 47, orange), including

inflammatory cytokines and their receptors (e.g., *IL1A*, *IL2RB*), several mediators of the IFNγ response (e.g., *JAK1*, *BATF2*) and complement factors (e.g., *C1S*, *CFH*). While genes activated by HIF1α functionally cluster in several gene families, repressed genes fall in only two functional categories: cholesterol homeostasis and p53 pathway. Moreover, few genes fall in these pathways and as consequence significance values are low (Adj.P.value =/>0.1). Nonetheless, these genes include the apoptosis inducing factor and DNA damage regulated autophagy modulator 1 (*DRAM1*), which partakes in p53-mediated autophagy and apoptosis, as well as the tumor protein P53 inducible nuclear protein 1 (*TP53INP1*) and the tumor protein P53 inducible protein 11 (*TP53I11*) involved in promoting and mediating p53 transcriptional functions. In addition, HIF1α repressed genes comprise few enzymes involved in cholesterol synthesis, such as the mevalonate kinase (*MVK*) and the phosphate cytidylyltransferase 2, ethanolamine (*PCYT2*). Interestingly, the same pathways are enriched among the gene families uniquely repressed by PML (figure 11), thus suggesting that HIF1α may cooperate with PML for their transcriptional inhibition.

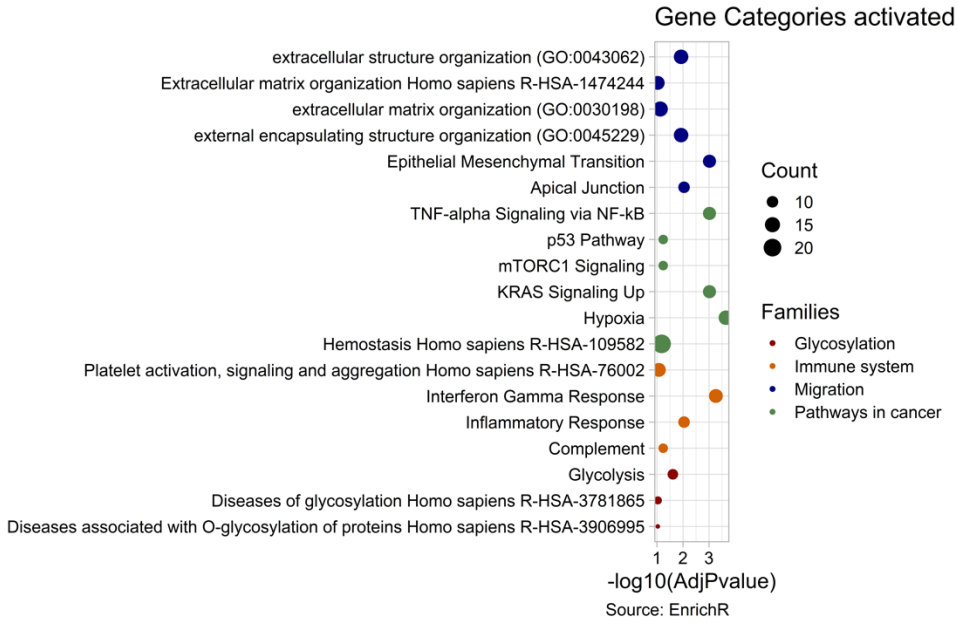

Figure 47. Gene set enrichment analysis of genes activated by HIF1α. *Genes activated by HIF1α (with log2FC<-0.3, FDR 0.05) were analysed with EnrichR. Significant pathways were filtered for adjusted p value<0.1 and clustered into functional families (blue, orange, red, green). Pathways are ordered according to their functional families and the size of the dots represents the number of HIF1α regulated genes falling in each pathway.*

These data suggest that in TNBC HIF1α mainly acts a transcriptional activator by promoting the expression of genes involved in tumour progression, metabolic pathways and immune regulation. In addition, suggest that it negatively regulate the activation of tumour suppressor pathways, especially those mediated by p53.

3.2.1.1 PML and HIF1α commonly regulate the expression of metastatic genes in TNBC

We previously demonstrated that PML and HIF1α commonly regulate the expression of a small set of metastatic genes that we had obtained by correlating the expression of bona fide HIF-target metagenes to PML expression in TNBC (Ponente *et al*, 2017). Because this analysis may have missed many genes, based on the tissue-specificity of HIF1α transcriptional regulation, we now aimed to identify all genes commonly regulated by PML and HIF1α in TNBC cells at the whole transcriptomic level. From the overlap of PML and HIF1α RNA-sequencing data we found a total of 249 genes commonly regulated (log2FC<-0.3/>0.3, FDR 0.05, figure 48A), 123 of which are activated and 104 repressed (figure. 49A). Interestingly, commonly regulated genes segregate into 4 clusters of high or low transcriptional regulation depending on their expression levels (or log2FC values) upon PML or HIF1α silencing. Although PML and HIF1α commonly activate and repress a comparable number of genes, PML activated genes show the highest degree of regulation in term of expression levels (figure 48B). Among these, we found *TNC*, *SPARC*, and *LOX*, which we previously showed to be PML regulated genes involved in promoting metastasis (figure 12). On the other hand, repressed genes appear to be equally regulated by PML and HIF1α, with the exception of a small group of genes highly repressed upon PML silencing (figure 48B). In this cluster falls the tumour protein p53 inducible protein 11 (*TP53I11*) and platelet-derived growth factors (*PDGFB*) gene.

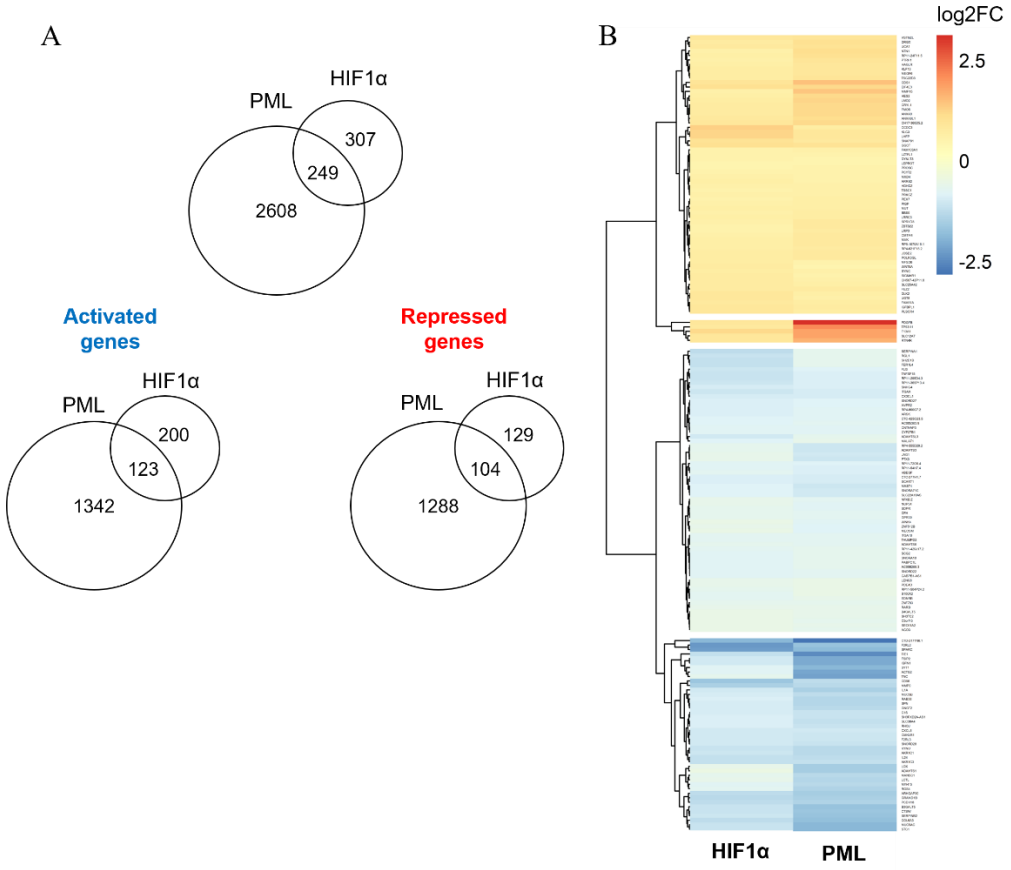

Figure 48. PML and HIF1α commonly regulate the expression of a subset of genes in TNBC. *A) Venn diagram showing the overlap of genes commonly deregulated in response to PML and HIF1α silencing. In both gene sets all deregulated genes with log2FC<-/>0.3 and FDR 0.05 were considered. Fisher's exact test, two-tailed P value is less than 0.0001 for both activated and repressed genes B) Heatmap of the log2FC values of genes commonly deregulated upon PML or HIF1α silencing in MDA-MB-231 cells.*

To characterize the gene categories enriched in genes commonly regulated by PML and HIF1α we performed gene set enrichment analysis on activated and repressed genes separately (log2FC<-0.3/>0.3, FDR 0.05, figure 48A). By this analysis we found that commonly activated genes were enriched in gene categories of metastasis, such as cell migration, extracellular matrix organization and EMT pathways, thus confirming our previous findings (Ponente *et al*, 2017) (figure 49, blue). In addition, we found enrichment of other HIF1α regulated pathways importantly involved in tumour progression, such as angiogenesis, inflammation and glycosylation (figure 49). On the contrary, commonly repressed genes do not fall in any significant functional category.

However, genes commonly repressed are involved in regulation of p53 related pathways (i.e., *DRAM1* and *TP53I11*), as well as in cholesterol synthesis (i.e. *MVK* and *PCYT2*).

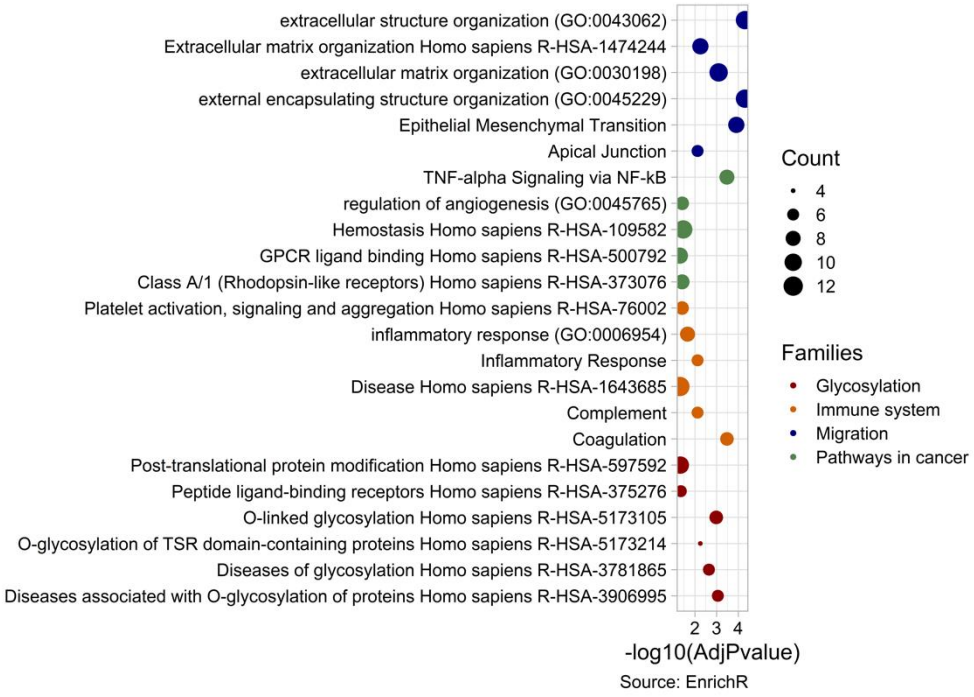

Figure 49. Gene set enrichment analysis of genes commonly activated by PML and HIF1α. *Genes commonly activated by PML and HIF1α (with log2FC<-0.3, FDR 0.05) were analysed with EnrichR. Significant pathways were filtered for adjusted p value<0.1 and clustered into functional families (blue, green, orange, red). Pathways are ordered according to their functional families and the size of the dots represents the number of HIF1α regulated genes falling in each pathway.*

To validate the transcriptomic data we performed qPCR analysis on cells independently silenced for PML and HIF1α. As important genes to validate, we selected *LOX*, *SPARC* and *TNC* which are involved in promoting metastasis and we have already shown to be regulated by PML. Consistently with the RNA-sequencing data, we confirmed that PML and HIF1α positively regulate the expression of these metastatic genes (figure 50).

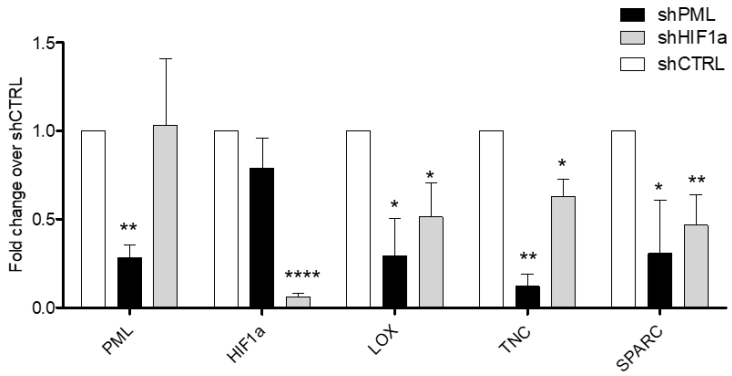

Figure 50. Validation of genes commonly regulated by PML and HIF1α in MDA-MB-231 cells. *qRT-PCR analysis on commonly activated genes involved in the metastatic process. Relative expression levels of each gene were compared to control cells (shCTRL). Data represent mean values ± SD of at least three independent experiments. Statistics was calculated with paired, two-tailed, Student t-test (*=p-value<0.05, **=p-value<0.01, ***=p-value<0.001, ****=p-value<0.001).*

Finally, to evaluate whether PML binds HIF1α-regulated genes, we overlapped library A PML ChIP-sequencing data with HIF1α RNA-sequencing data. With this analysis we found that PML associates to few HIF1α-regulated genes (24 activated genes and 15 repressed genes), which do not cluster in any functional categories. Nonetheless, genes bound by PML and activated by HIF1α include some hypoxia inducible genes, such as *NDRG1* and the lysine demethylase 3A (*KDM3A*), as well as genes bound and regulated by PML, like *MALAT1* and *SERPINB2*, involved in promoting metastasis in TNBC, suggesting that PML directly regulates transcription of this genes together with HIF1α. Instead, within HIF1α repressed genes we found PML bound to genes involved in different cellular process, such as the dimethylarginine dimethylaminohydrolase 1 (*DDAH1*), involved in the generation of nitric oxide, and the alpha and gamma adaptin binding protein (*AAGAB*), which promotes vesicle trafficking. Furthermore, among this genes we found *BLCAP*, which promotes apoptosis downstream p53 and is regulated by HIF1α, and few enzymes involved in cholesterol synthesis (i.e. *MVK* and *PCYT2*), which are regulated by both PML and HIF1α.

In conclusion, our data confirmed that PML and HIF1α commonly regulate the expression of metastatic genes in TNBC, as well as other tumour promoting pathways, like inflammation. In addition, we revealed a possible role of PML and HIF1α in inhibiting p53 signalling pathways and cholesterol synthesis. Interestingly, silencing of PML has a

greater effect on the expression level of coregulated genes, suggesting that PML may play an essential function in HIF1α mediated transcription. Nonetheless, most of the HIF1α-regulated genes co-regulated by PML are not bound by PML, indicating that PML mostly regulates HIF1α transcriptional activity indirectly, although few genes regulated by HIF1α are bound by PML and are in line with the tumour promoting and suppressive pathways regulated by HIF1α, such as migration and p53 signalling pathways.

3.2.2 PML and HIF1α localization in the nucleus of TNBC cells

To further elucidate the functional interaction of PML and HIF1α we analysed their nuclear localization in TNBC cells and luminal breast cancer cells as a control. Because HIF1α has a diffused nuclear staining in immunofluorescence, we applied PLA between PML and HIF1α to measure specific interactions. Few interaction foci were detected in the nuclei of MDA-MB-231 cells (figure 51). Therefore, to validate these results, we analysed another TNBC cell line, BT549 cells, and non-TNBC cells MCF7. PML and HIF1α interacting foci were higher in TNBC BT549 and MDA-MB-231 compared to non-TNBC cells MCF7. Specifically, we found that in MDA-MD-231 and BT549 cells PML and HIF1α colocalized in an average of 4 and 3 dots per nucleus (in 80% of cells), while in MCF7 cells PML and HIF1α colocalize in a minor fraction of foci (1 dots per nucleus in 60% of cells). Because both PML and HIF1α are expressed at lower levels in MCF7 cells (Ponente *et al*, 2017), these data suggest that albeit low in number the interaction foci detected in TNBC cells identify specific interactions between PML and HIF1α.

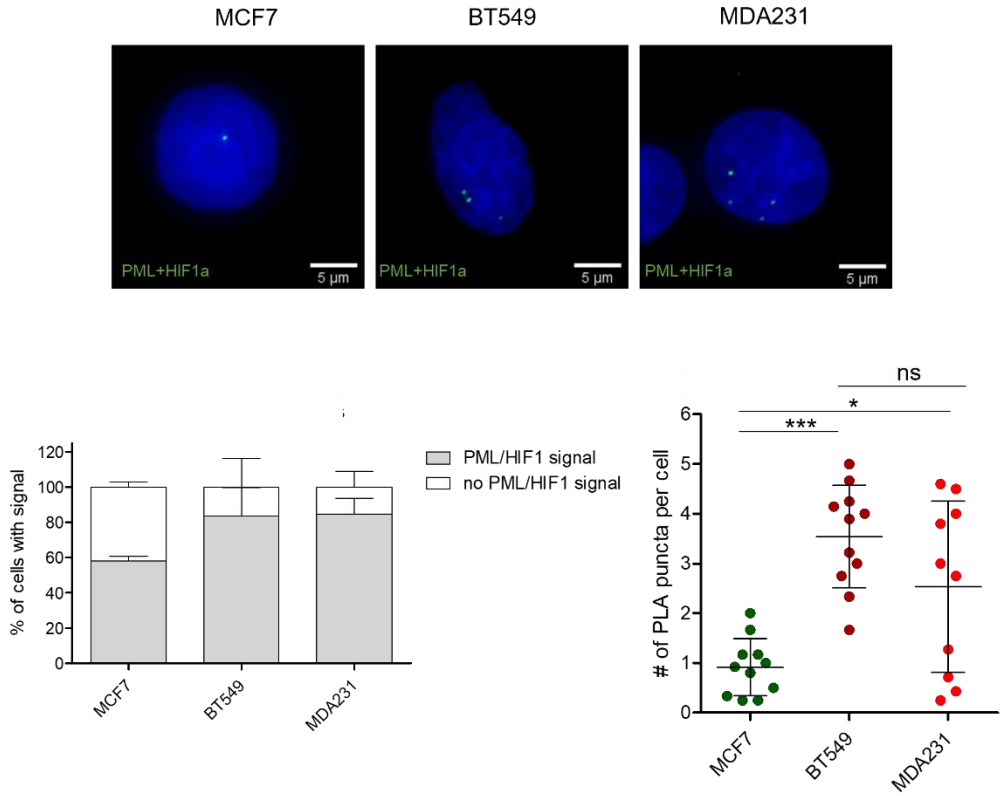

Figure 51. PLA between PML and HIF1α in breast cancer cell lines. *Upper panels show PLA (green) between PML and HIF1α in MCF7, BT549 and MDA-MB-231 cells. DNA was stained with DAPI (blue). Bar, 5 µm. Images shown are compressed z-stacks. Lower left bar plot indicates the percentage of cells positive to PML-HIF1α signals. Lower right scattered plot represents the number of PLA dots per cells. Data represent mean values ± SD of at least two independent experiments. On average, a total of 50 nuclei/condition were analysed. Statistics was calculated with One-way analysis of variance, Tukey's Multiple Comparison test (*=p-value<0.05, ***=p-value<0.001).*

Since the PML-NBs provide nuclear site for the storage and activation of several TFs, we tested the overlap of the PML-HIF1α complexes with the PML-NBs. Interestingly, we found that most PML and HIF1α complexes localize outside the PML-NBs both in non-TNBC and TNBC cells (figure 52). Specifically, 20% of the PML-NBs in MCF7 and 30% of the PML-NBs in BT549 and MDA-MB-231 cells colocalized with PML/HIF1α complexes. These data suggest that the association between the PML and HIF1α mostly occurs outside the PML-NBs. The colocalization with PML-NBs may represent a dynamic event, possibly associated to active transcription.

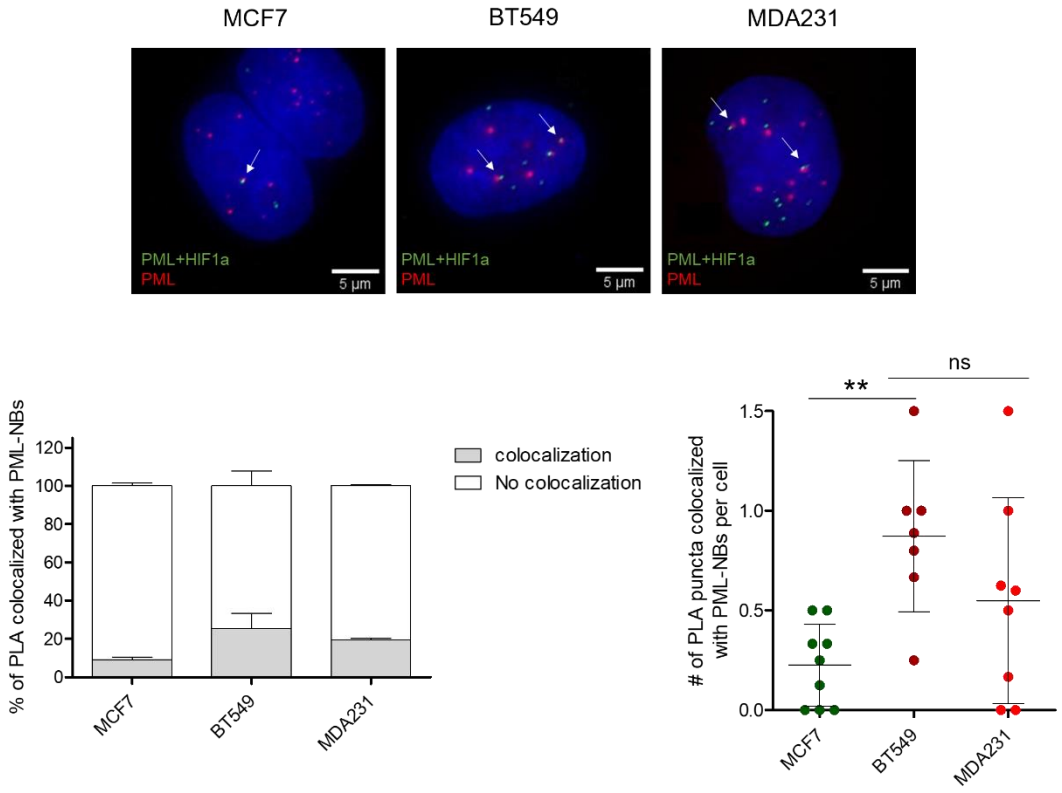

Figure 52. Colocalization of PML-HIF1α complexes and the PML-NBs. *Combined immunofluorescence against PML (red) and PLA (green) between PML and HIF1α in MCF7, BT549 and MDA-MB-231 cells. DNA was stained with DAPI (blue). Bar, 5 µm. Images shown are compressed z-stacks. Lower left bar plot indicates the percentage of PML-HIF1α signals colocalizing with the PML-NBs. Lower left scattered plots represent the number of PLA dots colocalizing with the PML-NBs per cells. Data represent mean values ± SD of at least three independent experiments. On average, a total of 50 nuclei/condition were analysed. Statistics was calculated with One-way analysis of variance, Tukey's Multiple Comparison test (**=p-value<0.01).*

3.2.2.1 PML and HIF1α are held together by active transcription.

Since we confirmed that PML and HIF1α commonly regulate the expression of metastatic genes in TNBC, we hypothesized that their interaction might be promoted by active transcription. Hence, to gain insights into the structural basis of PML and HIF1α interactions we decided to measure their colocalization upon transcription inhibition via Actinomycin D (AMD). This experiment however posed a problem, since the structural integrity of the PML-NBs is sustained by chromatin and inhibition of transcription, which promotes chromatin compaction, leads to the fission of PML-NBs into PML microbodies(Eskiw *et al*, 2004). For this reason, we performed a titration experiment with

decreasing AMD concentrations and selected the concentration of AMD that inhibits RNA Pol2 mediated transcription while maintaining PML-NBs numbers and size (figure 53).

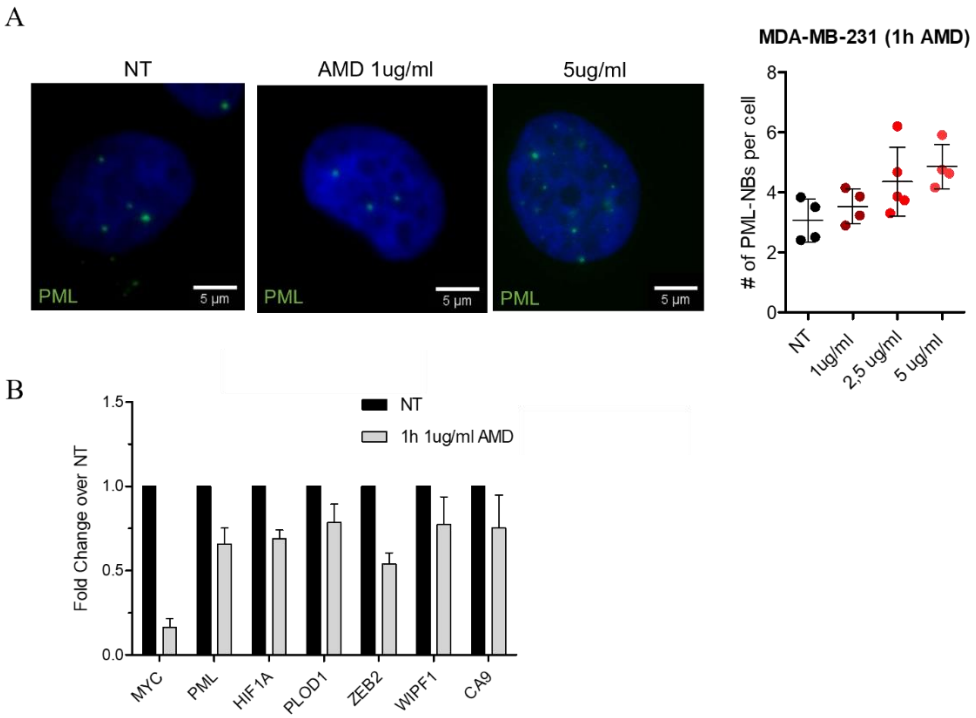

Figure 53. Transcription inhibition with AMD in MDA-MB-231 cells. *A) On the left, immunofluorescent of PML in control (NT) and AMD treated cells for 1h at the indicated concentrations. DNA was stained with DAPI (blue). Bar, 5 µm. Images shown are compressed z-stacks. On the right, scattered plots representing the number of PML-NBs in the nucleus of control (NT) and AMD treated. B) qRT-PCR analysis on PML, HIF1α and their co-regulated genes upon AMD treatment. Myc represents a positive control given the short half-life of its mRNA. Relative expression levels of each gene were compared to control cells (NT). Data represent mean values ± SD of at least two independent experiments.*

Under these experimental conditions we performed PLA between PML and HIF1α in MDA-MB231cells and found that the association between PML and HIF1α decreased upon transcriptional inhibition (figure 54). Specifically, while control cells showed an average of 2 dots per nucleus, upon AMD treatment most cells showed an average of 1 dot per nucleus (figure 54).

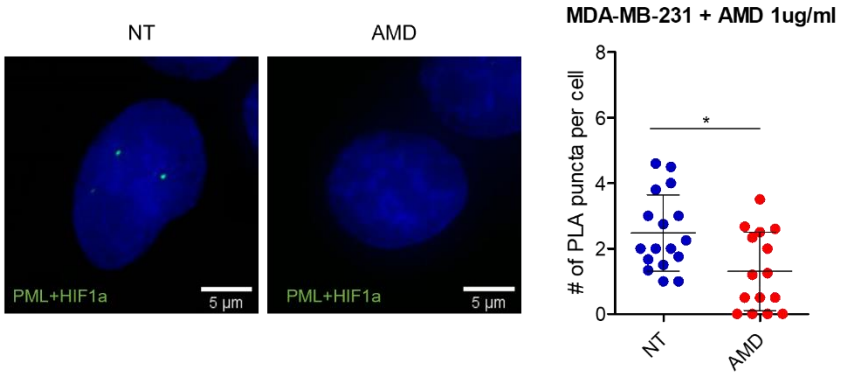

Figure 54. PLA between PML and HIF1α upon transcriptional inhibition. *On the left, PLA between PML and HIF1α in control (NT) and AMD treated cells. DNA was stained with DAPI (blue). Bar, 5 µm. Images shown are compressed z-stacks. On the right, scattered plot representing the number of PLA dots per cells. Data represent mean values ± SD of at least two independent experiments. A total of 50 nuclei/condition were analysed. Statistics was calculated with unpaired, two-tailed, Student t-test (*=p-value<0.05).*

Since our data suggest that PML and HIF1α associate during transcription, we tested the physical proximity between PML/HIF1α complexes and the phosphorylated form of RNA pol II (PS2), which represent foci of transcription initiation. By coupling PLA and immunofluorescence we observed that 30% of PML-HIF1α complexes colocalize with phospho-RNA pol II PS2 (on average 0.5 dots per cell) and that this colocalization decrease upon AMD treatment (figure 55).

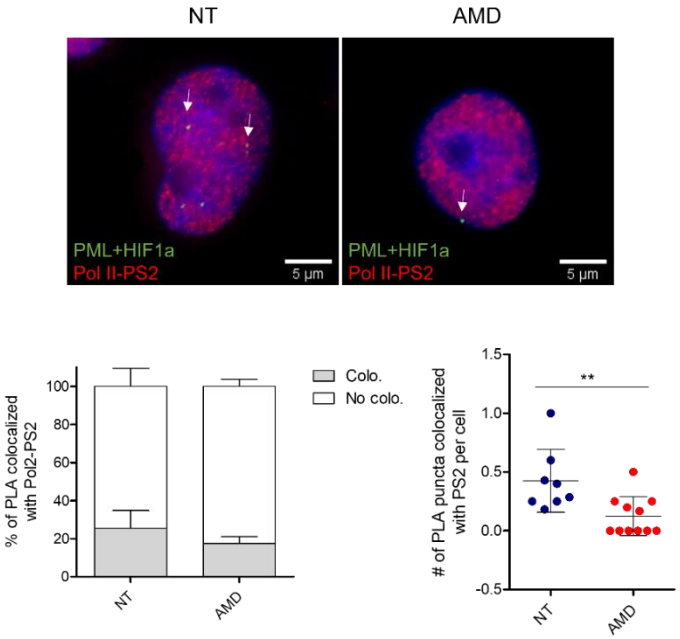

Figure 55. Colocalization of PML-HIF1α complexes and phospho-RNA pol II. *On the top, combined immunofluorescence against phospho-RNA pol II (red) and PLA (green) between PML and HIF1α in control (NT) and AMD treated cells. DNA was stained with DAPI (blue). Bar, 5 µm. Images shown are compressed z-stacks. Lower left bar plot indicates the percentage of PML-HIF1α signals colocalizing with phospho-RNA pol II. Lower right scatter plots represent the number of PLA dots colocalizing with phospho-RNA pol II per cells. Data represent mean values ± SD of at least three independent experiments. A total of 30 nuclei/condition were analysed. Statistics was calculated with unpaired, two-tailed, Student t-test (**=p-value<0.01).*

Overall, our data suggest that few, but specific PML-HIF1α complexes form in the nuclei of TNBC cells and are held together by active transcription. However, not all PML-HIF1α complexes localize with phosphorylated RNA pol2 (30% of colocalization), suggesting that this interaction may be highly dynamic. Interestingly, the same percentage of colocalization exists between PML-HIF1α complexes and phosphorylated RNA pol2 or the PML-NBs (30%). Thus, is tempting to speculate that the same PML-HIF1α complexes that colocalize with phospho-RNA pol II also associate with the PML-NBs, in a model in which PML-HIF1α complexes are dynamically formed in the nuclear space and then either coalesce into or induce nucleation of PML-NBs where transcriptional activity occurs.

To test this hypothesis, we plan to perform live imaging experiments with a PML-HIF1α-based bimolecular fluorescence complementation (BiFC) system and Halo-PML. To generate these tools, we fused PML and HIF1α to the N- and C- terminal portion of a YFP variant (Venus) respectively. Upon their expression in living cells, if an interaction occur between PML and HIF1α this will allow the reconstitution of the fluorescent protein and the formation of a stable complex that can be visualized by fluorescence microscopy. Since MDA-MB-231 cells are difficult to transfect, we set up our experimental conditions in BT549 cells. Also, given the tendency of PML to homo-multimerize and form large protein aggregates that may not be representative of PML physiological functions, to avoid biases of PML overexpression we titrated expression of the fusion protein VC155-PML to levels similar to PML expression in MDA-MB-231 cells (figure 56A). By transfecting VC155-PML at a very low concentration we were able express twice the amount of PML in MDA-MB-231 cells without affecting morphology of the PML-NBs (figure 56A). In the same way, we titrated HIF1α expression using decreasing vector concentrations, and compared expression of the fusion protein to $CoCl_2$-stabilized HIF1α

in MDA-MB-231, as the endogenous protein is not easily detected with current HIF1α antibodies. However, clear detection of HIF1α overexpression can be clearly detected only with the highest vector concentration (figure 56B). For this reason, we tested the complementation with PML of all three HIF1α concentrations.

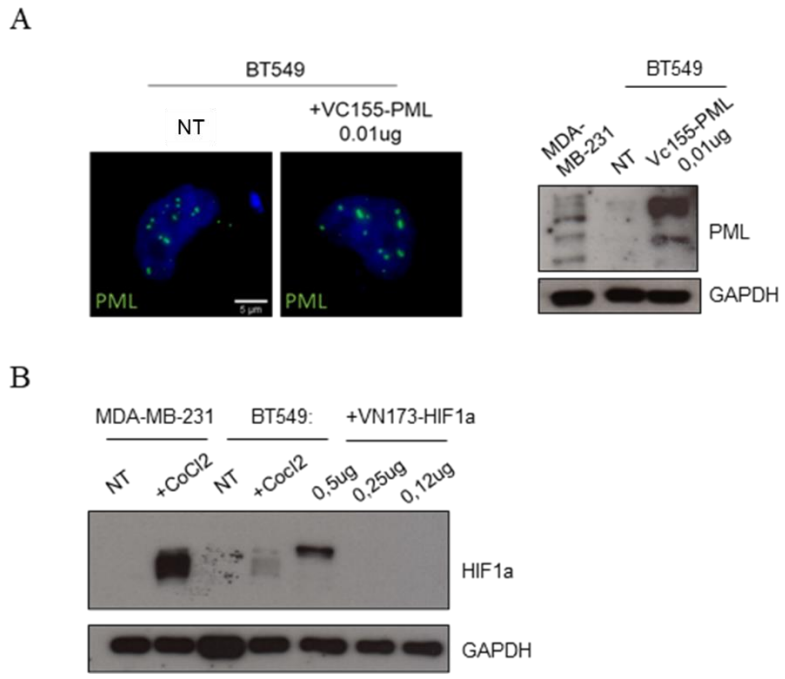

Figure 56. Expression of PML and HIF1α BiFc vectors in BT549 cells. *A) On the left, immunofluorescent of PML in control (NT) and cells transfected with 0.01µg of VC155-PML. DNA was stained with DAPI (blue). Bar, 5 µm. On the right, western blot analysis of endogenous PML in MDA-MB-231 cells, non-transfected BT549 cells and BT549 cells transfected with 0.01µg of VC155-PML. GAPDH was used as loading control. B) Western blot analysis of endogenous HIF1α in MDA-MB-231 and BT549 cells with or without cobalt chloride (CoCl2) and in BT549 cells transfected with 0.5, 0.25 and 0.12µg of VN173-HIF1α. GAPDH was used as loading control.*

We next looked at the degree of complementation among the fusion proteins on fixed cells by fluorescence microscopy. By expressing PML at a stable low concentration with decreasing HIF1α levels, we found in all conditions a higher number of complementation foci when compared to the number of PLA dots found in the same cell line (on average of 2.5 dots per cell). In addition, when decreasing HIF1α concentration, the complementation foci decrease in size rather than number (figure 57).

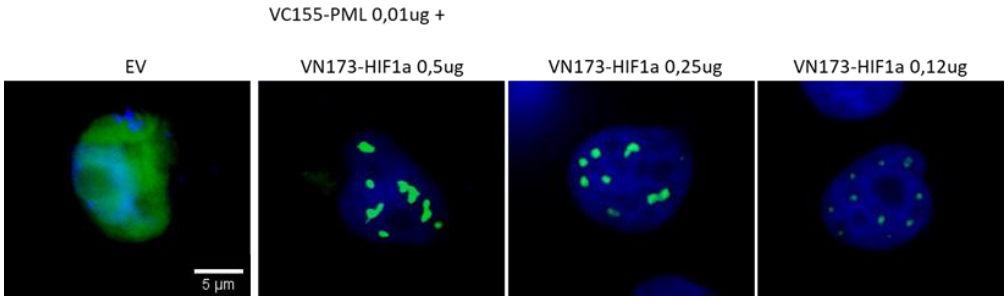

Figure 57. Direct visualization of PML-HIF1α complementation foci. *Fluorescent image of BT549 cells transfected with empty vectors (EV) and 0.01µg of VC155-PML together with decreasing concentrations of VN173-HIF1α (0.5, 0.25 and 0.12µg). DNA was stained with DAPI (blue). Bar, 5 µm. Images shown are compressed z-stacks.*

Interestingly, by combining the BiFC system with immunofluorescence we found that all PML-HIF1α complementation foci colocalized with all endogenous PML (figure 58). These data support a model in which the stabilization of PML-HIF1α complexes forces nucleation of PML-NBs or induces the coalescence of PML-HIF1α complexes in pre-existing PML-NBs.

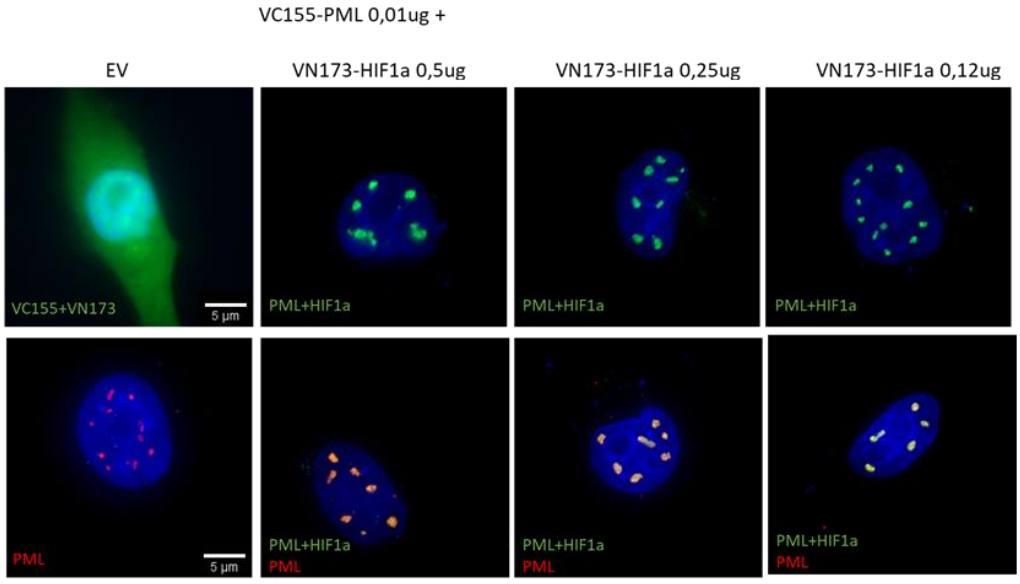

Figure 58. Colocalization of PML/HIF1α complementation foci and the PML-NBs. *Upper panels represent BT549 cells transfected with empty vectors (EV) and 0.01µg of VC155-PML together with decreasing concentrations of VN173-HIF1α (0.5, 0.25 and 0.12µg). Lower panels show immunofluorescence on endogenous PML (red) and the PML-HIF1α complementation foci (green). DNA was stained with DAPI (blue). Bar, 5 µm. Images shown are compressed z-stacks.*

Intriguingly, the PML-HIF1a complexes that formed upon medium or low HIF1a expression were transcriptionally active and able to induce upregulation of common PML and HIF1a target genes, while the expression of these genes was inhibited when HIF1a was highly expressed (figure 59). In this respect, it should be highlighted that at high concentration of HIF1a, the complementation foci appear as big protein aggregates (figure 58) which probably do not reflect the physiological interaction occurring between PML and HIF1α. Nonetheless, as our PML-HIF1a complementation system generates stable and active protein complexes, we are planning to use it in ChIP-qPCR experiments to validate the direct binding of PML and HIF1a on commonly regulated genes. Because the interaction between PML and HIF1α involves a minor fraction of these proteins, we will take advantage of the BiFC system to stabilize PML-HIF1a complexes and enrich their immunoprecipitation using anti-Venus antibody.

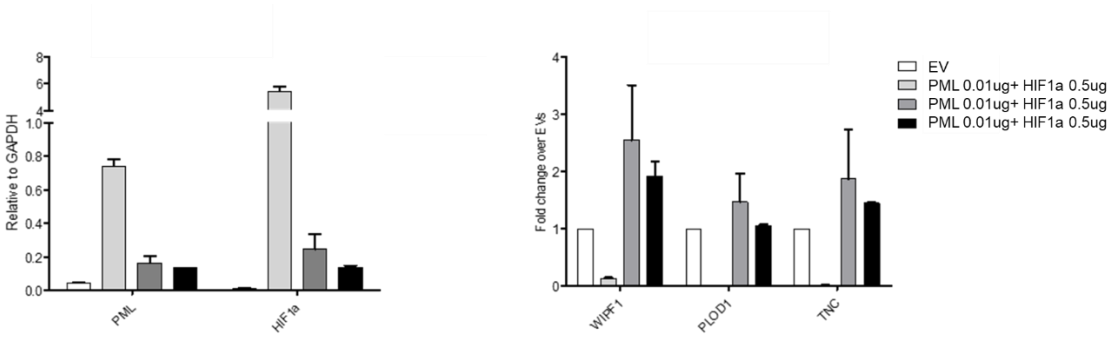

Figure 59. The PML-HIF1α complementation system is transcriptionally active. *qRT-PCR analysis on PML, HIF1α and their regulated genes upon expression of the PML-HIF1α complementation system in BT549 cells. On the left, relative expression levels of PML and HIF1α compared to the housekeeping gene GAPDH in control (EV) and transfected cells. On the right, relative expression levels of each PML-HIF1α coregulated gene in cells expressing PML-HIF1α complementation system over control cells (EV). Data represent mean values ± SD of at least two independent experiments.*

4. DISCUSSION

PML is the molecular scaffold of phase-separated organelles known as PML-NBs. The PML-NBs host a large number of resident and transient proteins, largely TFs, transcriptional regulators and chromatin remodelling proteins, which implicates PML in transcription regulation at various levels. In this respect, many studies have described PML as an indirect regulator of transcription, by acting as a transcriptional co-activator or co-repressor of TFs or by promoting or inhibiting the activity of chromatin modifiers (Zhong *et al*, 2000, Chang *et al*, 2011). However, other work implicated PML more directly into transcriptional regulation, via its association with specific DNA regions or larger chromatin domains, where it may regulate epigenetic profiles, chromatin composition and chromatin architecture (Corpet *et al*, 2020). In this context, several recent studies have attempted to define the DNA binding profile of PML in various cell types, and have described diverging profiles, with some work identifying binding patterns akin to those of TFs and others describing patterns that are typical of architectural proteins (Kurihara *et al*, 2020; Delbarre *et al*, 2017; Wang *et al*, 2020). At present, it is unknown if this heterogeneity derives from cell type specificity, biochemical diversity in PML conformations, different experimental approaches used to identify PML-bound DNA, or all of the above. In this respect, it must be emphasized that beside its concentration at PML-NBs, PML is also present in the nucleus as free moieties that shuttle dynamically between the nucleoplasm and insoluble PML aggregates, and it is presently unknown whether free and NB-condensed forms of PML have different functions in transcriptional regulation and chromatin organization.

Within this field of studies, in our laboratory we have recently demonstrated that PML acts as an oncogene in TNBC by promoting the expression of a specific HIF1α transcriptional program that triggers metastatic dissemination (Ponente *et al*, 2017). Specifically, we found that both PML and HIF1α associate to and regulate a subset of HIF1α target genes that promote metastatic dissemination (Ponente *et al*, 2017). However, this study lacked a general characterization of PML-mediated transcriptional output, as well as the molecular mechanism of PML mediated transcriptional cooperation with HIF1α. For these reasons, we set out to provide a comprehensive characterization of

the transcriptome and genome-wide DNA binding profile of PML in TNBC via RNA-sequencing, ChIP-sequencing and ATAC-sequencing approaches. In so doing, we also aimed to address the different and at times opposite DNA binding profiles identified for PML in different contexts and via different technical approaches. Hence, we performed ChIP-sequencing with two different protocols in the same TNBC cell line: a ChIP protocol designed to enrich for packed chromatin regions (PADs protocol) (Cabianca *et al*, 2012) and a ChIP protocol designed by the ENCODE project for the identification of TFs binding sites (narrow peaks protocol).

Notably, we found that these two protocols identified different DNA binding patterns within the same cell line that recapitulated what had been previously described in different cellular contexts: PML bound to either large heterochromatic and gene-poor DNA regions (PADs), or small regulatory regions of protein-coding genes (PML narrows peaks).

PML binds DNA in different modalities:

PADs identified in this work are similar to PADs described MEFs by the group of Dr. Collas (Delbarre *et al*, 2017). Specifically, they are enriched in the constitutive heterochromatin mark H3K9me3 and depleted of the facultative heterochromatin mark H3K27me3, which, along with active HPTMs, marks the flanking regions of PADs. However, we extended this characterization to show that PADs are gene-poor and enriched in structural components of heterochromatin including repetitive elements, MARs and LADs. Interestingly, LADs cover almost the whole PADs area, suggesting a possible interaction between PML and lamins in the organization of heterochromatic domains. In line with this, silencing of PML alters the nuclear distributions of both H3K9me3 and LMNB1, with H3K9me3 appearing less concentrated within nuclear foci and LMNB1 depleted from the nuclear interior and enriched at the nuclear lamina. Similarly, downregulation of LMNB1 during senescence has been shown to induce the nuclear re-positioning of H3K9me3 with a decrease of perinuclear foci (Sadaie *et al*, 2013). Furthermore, LMNB1 has been recently shown to regulate chromatin positioning in MDA-MB-231 cells and provide the right spatiotemporal regulation of pro-metastatic genes (Chang *et al*, 2020). In this respect, aggressive cancer cells are characterized by a variety of nuclear aberrations, such as a loosened nuclear envelope, twisted nuclei, and invagination, which may be identified by LMNB1 staining (Gauthier & Comaills, 2021).

These features are prominent in MDA-MB-231 cells in which we show that LMNB1 distributes both at the nuclear lamina and interior as disorganized filamentous structures. In this respect, the nuclear redistribution of LMNB1 a upon PML silencing may reflect the formation of a more organized nuclear structure which may perhaps indicate a less aggressive or cancerous state of cancer cells (Fischer, 2020). Moreover, upregulation of LMNB1 at the protein level may reflect an enhanced binding of LMNB1 to PADs, which may then result in a pronounced anchoring of these chromatin regions to the nuclear lamina and perhaps in a more stable nuclear structure (Tang *et al*, 2010).

Supporting a role of PADs in the maintenance of chromatin structure, ATAC-sequencing revealed that PADs are closed DNA compartments that are refractory to changes in chromatin conformation upon PML removal. These data confirm that PADs represent chromatin domains that must be maintained in a heterochromatin state as suggested by previous work where PML removal induced compensatory deposition of H3K27me3, thus allowing the conservation of a heterochromatic state within PADs (Delbarre *et al*, 2017).

In contrast to our data, a recent study has shown that in MDA-MB-231 cells silencing of PML induces LMNB1 downregulation as a consequence of PML-induced senescence (Arreal *et al*, 2020). The discrepancy among these phenotypes might be explained by the different silencing systems used to downregulate PML expression. Specifically, the authors of this recently published paper used an inducible lentiviral shRNA which causes rapid and reversible silencing of PML and thereby leads to an acute response to PML downregulation. Conversely, our system is based on constitutive silencing of PML. Therefore, cells constantly lacking PML experience a chronic condition of PML depletion which may lead to the activation of compensatory mechanisms.

Given the strong overlap of PADs with different structural components of heterochromatin and the functional implication of PML silencing in the nuclear distribution of heterochromatin marks, we conclude that PADs represent structural domains of heterochromatic DNA regions.

In addition to PADs, by applying a different ChIP protocol, we identified PML bound to narrow DNA peaks that are similar to those identified by the ENCODE project as well as by other groups using different technical approaches (i.e ALAP-sequencing and ImmunoTrap-ChIP-sequencing, Kurihara *et al*, 2020; Wang *et al*, 2020). Specifically,

PML-bound DNA is enriched in promoter regions and enhancers, as well as in epigenetic marks of active chromatin, thus resembling binding of a transcription factor.

To understand the reason for these diverging DNA binding profile, we compared technically the two protocols and identified three main differences: i) stringency of nuclear extraction buffer. The PAD protocol involves washing of nuclei with a high salt buffer, which increases the washout of soluble proteins, facilitates detection of highly packed protein complexes and masked chromatin regions (i.e heterochromatin) and decreases the background noise given by soluble proteins. ii) stringency of sonication buffer. The narrow peaks protocol involves use of a sonication buffer containing both ionic and non-ionic detergents, which increase the lysis of nuclear membranes improving epitope availability and chromatin yield. iii) amount of extracted and immunoprecipitated DNA. Starting from the same number of cells, a higher amount of DNA was obtained with the narrow peaks protocol compared to the PADs protocol. Interestingly, this occurs also after PML immunoprecipitation, suggesting that the different nuclear extraction and sonication buffers also lead to qualitatively different PML-associated chromatin. In this respect, it is possible that the higher amount of DNA that is immunoprecipitated with the narrow peaks protocol improves the signal to noise ratio thus allowing identification of PML bound at narrow peaks (regions of high enrichment) with MACS2. Conversely, the lower amount of chromatin obtained with the PADs protocol may allow specific identification of DNA regions that are bound by PML in a broad distribution and low enrichment, making them suitable for the analysis with EDD. Accordingly, when we attempted to call PADs on DNA obtained with the narrow peak protocol, EDD identified large domains covering almost the entire genome (data not shown), suggesting that the signal to noise ratio in ChIP-sequencing data obtained with the narrow peaks protocol makes them unsuitable for the analysis with EDD. Similarly, MACS2 peak calling of samples obtained with the PADs protocol didn't identify any PML associated peaks.

Of note, use of the narrow peaks protocol revealed two types of PML-bound DNA, similar to lamin A/C associated chromatin: low and high molecular weight chromatin (in this thesis work named library A and B respectively), possibly corresponding to euchromatic and heterochromatic regions, as demonstrated for lamin A/C (Gesson *et al*, 2016). However, albeit low and high molecular weight chromatin bound by PML contained different genomic regions, we could not conclusively analyse the composition of high

molecular weight chromatin and convincingly associate it to heterochromatic regions due to its high concentration and the inability to call broad DNA domains with EDD. Therefore, further studies are necessary to address this issue by optimizing the amount and concentration of chromatin that is immunoprecipitated with PML.

In conclusion, PML binds to different DNA regions and different types of chromatin, which may reflect the specific biochemical composition of PML aggregates, and a precise identification of all DNA associated with PML requires a combination of biochemical and bioinformatic approaches.

PML regulated transcription in TNBC:

Having characterized PML binding to DNA, we asked whether PML regulates gene expression via DNA association. Whole transcriptome analysis of genes regulated by PML in TNBC revealed that PML promotes the expression of several pro-metastatic genes, in line with previous work (Ponente *et al*, 2017), along with new gene sets that include immune modulators and glycosylation regulators. Transcriptional regulation of some of these genes is shared with HIF1α, thus expanding their crosstalk in TNBC. However, the majority of PML-regulated genes are not *bona fide* HIF1α targets, thus indicating that PML may also importantly regulate other TFs or transcriptional processes in this tumor context. In addition, in line with a described function of PML in regulating lipid metabolism (Carracedo *et al*, 2012, Cheng *et al*, 2013), PML suppresses the expression of genes belonging to the cholesterol and lysosome pathways also in TNBC. These analyses confirmed that PML is an important oncogenic factor in TNBC and that it partly regulates pro-tumorigenic functions in cooperation with HIF1α.

Not surprisingly, most PML regulated genes do not fall inside PADs (table 1), in line with their structural and gene-poor nature. However, genes that are positively regulated by PML are enriched in PADs-flanking regions, which contain active chromatin marks. This condition is reminiscent of LADs, which represent large heterochromatic domains associated with the nuclear lamina that promote the transcription of nearby genes in euchromatic flanking domains by preserving chromatin segregation (van Steensel & Belmont, 2017). Therefore, we conclude that one mechanism by which PML may promote transcription is by participating to the organization of chromatin domains.

In addition, we asked whether genes regulated by PML may also be located in the proximity of PML narrow peaks, which are mostly found at the regulatory regions of protein-coding genes. Intriguingly, we found that a minority of PML regulated genes overlap with PML-bound DNA (table 1). These include several metastatic and HIF1α target genes, confirming that PML functionally cooperates with HIF1α to promote metastasis in this tumor context (Ponente *et al*, 2017), along with genes regulated by few other transcription factors, mostly JUN and FOS complexes. Accordingly, our data indicate that PML and HIF1α dynamically interact in the nuclear space and either coalesce into or induce nucleation of PML-NBs where transcriptional activity occurs. This might occur also between PML and other transcription factors, such as JUN/FOS. However, the majority of genes regulated by PML do not overlap with PML bound genes, suggesting that they are regulated via indirect mechanisms such as the regulation of specific transcription factors like p53 inside the PML-NBs.

Therefore, altogether these data unveil a complex scenario where PML regulates transcription at various levels (figure 60): via binding and promoting expression of a sub-set of genes, via indirect mechanisms acting on specific transcription factors, and via organization of large chromatin domains that orchestrate chromatin activity. With respect to this last mechanism, we hypothesize that PML positively regulates transcription by organizing large heterochromatin regions that provide the correct spatial positioning of actively transcribed genomic regions.

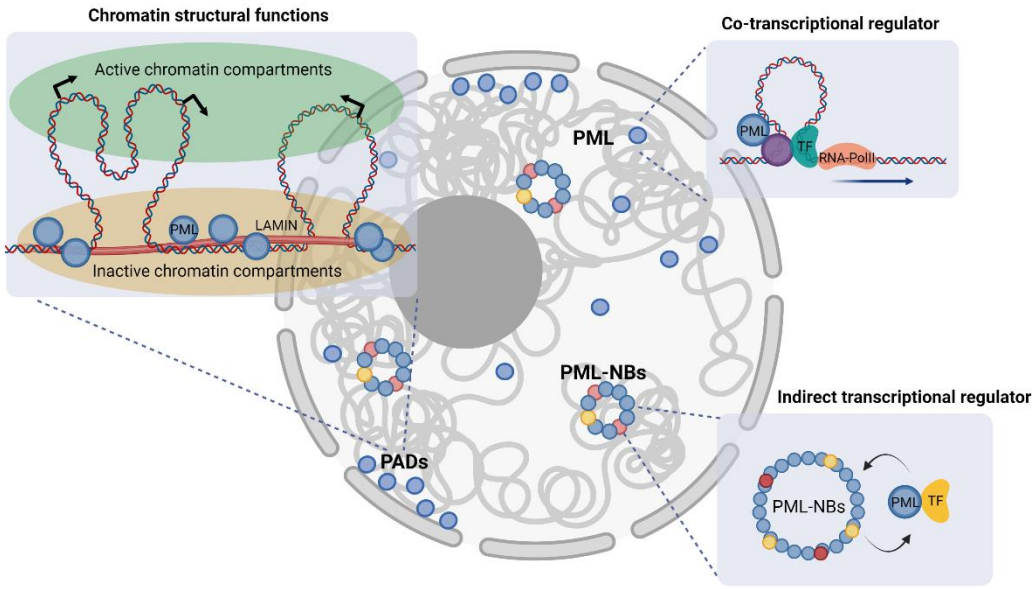

Figure 60. Model of PML mediated transcriptional regulation in TNBC. *PML binds DNA in different conformations in the same cellular context and modulates transcription at multiple levels: i) indirectly by acting as a chromatin structural protein (upper left); ii) directly on specific DNA sequences acting as a co-transcriptional regulator of TFs (upper right); iii) indirectly via the regulation of TFs activity inside the PML-NBs (lower right).*

Tissue specific and conserved transcriptional functions of PML:

Another intriguing finding that has emerged from our work is that there is a large number of genes that are bound but not regulated by PML (table 1). These genes cluster in stress response mechanisms, regulation of translation and regulation of splicing/transcription. These pathways recall the stress-induced functions of PML, which led us to hypothesize that they may represent conserved sites of PML binding which may be activated upon occurrence of stressful conditions. In line with this possibility, while PML bound regions associated with metastasis regulation show changes in chromatin structure in absence of PML by ATAC-sequencing, most PML associated DNA does not result in changes in chromatin accessibility (table 1). To better define these gene sets, we observed that part of these genes overlaps with PML-bound regions in the 3 other cells lines characterized by the ENCODE project, while other genes are uniquely bound by PML in TNBC cells. Also, genes conservatively bound by PML are particularly enriched in binding motifs of stress responsive ETS TFs and may thus represent gene sets regulated by PML upon the

occurrence of stress conditions. However, PML also binds cell type-specific genes, which in TNBC are enriched in AP-1 binding motifs. In this last category, it is tempting to speculate that binding of PML might provide recognition sites for tissue-specific and inducible AP-1 activity. Alternatively, these sites may represent regions transiently bound by PML, unlike DNA regions that are consistently bound by PML in different cell lines.

Genes	**PADs**	**PML narrow peaks**
Bound	4960	1497
Bound and regulated	102	204
Bound and NOT regulated genes	4858	1293
Bound and with changes in chromatin accessibility	335	345
Bound and regulated with changes with chromatin accessibility	47	62
Bound and NOT regulated with changes with chromatin accessibility	335	345

Table 1. Summary table of genomic and transcriptomic data.

PML binding profiles among different cell lines:

In order to determine the molecular mechanisms of PML mediated transcriptional regulation, several studies have characterized its DNA binding profile among different cell lines and with different technical approaches. Specifically, ChIP-experiments identified PML bound to DNA with distinct modalities and to epigenetically opposite chromatin regions, such as broad heterochromatin domains named PADs (Delbarre *et al*, 2017) and narrow peaks found on the regulatory region of coding genes (ENCODE data), the latter being confirmed also using different technical approaches (ALAP-seq and Immunotrap-ChIP-seq, Kurihara *et al*, 2020; Wang *et al*, 2020). Although these experiments have been performed in different cell lines, coming from different species and histological origins (i.e MEFs and several cancer cells), we were able to observe PML binding to DNA with opposing profiles occurring simultaneously in the same TNBC cell line. In doing so, we identified that PML binding to these DNA regions is partly conserved among all these different cell lines and technical approaches. Nevertheless, we also

identified PML bound to tissue-specific genes. Since PML does not bind DNA directly, both conserved and tissue-specific peaks should represent the binding of other proteins. In this concern, binding of PML to conserved sites on DNA may be mediated by constitutively expressed proteins, which possibly interact with PML independently of the cellular background and PML expression levels. As such, we confirmed that PML binds PADs both in MEFs and in TNBC and that PML narrow peaks are conserved among different cancer cell lines. Although not formally demonstrated, association of PML to these regions may reflect a structural role of PML on chromatin. This function may be either mediated by laminB1 or the ETS TFs that, perhaps, bind to PML in all cellular contexts. On the other hand, PML binding to tissue-specific DNA regions may reflect the interaction of PML with proteins differentially expressed among cell lines, which interact with PML depending on the cellular background or PML expression levels. In this concern, studying the DNA binding profile of PML in primary cells would be necessary to test all these possibilities. Nevertheless, it is tempting to speculate that PML generally acts as a chromatin structural protein which sustains the activity of proteins on DNA, either promoting the organization of chromatin domains or sustaining the assembly of inducible or tissue-specific transcription factories.

PML or the PML-NBs, who regulate transcription?:

Another important standing question is whether PML regulates transcription from within the PML-NBs or via its soluble nucleoplasmic moieties. We attempted to address this issue by studying the co-localization of PML with epigenetic chromatin marks that typify PADs as well as with the representative transcription factor HIF1α. Proximity ligation experiments revealed that PML interacts more significantly with the constitutive heterochromatic H3K9me3 mark and laminB1 than with an epigenetic mark of facultative heterochromatin and HIF1α, and these interactions are regulated throughout the cell cycle and occur predominantly in the S and G2 phases, when heterochromatin remodelling occurs. Intriguingly, none of these interactions appear to be enriched at the PML-NBs. Albeit DNA FISH experiments remain to be performed to formally demonstrate whether PAD heterochromatic regions are distal or proximal to PML-NBs, these data suggest that PML importantly regulates transcription outside the PML-NBs. The PML-NBs may still

participate to PML transcriptional functions by promoting the post-translational regulation of specific transcription factors or chromatin remodelling proteins.

In conclusion, our data for the first time reconcile the different and at times inconsistent transcriptional functions associated to PML and demonstrate that PML exerts these functions in the same cellular context, acting both as a transcriptional co-activator or repressor, as well as a structural protein involved in the organization of chromatin compartments.

5. MATERIAL AND METHODS

Cell culture, treatments and reagents

MCF7, BT-549, and MDA-MB-231 cells were maintained in DMEM. All media were from Lonza supplemented with 10% fetal bovine serum (FBS) (Euroclone) and 1% Pennicillin/Streptamycin antibiotics (Lonza). All cell lines were maintained at 37°C in a humidified atmosphere containing 5% CO2. For IF and PLA experiments with transcription inhibition, cells were seeded in a 12 well plate at a concentration of 20'000 cells per well and treated with actinomycin D (Sigma-Aldrich A1410) at a concentration of 1ug/ml for 1h. For cell cycle synchronization experiments cells were seeded at a concentration of 800'000 cells per dish and treated with 0.2ug/ml of Nocodazole (Sigma-Aldrich M1404) for 24h. After release from Nocodazole treatment cells were seeded for IF experiments in a concentration of 50'000 cells per well (12 well plate), while for FACs analysis cells were seeded at a concentration of 100'000 per well (6 well plate). For HIF1α stabilization, cells were treated with CoCl2 (Sigma-Aldrich C8661) at a concentration of 250uM for 6h.

Lentiviral vectors, and virus production and transduction

pLKO.1 vectors expressing shPML (TRCN0000003867), shHIF1α (TRCN0000003809) and shRNA control (SHC002) were purchased from SIGMA (MISSION®). Lentivirus were produced by transfecting HEK-293T with pLK0.1 and packaging plasmids (pRSV-Rev, pMDL-pRRE and pCMV-VSV-G), using calcium phosphate transfection. For each transfection, 9x10^6 HEK293T cells were plated 18h prior to transfection. Culture medium was replaced with fresh medium (DMEM), supplemented with 10% FBS and 1% Pennicillin/Streptamycin antibiotic cocktail, 2h before transfection. Respectively, 32ug, 9ug and 12,5ug of lentiviral vector, VSV-G and packaging vectors were diluted in 0.06X TE and brought to a final volume of 1,125mL. 125uL of ice-cold CaCl2 was added and the mix was allowed to incubate at RT for 10', following drop-wise addition of 1,250mL of 2X HBSS while vortexing the mix at full-speed. 2,5mL of the transfection mix was gently added drop-wise on HEK293T cells. After 16h the medium was replaced with fresh DMEM medium and cells were allowed in the incubator for 30h before

collection of the viral supernatant. Medium was then replaced and, after 24h of further incubation, a second round of virus collection was performed. Each time the supernatant from HEK-293T was collected and filtered and stored either at 4° (for subsequent use) or at -80° (for long term storage). Finally, the viral supernatant was diluted with complete growth medium and used to transduce MDA-MB-231 cells. After 24h the medium was replaced, and cells were allowed to recover before antibiotic selection. Optimal puromycin concentration was pre-determined by performing dose-response curves and used at a final concentration of 2,5 ug/ml.

Cloning

The PML/HIF1α based bimolecular fluorescent complementation system was performed by classical subcloning strategy. Briefly, the ORF of PML-I was subcloned from a pEGFP-C3-PML I (kindly provided by the group of Peter Hemmerich Stefanie, Weidtkamp-Peters *et al*, 2008) into the pBiFC-VC155 plasmid containing the C terminal portion of the Venus protein (Shyu *et al*, 2006). PML-I was amplified with PCR primers containing the Sal1 and BglII restriction sites (table 2), digested and ligated with the linearized pBiFC-VC155 vector. Similarly, the ORF of HIF1α was subcloned form a pCMV3- HIF1α vector (Sino Biological Inc HG11977-UT) into the pBiFC-VN173 plasmid encoding the N-terminal portion of the Venus protein. HIF1α was amplified with PCR primers containing the Not1 and Acc65I restriction sites (table 2), digested and ligated with linear pBiFC-VN173 vector. The indicated concentrations of vectors were transfected into cells with the Lipofectamine LTX and PLUS reagent (ThermoFisher scientific) following the manufactured instructions.

Primer		**Sequence (5'-3')**
PMLI-Sal1/ BglII	Fw	ACGCGTCGACAGAGCCTGCACCCGC
	Rev	GGAAGATCTGGCTCTGCTGGGAGGC
HIF1α- Not1/ Acc65I	Fw	AAATATGCGGCCGCAGAGGGCGCCGGCGG
	Rev	CGGGGTACCCCGTTAACTTGATCCAAAGCTC

Table 2. Sets of primers used for PML/HIF1α BiFC cloning.

Flow cytometry analysis (FACS)

FACS analysis was carried out using the Propidium Iodide (PI) staining for DNA (Sigma, P4170). Briefly cells were fixed in 70% EtOH for at least 1h at 4°. After wash in PBS, cell were permeabilized with 0.25% Triton X-100 for 15 min on ice. Staining was performed in PBS containing 10ug/ml RNAse A and 20 ug/ml PI stock solution at RT in the dark for 30min. All FACS analyses were performed with the BD FACSCantoTM III (Becton Dickinson) analyser. Downstream analysis was performed with FCS Express 7.

Immunoblot (Western Blot, WB)

Proteins were extracted with RIPA buffer and sonicated with 3 cycle at 30% of amper, 1s ON and 1s OFF. Next, samples concentration was determined via Bradford assay, 10ug of protein was diluted in 4X Laemmli buffer and b-mercapthoetanol and boiled 5' at 95°. Standard SDS-PAGE was performed at different polyacrylamide concentrations (4-15%) and transferred on polyvinylidene difluoride (PVDF) membrane through transBlot Turbo Transfer System (Bio-Rad). Blocking and dilution of primary and secondary antibodies (Table 3) have been performed in 5% Milk in PBS 0.5% Tween20. Finally, immunoreactive proteins were detected using the ECL Western Blotting Detection Reagents (GE Healthcare)

Quantitative real time (qRT)-PCR

Total RNA was isolated from cell lines using the RNeasy Kit (Qiagen). cDNA was synthesized by retro-transcription of 1ug of RNA, using Advantage RT-for-PCR Kit (Ambion). Real-time PCR (RT-PCR) was performed by using the SsoAdvanced Universal Probes Supermix (Biorad) assay, using 12,5g of cDNA and 0,4uM concentration of primers (table 3) in the 96 well plates, respectively. The real-time qPCR program used, on the u7900 Fast-Real Time PCR System (Applied Biosystem), was: 10' - 95°C, 30'' - 95°C, 30'' - 58°C, 30'' - 72°C, repeated 39 times, 5'' – 65°C and 30'' - 65°C to terminate the reaction. All primers have been manually designed and purchase by Eurofins (Table 2). The relative fold-change expression of each mRNA was calculated using the $2^{-\Delta\Delta CT}$ method.

Gene		Sequence (5'-3')
GAPDH	Fw	TCAAGAAGGTGGTGAAGCAGG
	Rev	ACCAGGAAATGAGCTTGACAAA
HLA-A	Fw	CGACGCCGCGAGCCAGA
	Rev	GCGATGTAATCCTTGCCGTCGTAG
HLA-B	Fw	CTACCCTGCGGAGATCA
	Rev	ACAGCCAGGCCAGCAACA
HLA-C	Fw	GGAGACACAGAAGTACAAGCG
	Rev	CGTCGTAGGCGTACTGGTCATA
TNC	Fw	ATGTACTGCAGGAGCAGG
	Rev	CTCGAAGGTGACAGTTGCCT
SPARC	Fw	GCTCAAGAACGTCCTGGTCA
	Rev	TCCAGGCGCTTCTCATTCTC
PML	Fw	TCTTCTGCTCCAACCCCAAC
	Rev	TGTGGCTGCTGTCAAGGAG
HIF1a	Fw	GCCTTGGATGGTTTTGTTATGGT
	Rev	CCTCATGGTCACATGGATGAGTA
CIITA	Fw	GTGGCTACCTGGAGCTTCTT
	Rev	ATGGTGTCTGTGTCGGGTTC
PDL1/CD274	Fw	CGACTACAAGCGAATTACTG
	Rev	CTGCTTGTCCAGATGACTTC
CSF1	Fw	ACTCTCTTTGAGGCTGAAG
	Rev	GTCCTTGTCAAGGAGATTC
LOX	Fw	AATGGCACAGTTGTCATCA
	Rev	TGTGGTAGCCATAGTCACAG

Table 3. Sets of primers for qRT-PCR experiments.

Immunofluorescence (IF)

Cells were seeded the day before the experiment on glasses in a 12 multi well plate at a concentration of 20'000 cells in each well. The day after, cells were fixed with 4% PFA for 10' at RT. After 3 washes in PBS 1x cells were permeabilized with PBS+ 1% triton for 5'. Alternatively, for the detection of histone proteins the permeabilization step was performed before fixation with PBS+0.5% triton X100 for 5' at RT. After 3 washes in PBS 1X, blocking was performed in PBS 0.05% tween+10% FBS for 30' at RT. Cells were then washes 3 times in PBS 1X and incubated with primary antibodies (table 4), diluted in in PBS 0.05% tween+1% FBS, for 1h at RT or overnight at 4°. Next, cells were washed 3 times in PBS 1X and incubated with secondary antibodies (table 4), diluted in

in PBS 0.05% tween+10% FBS, for 1h at RT. Finally, after 3 washes in PBS 1X, cells were counterstained with DAPI 1X and placed on microscope slides. Mounting was performed with home-made Mowiol solution.

Proximity ligation assay (PLA)

PLA was performed with the Duolink in situ detection reagents green (Sigma-Aldrich DUO92014). Cells were seeded the day before the experiment on glasses in a 12 multi well at a concentration of 20'000 cells in each well. The day after, cells were fixed with 4% PFA for 10' at RT. After 3 washes in PBS 1X cells were permeabilized with PBS+ 1% triton for 5'. The permeabilization buffer was washed away 3 times with PBS 1X and blocking was performed with the Duolink Blocking solution 30' at 37°. Without any intermediate wash, cells were incubated with primary antibodies (table 4) diluted in the Duolink antibody diluent solution, either 1h at RT or overnight at 4°. The next day, cells were washed with the Duolink washing buffer A 1X 2 times, with each wash performed at RT while oscillating for 5'. Cells were then incubated with the Duolink mouse and rabbit probes, diluted 1:5 in the Duolink antibody diluent, for 1h at 37°. After 2 washes in Duolink washing buffer A 1X, performed at RT while oscillating for 5', cells were incubated with the Duolink ligation mix (1:5 of ligation mix, 1:40 of ligase in pure H20) for 30' at 37°. Next the duolink signal was amplified by incubating cells with the Duolink amplification mix (1:5 amplification mix, 1:80 od polymerase in H20) for 100' at 37°. Cells were then washed 2 times in the Duolink wash buffer B 1X, each 5' while oscillating, and 1 time in the Duolink wash buffer B 0.01X for 1'. Finally, cells were stained with the Duolink DAPI and placed on microscope slides.

When PLA was coupled with IF, first PLA was performed until the last wash in the Duolink buffer B 1X then IF was performed without any further blocking step.

In order to set up the antibody specificity for PLA, we included both technical and biological controls: i) Omission of each probe separately; ii) titration of primary antibodies; iii) use of PML knockdown cells.

Antibody	Species	Working dilution	Application
PML (PG-M3)	M	1:200	IF
		1:1000	PLA
PML (NB100-59787)	R	1:200	IF
		1:1000	PLA
		1:1000	WB
PML (5G191)	M	20ug	ChIP
HIF1α (BD-610959)	M	1:250	WB
		1:200	IF/PLA
HIF1α (NB100-479)	R	1:200	IF/PLA
H3K9me3 (Ab8898)	R	1:5000	IF
		1:10'000	WB
H3K27me3 (Ab6002)	R	1:1000	IF
		1:1000	PLA
LMNB1 (Ab16048)	R	1:500	IF
		1:1000	PLA
		1:1000	WB
RNA Pol2-PS2 (Diagenode C15200005-50)	M	1:500	IF
		1:10000	PLA
GAPDH (sc47724)	M	1:10’000	WB
Beta-Actin (sc69879)	M	1:10’000	WB
Normal IgG-HRP (sc2005/2357)	R/M	1:5000	WB
Normal IgM (sc2025)	M	20ug	ChIP
Alexafluor 546/488	R/M	1:500	IF

Table 4. Sets of antibodies for WB, IF, PLA and ChIP experiments.

Microscopy, imaging, and quantification

Images were acquired with the Zeiss Axio Observer Z1 inverted wide-field epifluorescence microscope (63X objectives) or with the GE HealthCare DeltaVision Ultra microscope (60X objectives). Images were acquired in stacks and identical settings and contrast were applied for all images of the same experiment to allow data comparison. Raw images were treated with Fiji software. Colocalization among IF and PLA signals were performed by manual counting the number of colocalization occurring in each nucleus and on the same stack. The same number of cells were counted for each experimental condition to allow data comparison. Quantification of the number of nuclear

H3K9me3 foci was performed with Fiji. Briefly, the H3K9me3 staining in control cells (shCTRL) was used to define masks of each H3K9me3 foci with the threshold function. The number of H3K9me3 foci was quantified within each nucleus with the analyse particles function. Line and profile plots were performed with Fiji on grayscale images with the corresponding functions.

Chromatin-Immunoprecipiation (ChIP)

Human MDA-MB-231 cells were seeded 24h before the experiment at 60-70% confluence in 15cm dishes plate. In order to extract chromatin, a total of $4*10^8$ cells were collected, and double crosslinking was performed in suspension. Firstly, cells were resuspended in PBS + DSG 2 mM (Sigma-Aldrich 80424) for 45 min at RT on gentle rotation. Next, the cells were centrifuged at 1200 rpm and RT, for 5 min. The resulting pellet was resuspended in PBS + 1% formaldehyde for 10 min at RT on gentle rotation (from a 37.5% formaldehyde/10% methanol stock, Sigma- Aldrich 252549). After formaldehyde quenching with Glycine (final concentration 125 mM) for 5 min, cells were centrifuged 1350 x g 4°C 5 min, and the supernatant was discarded.

Cell lysis PADs protocol (modified from Cabianca et. al., 2012)

Each pellet was lysed in 1 ml (per plate, ~$20*10^6$) of LB1 solution and incubated 10′ in ice. Next, the samples were centrifuged at 1350 g for 5′ at 4°C. The resulting pellet was washed in 1 ml (per plate) of LB2 with gentle rotation 10 min at RT and centrifuged at 1350 g for 5′ at 4°C. The resulting pellet was resuspended in 0.5 ml (per plate) of LB3 and directly sonicated.

Buffer recipes:

LB1	50 mM HEPES-KOH pH 7.5, 140 mM NaCl, 1 mM EDTA, 10% glycerol, 0.5% NP40, 0.25% Triton X-100
LB2	10 mM Tris-HCl pH 8.0, 200 mM NaCl, 1 mM EDTA, 0.5 mM EGTA
LB3	10 mM Tris-HCl pH 8.0, 100 mM NaCl, 1 mM EDTA, 0.5 mM EGTA, 0.1% Na-Deoxycholate, 0.5% N-laurylsarcosine

All buffers were filtered 0.2 -0.45-micron filter unit and supplemented with protease inhibitor (Complete EDTA-free Protease Inhibitor Cocktail Tablets; Roche).

Cell lysis narrow peaks protocol (modified from Myers Lab ChIP-seq Protocol V042211.1)

Each pellet was resuspended in 1 ml (per plate) of Farnham Lysis Buffer, mixed gently by flicking the test tube and incubated 10 min in ice. Next, sample were centrifuge at 2,000 rpm at 4°C for 5 min and the resulting pellet was resuspended in 1ml (per plate) of RIPA buffer and directly sonicated.

Buffer recipes:

Farnham Lysis buffer	5 mM PIPES pH 8.0 / 85 mM KCl / 0.5% NP-40
RIPA buffer	1XPBS / 1% NP-40 / 0.5% sodium deoxycholate / 0.1% SDS

All buffers were filtered 0.2 -0.45-micron filter unit and supplemented with protease inhibitor (Complete EDTA-free Protease Inhibitor Cocktail Tablets; Roche).

Chromatin sonication and quantification

Sonication was performed using the Bioruptor (Diagenode Bioruptor 300) at high intensity 30s ON 40s OFF, for 12 cycles. After sonication, an aliquot (30-60 µl) was collected to determine the quality of the chromatin. To reverse crosslinking, 0.1M $NaHCO_3$, 1% SDS (100 µl) was added to the chromatin aliquot overnight at 65°c, and 12 ul Proteinase K (20 mg/ml in 50 mM Tris-HCl pH 8.0, 10 mM $CaCl_2$, 50% glycerol; Promega) for 1hr at 55°C. Next, the sample was purified using QIAquick PCR purification kit, following the manufacturer's recommendations, and chromatin was quantified with Nanodrop spectrophotometer. Efficiency of sonication was checked by loading 1ug on 1% agarose gel for electrophoresis. We considered good a chromatin enriched in fragments of 500-100 bp.

Immunoprecipitation

Before ChIP, Triton X-100 was added to chromatin samples at a final concentration of 1% and a clarification step was performed for 10 min, 13'000 rpm at 4°C. Then the supernatant was transferred into a new tube to perform immunoprecipitation. For each

ChIP, were used 25ug to 50ug (the latter concentration was used for ChIP-sequencing) of chromatin and the corresponding 5% of the immunoprecipitated chromatin was collected as input sample and stored at -20°c for downstream analysis. Chromatin was pre-coupled to target-antibody overnight at 4°c, on rotation. For 50ug of chromatin we uses 20ug of specific antibody and IgG (table 3), which in the case of the cell lysis protocol modified from (Cabianca *et al*, 2012) was diluted in 9 volumes of RIPA buffer without SDS. The day after, beads were added (25ul of beads each 6ug of antibody, ChIP-IT Protein G magnetic beads 53033) for 4h on rotation at 4°c and finally washed three times in ice-cold RIPA buffer+1% SDS. The supernatant was discarded and 250 ul of Elution buffer was added to the beads-antibody-chromatin complex and placed on rotation for 6h at 37°c. Finally, beads were removed, and samples were incubated overnight at 65°c, together with the input sample, that was resuspended in 3 volume of Elution buffer. Sample purification was performed with the QIAquick PCR purification kit was used (QIAGEN), following the manufacturer recommendations.

Buffer recipes:

RIPA buffer	Tris-HCl pH8 10mM, NaCl 140mM, Triton-x100 1%, Na-deoxycholate 0.1%, EDTA 1mM, EGTA 0.5mM
Elution buffer	NaCl 50mM, TrisHCl pH7.5 20mM, EDTA 5mM, SDS 1%, RNAse-A 0.5ug/ml, Proteinase K 2ug/ml

ChIP q-PCR Analysis

DNA was eluted in 30 µl of pure water and 2 µl were used for downstream qPCR analysis. To determine the ChIP enrichments, we normalized ChIP-qPCR data for input chromatin (reported as % input in the figures). All primers have been manually designed and purchase by Eurofins (Table 4). Real-time PCR (RT-PCR) was performed by using the SsoAdvanced Universal Probes Supermix (Biorad) and a 7900 Fast-Real Time PCR System (Applied Biosystem). Real-time PCR (RT-PCR) was performed using 2ul of DNA and 0,4uM concentration of primers (table 5) in the 96 well plates, respectively. The real-time qPCR program used, on the u7900 Fast-Real Time PCR System (Applied Biosystem), was: 10’ - 95°C, 30’’ - 95°C, 30’’ - 58°C, 30’’ - 72°C, repeated 39 times, 5’’ – 65°C and 30’’ - 65°C to terminate the reaction.

Gene		Sequence (5'-3')
SPARC	Fw	AGGCAAAGAGAGACTGTGAAAGA
	Rev	CCAGTGTACCTGTCCTTGCT
LINE_hORF2-s1	Fw	TGCGGAGAAATAGGAACACTTTT
	Rev	TGAGGAATCGCCACACTGACT
LOX	Fw	AGGTCACACTGGAAATTTGTCT
	Rev	CAATGCCTGCTCTGTGTCCT

Table 5. Sets of primers for ChIP-qPCR experiments.

ChIP-sequencing and ATAC-sequencing

All sequencing were performed by the Center for Omics Sciences at the IRCCS Ospedale San Raffaele (COSR).

DNA quality was evaluated with a High Sensitivity D5000 ScreenTape (Agilent). To generate the libraries, the ChIPSeq Illumina protocol was used. Libraries were barcoded, pooled and sequenced on an Illumina Nova-Seq sequencing system. ChIP-sequencing experiments were performed generating 30M reads, 150 nucleotide long, in paired end.

ATAC-sequencing experiments are representative of two independent experiments performed at different cell passages, while ChIP-sequencing experiments have been performed in single replicate.

After sequencing, reads were trimmed using BBDuk from BBTools suite version 37.36 [http://sourceforge.net/projects/bbmap/] with suggested settings (ktrim=r k=23 mink=11 hdist=1), then mapped using BWA-MEM version 0.7.12-r1039 (Li & Durbin, 2010) on the human genome assembly GRCh38 (hg38, containing only autosomes). Uniquely mapped reads were selected with MarkDuplicates from Picard Tools version 1.104 [http://broadinstitute.github.io/picard/]. Further filtering was done on reads mapping in regions present in the ENCODE hg38 blacklist (Amemiya *et al*, 2019) and regions flagged as not primary alignment or with mapping quality score less than 15.

ChIP-sequencing experiment performed with the cell lysis protocol modified from (Cabianca *et al*, 2012) and identified as "PADs protocol", were used to call peaks using the Enriched Domain Detector (EDD) algorithm (Lund *et al*, 2014).

Mapped PML ChIP-sequencing reads, obtained from the ChIP-sequencing performed with the cell lysis protocol modified from Myers lab protocol, identified as "Narrow peaks protocol", and ATAC-sequencing reads were used to call peaks using MACS2 software version 2.1.1 (Zhang *et al*, 2008) with automatic broad and narrow peaks setting. Consistent peaks between replicates were obtained using the irreproducible discovery rate (IDR) methods version 2.0.3 (Li *et al*, 2011) using a cutoff of 0.05. For ATAC-sequencing, differential peak calling was performed using Diffbind version2 (2.16.2) with the EDGER normalization method.

Browser views are shown using Integrated Genomics Viewer (Robinson *et al*, 2011).

Additional ChIP-sequencing data were retrieved from the NCBI Gene Expression Omnibus (GEO; http://www.ncbi.nlm.nih.gov/geo/, Table 6). In alternative, ChIP-sequencing data were retrieved from the Cistrome DB database (Zheng *et al*, 2019).

Protein	**GSE**	**GSM**		**Cell line**
PML	GSE32465	GSM1010722	HudsonAlpha_ChipSeq_K562_PML_(SC-71910)_v042211.1	K562
		GSM1010771	HudsonAlpha_ChipSeq_GM12878_PML_(SC-71910)_v042211.1	GM12878
		GSM1010838	HudsonAlpha_ChipSeq_MCF-7_PML_(SC-71910)_v042211.1	MCF7
HPTMs	GSE124379	GSM3530736	MDA231-H3K4me1	MDA-MB-231
		GSM3530737	MDA231-H3K4me3	MDA-MB-231
		GSM3530738	MDA231-H3K9me3	MDA-MB-231
		GSM3530740	MDA231-H3K27me3	MDA-MB-231
MARs	GSE87671	GSM2338032	MDA-MB-231 nuclear matrix	MDA-MB-231
LADs	GSE124409	GSE124409	WT_merged_peaks	MDA-MB-231

Table 6. Sets of GEO accession number for ChIP-sequencing experiments.

RNA-sequencing

Total RNA from shPML, shHIF1α and shCTRL from MDA-MB-231 cells was isolated with QIAGEN RNeasy Plus Micro Kit according to the manufacturer's instructions. RNA-sequencing experiments are representative of three independent experiments performed at different cell passages and lentiviral transfections. RNA quality was evaluated with a 2100 Bioanalyzer (Agilent). To generate the libraries, the TruSeq stranded mRNA protocol was used. Libraries were barcoded, pooled and sequenced on an Illumina Nova-Seq 6000 sequencing system. RNA-sequencing experiments were

performed generating 30M reads, 100 nucleotide long, for each run. After trimming, sequences generated within RNASeq experiments were aligned using the STAR aligner (Dobin *et al*, 2013) and counted with featureCounts (Liao *et al*, 2014) on the last Gencode (Harrow *et al*, 2012) release for RNAseq. Differential genes expression was evaluated in R/BioConductor (Huber *et al*, 2015) using the DESeq2 package (Love *et al*, 2014). Finally, EnrichR v3.0 (Kuleshov *et al*, 2016) was used to perform gene set enrichment analysis and find common annotated biological features in the analysed gene lists. Reactome, Hallmark and GO Biological process were used as gene sets for all the analysis performed. Gene sets were obtained by filtering DEGs with logFC<-/>0.3 and FDR 0.05, while significant gene categories were filtered for Adjusted p-value <0.1.

Data processing

All personal scripts were written in R or phyton, and graphs were plotted using ggplot2 in R (R Core Team) or GraphPad Prism (version 5, GraphPad Software, San Diego, California, USA, www.graphpad.com).

Gene annotation

Gene annotation have been performed using the Bioconductor ChIPseeker package (version 1.28.3). The *annotatePeak* function has been used to annotate ChIP-sequencing and ATAC-sequencing peaks. *AnnotatePeak* annotate the location of a given peak in terms of genomic features by assigns peaks to genomic annotations, including TSS, Exon, 5' UTR, 3' UTR, Intronic or Intergenic regions. All annotations have been performed setting the TSS region from -2kb to +2kb. TxDb.Hsapiens.UCSC.hg38.knownGene have been used as gene annotation for human genome hg38. Since PADs comprise non-coding genes, gene annotation was performed by counting the overlap of PADs with the GencodeV28 gene annotation for human genome hg38. Overlaps were counted with the *find_overlaps* function from the Bioconductor plyranges package (version 3.14).

Lift over

LiftOver was performed to bring all genetical analysis to the same reference build. It has been performed by using the liftOver Bioconductor package (version 1.16.0) which use chain file provided by UCSC

(http://hgdownload.soe.ucsc.edu/goldenPath/hg19/liftOver/hg19ToHg38.over.chain.gz or http://hgdownload.soe.ucsc.edu/goldenPath/hg38/liftOver/hg38ToHg19.over.chain.gz).

Intersects and Overlaps

Intersections and overlaps were computed using the Bioconductor packages GenomicRanges (version 1.44.0) and plyranges (version 1.12.1).

Intersect: The intersect method use the triplet (sequence name, range, strand) contained in GRanges objects to determine intersection of features, where a strand value of "*" is treated as occurring on both the "+" and "-" strand. It returns the sequences common to both GRanges objects.

Overlap: Peaks overlaps, gene and features annotations have been performed using the *find_overlaps* function form the plyranges library (version 1.12.1). This function search for any overlaps between ranges x and y and return a GRanges object of length equal to the number of times x overlaps y. Overlaps may be counted in a defined region measured by the max and min gap.

Motif Calling

Motif calling was performed with the HOMER software (v4.11, 10-24-2019), using hg38 as refence genome and default parameters (findMotifsGenome.pl <peak file> <genome> <output directory> -size 200).

Profile plots (DeepTools)

Profile plots of the represented ChIP-sequencing scores (values corresponding to each reads) associated with specific genomic regions were performed using the *computeMatrix* and *plotProfile* functions from DeepTools 2.0.

Coverage boxplots (BedTools)

To quantify the distribution of HPTMs associated scores inside and outside PADs, the mean coverage of each read was measured in a window of 3mb inside and outside PADs.

PADs flanking regions were extracted with the *bedtoolflank* function, while the coverage was measured with the *coverage* function from BedTools (version 2.18).

Statistical analyses

All analyses were performed using GraphPad Prism (version 5, GraphPad Software, San Diego, California, USA, www.graphpad.com) or R.

Permutation tests were performed on R. Randomizations were computed using the Bioconductor packages RegioneR (version 3.14). Particularly, in permutation-based approaches "random PADs" were defined as non-overlapping regions of the same sizes as PADs distributed in a genome subtracted of PADs and containing unmasked genomic regions.

Synthetic genomic regions used as negative control of our experimentally identified PADs were generated by using the *createRandomRegions* function with the following parameters: nregions=123; length.mean=3000000 (bp); length.sd=20; non.overlapping=TRUE.

6. REFERENCES

Altemus MA, Goo LE, Little AC, Yates JA, Cheriyan HG, Wu ZF & Merajver SD (2019) Breast cancers utilize hypoxic glycogen stores via PYGB, the brain isoform of glycogen phosphorylase, to promote metastatic phenotypes. *PLoS One* 14: e0220973

Amemiya HM, Kundaje A & Boyle AP (2019) The ENCODE Blacklist: Identification of Problematic Regions of the Genome. *Sci Rep* 9: 9354

Arreal L, Piva M, Fernández S, Revandkar A, Schaub- Clerigué A, Villanueva J, Zabala-Letona A, Pujana M, Astobiza I, Cortazar AR, *et al* (2020) Targeting PML in triple negative breast cancer elicits growth suppression and senescence. *Cell Death Differ* 27: 1186–1199

Bahrami S & Drabløs F (2016) Gene regulation in the immediate-early response process. *Adv Biol Regul* 62: 37–49

Banani SF, Lee HO, Hyman AA & Rosen MK (2017) Biomolecular condensates: organizers of cellular biochemistry. *Nat Rev Mol Cell Biol* 18: 285–298

Banani SF, Rice AM, Peeples WB, Lin Y, Jain S, Parker R & Rosen MK (2016) Compositional Control of Phase-Separated Cellular Bodies. *Cell* 166: 651–663

Bejjani F, Tolza C, Boulanger M, Downes D, Romero R, Maqbool MA, Zine El Aabidine A, Andrau J-C, Lebre S, Brehelin L, *et al* (2021) Fra-1 regulates its target genes via binding to remote enhancers without exerting major control on chromatin architecture in triple negative breast cancers. *Nucleic Acids Res* 49: 2488–2508

Bernardi R, Guernah I, Jin D, Grisendi S, Alimonti A, Teruya-Feldstein J, Cordon-Cardo C, Celeste Simon M, Rafii S & Pandolfi PP (2006) PML inhibits HIF-1α translation and neoangiogenesis through repression of mTOR. *Nature* 442: 779–785

Bernardi R & Pandolfi PP (2007) Structure, dynamics and functions of promyelocytic leukaemia nuclear bodies. *Nat Rev Mol Cell Biol* 8: 1006–1016

Bernardi R, Papa A & Pandolfi PP (2008) Regulation of apoptosis by PML and the PML-NBs. *Oncogene* 27: 6299–6312

Boichuk S, Hu L, Makielski K, Pandolfi PP & Gjoerup O V. (2011) Functional Connection between Rad51 and PML in Homology-Directed Repair. *PLoS One* 6: e25814

Boisvert F-M, Hendzel MJ & Bazett-Jones DP (2000) Promyelocytic Leukemia (Pml) Nuclear Bodies Are Protein Structures That Do Not Accumulate RNA. *J Cell Biol* 148: 283–292

Bonev B & Cavalli G (2016) Organization and function of the 3D genome. *Nat Rev Genet* 17: 661–678

Boyer LA, Lee TI, Cole MF, Johnstone SE, Levine SS, Zucker JP, Guenther MG, Kumar RM, Murray HL, Jenner RG, *et al* (2005) Core Transcriptional Regulatory Circuitry in Human Embryonic Stem Cells. *Cell* 122: 947–956

Bracken CP, Fedele AO, Linke S, Balrak W, Lisy K, Whitelaw ML & Peet DJ (2006) Cell-specific Regulation of Hypoxia-inducible Factor (HIF)-1α and HIF-2α Stabilization and Transactivation in a Graded Oxygen Environment. *J Biol Chem* 281: 22575–22585

Brand P, Lenser T & Hemmerich P (2010) Assembly dynamics of PML nuclear bodies in living cells. *PMC Biophys* 3: 3

Briand N & Collas P (2020) Lamina-associated domains: peripheral matters and internal affairs. *Genome Biol* 21: 85

Briggs KJJ, Koivunen P, Cao S, Backus KMM, Olenchock BAA, Patel H, Zhang Q, Signoretti S, Gerfen GJJ, Richardson ALL, *et al* (2016) Paracrine Induction of HIF by Glutamate in Breast Cancer: EglN1 Senses Cysteine. *Cell* 166: 126–139

Buchwalter A, Kaneshiro JM & Hetzer MW (2019) Coaching from the sidelines: the nuclear periphery in genome regulation. *Nat Rev Genet* 20: 39–50

Buczek ME, Miles AK, Green W, Johnson C, Boocock DJ, Pockley AG, Rees RC, Hulman G, van Schalkwyk G, Parkinson R, *et al* (2016) Cytoplasmic PML promotes TGF-β-associated epithelial–mesenchymal transition and invasion in prostate cancer. *Oncogene* 35: 3465–3475

Butler JT, Hall LL, Smith KP & Lawrence JB (2009) Changing nuclear landscape and unique PML structures during early epigenetic transitions of human embryonic stem cells. *J Cell Biochem* 107: 609–621

Cabianca DS, Casa V, Bodega B, Xynos A, Ginelli E, Tanaka Y & Gabellini D (2012) A Long ncRNA Links Copy Number Variation to a Polycomb/Trithorax Epigenetic Switch in FSHD Muscular Dystrophy. *Cell* 149: 819–831

Carracedo A, Weiss D, Leliaert AK, Bhasin M, de Boer VCJ, Laurent G, Adams AC, Sundvall M, Song SJ, Ito K, *et al* (2012) A metabolic prosurvival role for PML in breast cancer. *J Clin Invest* 122: 3088–3100

Catez, F, Picard, C, Held, K, Gross, S, Rousseau, A, Theil, D, Sawtell, N, Labetoulle, M, & Lomonte, P (2012). HSV-1 genome subnuclear positioning and associations with host-cell PML-NBs and centromeres regulate LAT locus transcription during latency in neurons. *PLoS pathogens*, *8*(8): e1002852.

Chang C-C, Naik MT, Huang Y-S, Jeng J-C, Liao P-H, Kuo H-Y, Ho C-C, Hsieh Y-L, Lin C-H, Huang N-J, *et al* (2011) Structural and Functional Roles of Daxx SIM Phosphorylation in SUMO Paralog-Selective Binding and Apoptosis Modulation. *Mol Cell* 42: 62–74

Chang FTM, McGhie JD, Chan FL, Tang MC, Anderson MA, Mann JR, Andy Choo KH & Wong LH (2013) PML bodies provide an important platform for the maintenance of telomeric chromatin integrity in embryonic stem cells. *Nucleic Acids Res* 41: 4447–4458

Chang L, Li M, Shao S, Li C, Ai S, Xue B, Hou Y, Zhang Y, Li R, Fan X, *et al* (2020) Nuclear peripheral chromatin-lamin B1 interaction is required for global integrity of chromatin architecture and dynamics in human cells. *Protein Cell*

Chen S, Luperchio TR, Wong X, Doan EB, Byrd AT, Roy Choudhury K, Reddy KL & Krangel MS (2018) A Lamina-Associated Domain Border Governs Nuclear Lamina Interactions, Transcription, and Recombination of the Tcrb Locus. *Cell Rep* 25: 1729-1740.e6

Cheng X, Guo S, Liu Y, Chu H, Hakimi P, Berger NA, Hanson RW & Kao H-Y (2013) Ablation of Promyelocytic Leukemia Protein (PML) Re-patterns Energy Balance and Protects Mice from Obesity Induced by a Western Diet. *J Biol Chem* 288: 29746–29759

Cheng X, Liu Y, Chu H & Kao HY (2012) Promyelocytic Leukemia Protein (PML) regulates endothelial cell network formation and migration in response to tumor necrosis factor α (TNFα) and interferon α (IFNα). *J Biol Chem* 287: 23356–23367

Ching RW, Ahmed K, Boutros PC, Penn LZ & Bazett-Jones DP (2013) Identifying gene locus associations with promyelocytic leukemia nuclear bodies using immuno-TRAP. *J Cell Biol* 201: 325–335

Ching RW, Dellaire G, Eskiw CH & Bazett-Jones DP (2005) PML bodies: A meeting place for genomic loci? *J Cell Sci* 118: 847–854

Cho S, Park JS & Kang Y-K (2011) Dual Functions of Histone-Lysine N-Methyltransferase Setdb1 Protein at Promyelocytic Leukemia-Nuclear Body (PML-NB). *J Biol Chem* 286: 41115–41124

Choudhry H, Albukhari A, Morotti M, Haider S, Moralli D, Smythies J, Schödel J, Green CM, Camps C, Buffa F, *et al* (2015) Tumor hypoxia induces nuclear paraspeckle formation through HIF-2α dependent transcriptional activation of NEAT1 leading to cancer cell survival. *Oncogene* 34: 4482–4490

Cohen C, Corpet A, Roubille S, Maroui MA, Poccardi N, Rousseau A, Kleijwegt C, Binda O, Texier P, Sawtell N, *et al* (2018) Promyelocytic leukemia (PML) nuclear bodies (NBs) induce latent/quiescent HSV-1 genomes chromatinization through a PML NB/Histone H3.3/H3.3 Chaperone Axis. *PLOS Pathog* 14: e1007313

Condemine W, Takahashi Y, Bras M Le & Thé H De (2007) A nucleolar targeting signal in PML-I addresses PML to nucleolar caps in stressed or senescent cells. 3219–3227

Condemine W, Takahashi Y, Zhu J, Puvion-Dutilleul F, Guegan S, Janin A & de Thé H (2006) Characterization of Endogenous Human Promyelocytic Leukemia Isoforms. *Cancer Res* 66: 6192–6198

Corpet A, Kleijwegt C, Roubille S, Juillard F, Jacquet K, Texier P & Lomonte P (2020) PML nuclear bodies and chromatin dynamics: catch me if you can! *Nucleic Acids Res* 48: 11890–11912

Corpet A & Stucki M (2014) Chromatin maintenance and dynamics in senescence: a spotlight on SAHF formation and the epigenome of senescent cells. *Chromosoma* 123: 423–436

Cournac A, Koszul R & Mozziconacci J (2016) The 3D folding of metazoan genomes correlates with the association of similar repetitive elements. *Nucleic Acids Res* 44:

245–255

Crowder C, Dahle Ø, Davis RE, Gabrielsen OS & Rudikoff S (2005) PML mediates IFN-α–induced apoptosis in myeloma by regulating TRAIL induction. *Blood* 105: 1280–1287

Cuchet-Lourenco D, Vanni E, Glass M, Orr A & Everett RD (2012) Herpes Simplex Virus 1 Ubiquitin Ligase ICP0 Interacts with PML Isoform I and Induces Its SUMO-Independent Degradation. *J Virol* 86: 11209–11222

Curtis, C. et al (2012) Comprehensive molecular portraits of human breast tumours. *Nature* 490: 61–70

Van Damme E, Laukens K, Dang TH & Van Ostade X (2010) A manually curated network of the PML nuclear body interactome reveals an important role for PML-NBs in SUMOylation dynamics. *Int J Biol Sci* 6: 51–67

Dayan F, Roux D, Brahimi-Horn MC, Pouyssegur J & Mazure NM (2006) The oxygen sensor factor-inhibiting hypoxia-inducible factor-1 controls expression of distinct genes through the bifunctional transcriptional character of hypoxia-inducible factor-1α. *Cancer Res* 66: 3688–3698

Delbarre E, Ivanauskiene K, Spirkoski J, Shah A, Vekterud K, Moskaug JØ, Bøe SO, Wong LH, Küntziger T & Collas P (2017) PML protein organizes heterochromatin domains where it regulates histone H3.3 deposition by ATRX/DAXX. *Genome Res* 27: 913–921

Delbarre E & Janicki SM (2021) Modulation of H3.3 chromatin assembly by PML: A way to regulate epigenetic inheritance. *BioEssays* 43: 2100038

Dellaire G, Ching RW, Ahmed K, Jalali F, Tse KCK, Bristow RG & Bazett-Jones DP (2006a) Promyelocytic leukemia nuclear bodies behave as DNA damage sensors whose response to DNA double-strand breaks is regulated by NBS1 and the kinases ATM, Chk2, and ATR. *J Cell Biol* 175: 55–66

Dellaire G, Ching RW, Dehghani H, Ren Y & Bazett-Jones DP (2006b) The number of PML nuclear bodies increases in early S phase by a fission mechanism. *J Cell Sci* 119: 1026–1033

Dellaire G, Eskiw CH, Dehghani H, Ching RW & Bazett-jones DP (2006c) Mitotic accumulations of PML protein contribute to the re-establishment of PML nuclear bodies in G1. 1034–1042

Dengler VL, Galbraith MD & Espinosa JM (2014) Transcriptional regulation by hypoxia inducible factors. *Crit Rev Biochem Mol Biol* 49: 1–15

Dixon JR, Selvaraj S, Yue F, Kim A, Li Y, Shen Y, Hu M, Liu JS & Ren B (2012) Topological domains in mammalian genomes identified by analysis of chromatin interactions. *Nature* 485: 376–380

Dobin A, Davis CA, Schlesinger F, Drenkow J, Zaleski C, Jha S, Batut P, Chaisson M & Gingeras TR (2013) STAR: ultrafast universal RNA-seq aligner. *Bioinformatics* 29: 15–21

Dobson JR, Hong D, Barutcu AR, Wu H, Imbalzano AN, Lian JB, Stein JL, van Wijnen AJ, Nickerson JA & Stein GS (2017) Identifying Nuclear Matrix-Attached DNA Across the Genome. *J Cell Physiol* 232: 1295–1305

Draskovic I, Arnoult N, Steiner V, Bacchetti S, Lomonte P & Londoño-Vallejo A (2009) Probing PML body function in ALT cells reveals spatiotemporal requirements for telomere recombination. *Proc Natl Acad Sci* 106: 15726–15731

Duan C (2016) Hypoxia-inducible factor 3 biology: complexities and emerging themes. *Am J Physiol Physiol* 310: C260–C269

Dunwoodie SL (2009) The Role of Hypoxia in Development of the Mammalian Embryo. *Dev Cell* 17: 755–773

Dvorkina M, Nieddu V, Chakelam S, Pezzolo A, Cantilena S, Leite AP, Chayka O, Regad T, Pistorio A, Sementa AR, *et al* (2016) A Promyelocytic Leukemia Protein–Thrombospondin-2 Axis and the Risk of Relapse in Neuroblastoma. *Clin Cancer Res* 22: 3398–3409

Ernst J, Kheradpour P, Mikkelsen TS, Shoresh N, Ward LD, Epstein CB, Zhang X, Wang L, Issner R, Coyne M, *et al* (2011) Mapping and analysis of chromatin state dynamics in nine human cell types. *Nature* 473: 43–49

Eskiw CH, Dellaire G & Bazett-jones DP (2004a) Chromatin Contributes to Structural Integrity of Promyelocytic Leukemia Bodies through a SUMO-1-independent Mechanism * □. 279: 9577–9585

Eskiw CH, Dellaire G & Bazett-Jones DP (2004b) Chromatin Contributes to Structural Integrity of Promyelocytic Leukemia Bodies through a SUMO-1-independent Mechanism. *J Biol Chem* 279: 9577–9585

Eskiw CH, Dellaire G, Mymryk JS & Bazett-jones DP (2003) Size , position and dynamic behavior of PML nuclear bodies following cell stress as a paradigm for supramolecular trafficking and assembly.

Everett RD & Chelbi-alix MK (2007) PML and PML nuclear bodies : Implications in antiviral defence PML : Structure and Localization. 89

Filion GJ, van Bemmel JG, Braunschweig U, Talhout W, Kind J, Ward LD, Brugman W, de Castro IJ, Kerkhoven RM, Bussemaker HJ, *et al* (2010) Systematic Protein Location Mapping Reveals Five Principal Chromatin Types in Drosophila Cells. *Cell* 143: 212–224

Fischer EG (2020) Nuclear Morphology and the Biology of Cancer Cells. *Acta Cytol* 64: 511–519

Fonin A V., Silonov SA, Shpironok OG, Antifeeva IA, Petukhov A V., Romanovich AE, Kuznetsova IM, Uversky VN & Turoverov KK (2021) The Role of Non-Specific Interactions in Canonical and ALT-Associated PML-Bodies Formation and Dynamics. *Int J Mol Sci* 22: 5821

Fortini ME (2009) Notch Signaling: The Core Pathway and Its Posttranslational Regulation. *Dev Cell* 16: 633–647

Galbraith MD, Allen MA, Bensard CL, Wang X, Schwinn MK, Qin B, Long HW, Daniels DL, Hahn WC, Dowell RD, *et al* (2013) HIF1A Employs CDK8-Mediator to Stimulate RNAPII Elongation in Response to Hypoxia. *Cell* 153: 1327–1339

Gallant S & Gilkeson G (2006) ETS transcription factors and regulation of immunity. *Arch Immunol Ther Exp (Warsz)* 54: 149–163

Gauthier BR & Comaills V (2021) Nuclear Envelope Integrity in Health and Disease: Consequences on Genome Instability and Inflammation. *Int J Mol Sci* 22: 7281

Geng Y, Monajembashi S, Shao A, Cui D, He W, Chen Z, Hemmerich P & Tang J (2012) Contribution of the C-terminal Regions of Promyelocytic Leukemia Protein (PML) Isoforms II and V to PML Nuclear Body Formation. *J Biol Chem* 287: 30729–30742

Geoffroy M-C & Chelbi-Alix MK (2011) Role of Promyelocytic Leukemia Protein in Host Antiviral Defense. *J Interf Cytokine Res* 31: 145–158

Gesson K, Rescheneder P, Skoruppa MP, von Haeseler A, Dechat T & Foisner R (2016) A-type lamins bind both hetero- and euchromatin, the latter being regulated by lamina-associated polypeptide 2 alpha. *Genome Res* 26: 462–473

Gialitakis M, Arampatzi P, Makatounakis T & Papamatheakis J (2010) Gamma Interferon-Dependent Transcriptional Memory via Relocalization of a Gene Locus to PML Nuclear Bodies. *Mol Cell Biol* 30: 2046–2056

Gilkes DM & Semenza GL (2013) Role of hypoxia-inducible factors in breast cancer metastasis. *Futur Oncol* 9: 1623–1636

Giorgetti L, Lajoie BR, Carter AC, Attia M, Zhan Y, Xu J, Chen CJ, Kaplan N, Chang HY, Heard E, *et al* (2016) Structural organization of the inactive X chromosome in the mouse. *Nature* 535: 575–579

Grobelny JV, Godwin AK & Broccoli D (2000) ALT-associated PML bodies are present in viable cells and are enriched in cells in the G(2)/M phase of the cell cycle. *J Cell Sci* 113: 4577–4585

Groh S, Milton AV, Marinelli LK, Sickinger C V., Russo A, Bollig H, de Almeida GP, Schmidt A, Forné I, Imhof A, *et al* (2021) Morc3 silences endogenous retroviruses by enabling Daxx-mediated histone H3.3 incorporation. *Nat Commun* 12: 5996

Guelen L, Pagie L, Brasset E, Meuleman W, Faza MB, Talhout W, Eussen BH, de Klein A, Wessels L, de Laat W, *et al* (2008) Domain organization of human chromosomes revealed by mapping of nuclear lamina interactions. *Nature* 453: 948–951

Guo L, Giasson BI, Glavis-Bloom A, Brewer MD, Shorter J, Gitler AD & Yang X (2014) A Cellular System that Degrades Misfolded Proteins and Protects against Neurodegeneration. *Mol Cell* 55: 15–30

Gurrieri C, Capodieci P, Bernardi R, Scaglioni PP, Nafa K, Rush LJ, Verbel DA, Cordon-Cardo C & Pandolfi PP (2004) Loss of the Tumor Suppressor PML in Human Cancers of Multiple Histologic Origins. *JNCI J Natl Cancer Inst* 96: 269–279

Guttlein LN, Benedetti LG, Fresno C, Spallanzani RG, Mansilla SF, Rotondaro C, Iraolagoitia XLR, Salvatierra E, Bravo AI, Fernandez EA, *et al* (2017) Predictive outcomes for HER2-enriched cancer using growth and metastasis signatures driven by SPARC. *Mol Cancer Res* 15: 304–316

Hanahan D & Weinberg RA (2011) Hallmarks of Cancer: The Next Generation. *Cell* 144: 646–674

Harr JC, Luperchio TR, Wong X, Cohen E, Wheelan SJ & Reddy KL (2015) Directed targeting of chromatin to the nuclear lamina is mediated by chromatin state and A-type lamins. *J Cell Biol* 208: 33–52

Harrow J, Frankish A, Gonzalez JM, Tapanari E, Diekhans M, Kokocinski F, Aken BL, Barrell D, Zadissa A, Searle S, *et al* (2012) GENCODE: The reference human genome annotation for The ENCODE Project. *Genome Res* 22: 1760–1774

Hayashi Y, Yokota A, Harada H & Huang G (2019) Hypoxia/pseudohypoxia-mediated activation of hypoxia-inducible factor-1α in cancer. *Cancer Sci* 110: 1510–1517

de Heer EC, Jalving M & Harris AL (2020) HIFs, angiogenesis, and metabolism: elusive enemies in breast cancer. *J Clin Invest* 130: 5074–5087

Henikoff S & Smith MM (2015) Histone Variants and Epigenetics. *Cold Spring Harb Perspect Biol* 7: a019364

Hildebrand EM & Dekker J (2020) Mechanisms and Functions of Chromosome Compartmentalization. *Trends Biochem Sci* 45: 385–396

Hirsilä M, Koivunen P, Günzler V, Kivirikko KI & Myllyharju J (2003) Characterization of the Human Prolyl 4-Hydroxylases That Modify the Hypoxia-inducible Factor. *J Biol Chem* 278: 30772–30780

Hoischen C, Monajembashi S, Weisshart K & Hemmerich P (2018) Multimodal light microscopy approaches to reveal structural and functional properties of promyelocytic leukemia nuclear bodies. *Front Oncol* 8

Hsu K-S, Zhao X, Cheng X, Guan D, Mahabeleshwar GH, Liu Y, Borden E, Jain MK & Kao H-Y (2017) Dual regulation of Stat1 and Stat3 by the tumor suppressor protein PML contributes to interferon α-mediated inhibition of angiogenesis. *J Biol Chem* 292: 10048–10060

Huber W, Carey VJ, Gentleman R, Anders S, Carlson M, Carvalho BS, Bravo HC, Davis S, Gatto L, Girke T, *et al* (2015) Orchestrating high-throughput genomic analysis with Bioconductor. *Nat Methods* 12: 115–121

Humphries BA, Buschhaus JM, Chen Y-C, Haley HR, Qyli T, Chiang B, Shen N, Rajendran S, Cutter A, Cheng Y-H, *et al* (2019) Plasminogen activator inhibitor 1 (PAI1) promotes actin cytoskeleton reorganization and glycolytic metabolism in triple negative breast cancer. *Mol Cancer Res* 17: molcanres.0836.2018

Iommarini L, Porcelli AM, Gasparre G & Kurelac I (2017) Non-canonical mechanisms regulating hypoxia-inducible factor 1 alpha in cancer. *Front Oncol* 7: 1–9

Ito K, Bernardi R, Morotti A, Matsuoka S, Saglio G, Ikeda Y, Rosenblatt J, Avigan DE,

Teruya-Feldstein J & Pandolfi PP (2008) PML targeting eradicates quiescent leukaemia-initiating cells. *Nature* 453: 1072–1078

Jeanne M, Lallemand-Breitenbach V, Ferhi O, Koken M, Le Bras M, Duffort S, Peres L, Berthier C, Soilihi H, Raught B, *et al* (2010) PML/RARA Oxidation and Arsenic Binding Initiate the Antileukemia Response of As2O3. *Cancer Cell* 18: 88–98

Jensen K, Shiels C & Freemont PS (2001) PML protein isoforms and the RBCC/TRIM motif. *Oncogene* 20: 7223–7233

Jiang S & Mortazavi A (2018) Integrating ChIP-seq with other functional genomics data. *Brief Funct Genomics* 17: 104–115

Jin F, Brockmeier U, Otterbach F & Metzen E (2012) New Insight into the SDF-1/CXCR4 Axis in a Breast Carcinoma Model: Hypoxia-Induced Endothelial SDF-1 and Tumor Cell CXCR4 Are Required for Tumor Cell Intravasation. *Mol Cancer Res* 10: 1021–1031

Kang Y, Siegel PM, Shu W, Drobnjak M, Kakonen SM, Cordón-Cardo C, Guise TA & Massagué J (2003) A multigenic program mediating breast cancer metastasis to bone. *Cancer Cell* 3: 537–549

Kawasaki A, Matsumura I, Kataoka Y, Takigawa E, Nakajima K & Kanakura Y (2003) Opposing effects of PML and PML/RARα on STAT3 activity. *Blood* 101: 3668–3673

Kepkay R, Attwood KM, Ziv Y, Shiloh Y, Kepkay R, Attwood KM, Ziv Y, Shiloh Y & Dellaire G (2011) KAP1 depletion increases PML nuclear body number in concert with ultrastructural changes in chromatin KAP1 depletion increases PML nuclear body number in concert with ultrastructural changes in chromatin. 4101

Khosraviani N, Ostrowski LA, Mekhail K & Dimitri P (2019) Roles for Non-coding RNAs in Spatial Genome Organization. *Front Cell Dev Biol* 7: 1–16

Kietzmann T, Mennerich D & Dimova EY (2016) Hypoxia-Inducible Factors (HIFs) and Phosphorylation: Impact on Stability, Localization, and Transactivity. *Front Cell Dev Biol* 4: 1–14

Kim MK, Yang S, Lee K-H, Um J-H, Liu M, Kang H, Park SJ & Chung JH (2011) Promyelocytic leukemia inhibits adipogenesis, and loss of promyelocytic leukemia results in fat accumulation in mice. *Am J Physiol Metab* 301: E1130–E1142

Kim Y-J, Zhao Y, Myung JK, Yi JM, Kim M-J & Lee S-J (2021) Suppression of breast cancer progression by FBXL16 via oxygen-independent regulation of HIF1α stability. *Cell Rep* 37: 109996

Kleijwegt C, Bressac F, Cohen C, Texier P, Simonet T, Schaeffer L, Lomonte P & Corpet A (2021) Interplay between PML NBs and HIRA for H3.3 deposition on transcriptionally active interferon-stimulated genes. *bioRxiv*: 2021.11.30.470516

Koivunen P, Hirsilä M, Günzler V, Kivirikko KI & Myllyharju J (2004) Catalytic Properties of the Asparaginyl Hydroxylase (FIH) in the Oxygen Sensing Pathway Are Distinct from Those of Its Prolyl 4-Hydroxylases. *J Biol Chem* 279: 9899–

9904

Kuleshov M V., Jones MR, Rouillard AD, Fernandez NF, Duan Q, Wang Z, Koplev S, Jenkins SL, Jagodnik KM, Lachmann A, *et al* (2016) Enrichr: a comprehensive gene set enrichment analysis web server 2016 update. *Nucleic Acids Res* 44: W90–W97

Kulshreshtha R, Ferracin M, Wojcik SE, Garzon R, Alder H, Agosto-Perez FJ, Davuluri R, Liu C-G, Croce CM, Negrini M, *et al* (2007) A MicroRNA Signature of Hypoxia. *Mol Cell Biol* 27: 1859–1867

Kumar P, Bischof O, Purbey PK, Notani D, Urlaub H, Dejean A & Galande S (2007) Functional interaction between PML and SATB1 regulates chromatin-loop architecture and transcription of the MHC class I locus. *Nat Cell Biol* 9: 45–56

Kurihara M, Kato K, Sanbo C, Shigenobu S, Ohkawa Y, Fuchigami T & Miyanari Y (2020) Genomic Profiling by ALaP-Seq Reveals Transcriptional Regulation by PML Bodies through DNMT3A Exclusion. *Mol Cell* 78: 493-505.e8

Lallemand-Breitenbach V & de The H (2010) PML Nuclear Bodies. *Cold Spring Harb Perspect Biol* 2: a000661–a000661

Lång A, Eriksson J, Schink KO, Lång E, Blicher P, Połeć A, Brech A, Dalhus B & Bøe SO (2017) Visualization of PML nuclear import complexes reveals FG-repeat nucleoporins at cargo retrieval sites. *Nucleus* 8: 404–420

Laughner E, Taghavi P, Chiles K, Mahon PC & Semenza GL (2001) HER2 (neu) Signaling Increases the Rate of Hypoxia-Inducible Factor 1α (HIF-1α) Synthesis: Novel Mechanism for HIF-1-Mediated Vascular Endothelial Growth Factor Expression. *Mol Cell Biol* 21: 3995–4004

Lawrence M, Daujat S & Schneider R (2016) Lateral Thinking: How Histone Modifications Regulate Gene Expression. *Trends Genet* 32: 42–56

Lendahl U, Lee KL, Yang H & Poellinger L (2009) Generating specificity and diversity in the transcriptional response to hypoxia. *Nat Rev Genet* 10: 821–832

Li H & Durbin R (2010) Fast and accurate long-read alignment with Burrows–Wheeler transform. *Bioinformatics* 26: 589–595

Li H, Leo C, Zhu J, Wu X, O'Neil J, Park E-J & Chen JD (2000) Sequestration and Inhibition of Daxx-Mediated Transcriptional Repression by PML. *Mol Cell Biol* 20: 1784–1796

Li Q, Brown JB, Huang H & Bickel PJ (2011) Measuring reproducibility of high-throughput experiments. *Ann Appl Stat* 5: 1752–1779

Li S (2019) Regulation of Ribosomal Proteins on Viral Infection. *Cells* 8: 508

Liao K-C & Garcia-Blanco MA (2021) Role of Alternative Splicing in Regulating Host Response to Viral Infection. *Cells* 10: 1720

Liao Y, Smyth GK & Shi W (2014) featureCounts: an efficient general purpose program for assigning sequence reads to genomic features. *Bioinformatics* 30:

923–930

Lin A, Li C, Xing Z, Hu Q, Liang K, Han L, Wang C, Hawke DH, Wang S, Zhang Y, *et al* (2016) The LINK-A lncRNA activates normoxic HIF1α signalling in triple-negative breast cancer. *Nat Cell Biol* 18: 213–224

Lin Y-C, Lu L-T, Chen H-Y, Duan X, Lin X, Feng X-H, Tang M-J & Chen R-H (2014) SCP Phosphatases Suppress Renal Cell Carcinoma by Stabilizing PML and Inhibiting mTOR/HIF Signaling. *Cancer Res* 74: 6935–6946

Liu S-B, Shen Z-F, Guo Y-J, Cao L-X & Xu Y (2017) PML silencing inhibits cell proliferation and induces DNA damage in cultured ovarian cancer cells. *Biomed Reports* 7: 29–35

Liu Y, van den Berg A, Veenstra R, Rutgers B, Nolte I, van Imhoff G, Visser L & Diepstra A (2013) PML Nuclear Bodies and SATB1 Are Associated with HLA Class I Expression in EBV+ Hodgkin Lymphoma. *PLoS One* 8: e72930

Lo Y-H, Huang Y-W, Wu Y-H, Tsai C-S, Lin Y-C, Mo S-T, Kuo W-C, Chuang Y-T, Jiang S-T, Shih H-M, *et al* (2013) Selective inhibition of the NLRP3 inflammasome by targeting to promyelocytic leukemia protein in mouse and human. *Blood* 121: 3185–3194

Loe TK, Li JSZ, Zhang Y, Azeroglu B, Boddy MN & Denchi EL (2020) Telomere length heterogeneity in ALT cells is maintained by PML-dependent localization of the BTR complex to telomeres. *Genes Dev* 34: 650–662

Love MI, Huber W & Anders S (2014) Moderated estimation of fold change and dispersion for RNA-seq data with DESeq2. *Genome Biol* 15: 550

Lu JY, Chang L, Li T, Wang T, Yin Y, Zhan G, Han X, Zhang K, Tao Y, Percharde M, *et al* (2021) Homotypic clustering of L1 and B1/Alu repeats compartmentalizes the 3D genome. *Cell Res* 31: 613–630

Lu JY, Shao W, Chang L, Yin Y, Li T, Zhang H, Hong Y, Percharde M, Guo L, Wu Z, *et al* (2020) Genomic Repeats Categorize Genes with Distinct Functions for Orchestrated Regulation. *Cell Rep* 30: 3296-3311.e5

Luciani JJ, Depetris D, Usson Y, Metzler-Guillemain C, Mignon-Ravix C, Mitchell MJ, Megarbane A, Sarda P, Sirma H, Moncla A, *et al* (2006) PML nuclear bodies are highly organised DNA-protein structures with a function in heterochromatin remodelling at the G2 phase. *J Cell Sci* 119: 2518–2531

Lunardi A, Gaboli M, Giorgio M, Rivi R, Bygrave A, Antoniou M, Drabek D, Dzierzak E, Fagioli M, Salmena L, *et al* (2011) A Role for PML in Innate Immunity. *Genes Cancer* 2: 10–19

Lund E, Oldenburg AR & Collas P (2014) Enriched domain detector: a program for detection of wide genomic enrichment domains robust against local variations. *Nucleic Acids Res* 42: e92–e92

Majmundar AJ, Wong WJ & Simon MC (2010) Hypoxia-Inducible Factors and the Response to Hypoxic Stress. *Mol Cell* 40: 294–309

Martín-Martín N, Piva M, Urosevic J, Aldaz P, Sutherland JD, Fernández-Ruiz S, Arreal L, Torrano V, Cortazar AR, Planet E, *et al* (2016) Stratification and therapeutic potential of PML in metastatic breast cancer. *Nat Commun* 7

Mazza M & Pelicci PG (2013) Is PML a Tumor Suppressor? *Front Oncol* 3: 1–9

McFarlane S, Orr A, Roberts APE, Conn KL, Iliev V, Loney C, da Silva Filipe A, Smollett K, Gu Q, Robertson N, *et al* (2019) The histone chaperone HIRA promotes the induction of host innate immune defences in response to HSV-1 infection. *PLOS Pathog* 15: e1007667

El Mchichi B, Regad T, Maroui M-A, Rodriguez MS, Aminev A, Gerbaud S, Escriou N, Dianoux L & Chelbi-Alix MK (2010) SUMOylation Promotes PML Degradation during Encephalomyocarditis Virus Infection. *J Virol* 84: 11634–11645

Mcnally BA, Trgovcich J, Maul GG, Liu Y & Zheng P (2008) A Role for Cytoplasmic PML in Cellular Resistance to Viral Infection. 3

Mehner C, Hockla A, Miller E, Ran S, Radisky DC & Radisky ES (2014) Tumor cell-produced matrix metalloproteinase 9 (MMP-9) drives malignant progression and metastasis of basal-like triple negative breast cancer. *Oncotarget* 5: 2736–2749

Melnick A & Licht JD (1999) Deconstructing a Disease: RAR□, Its Fusion Partners, and Their Roles in the Pathogenesis of Acute Promyelocytic Leukemia. *Blood* 93: 3167–3215

Merino-Gracia J, García-Mayoral MF & Rodríguez-Crespo I (2011) The association of viral proteins with host cell dynein components during virus infection. *FEBS J* 278: 2997–3011

Moir RD, Spann TP, Lopez-Soler RI, Yoon M, Goldman AE, Khuon S & Goldman RD (2000) Review: The Dynamics of the Nuclear Lamins during the Cell Cycle—Relationship between Structure and Function. *J Struct Biol* 129: 324–334

Mole DR, Blancher C, Copley RR, Pollard PJ, Gleadle JM, Ragoussis J & Ratcliffe PJ (2009) Genome-wide Association of Hypoxia-inducible Factor (HIF)-1α and HIF-2α DNA Binding with Expression Profiling of Hypoxia-inducible Transcripts. *J Biol Chem* 284: 16767–16775

Nefkens I, Negorev DG, Ishov AM, Michaelson JS, Yeh ETH, Tanguay RM, Müller WEG & Maul GG (2003) Heat shock and Cd2+ exposure regulate PML and Daxx release from ND10 by independent mechanisms that modify the induction of heat-shock proteins 70 and 25 differently. *J Cell Sci* 116: 513–524

Nisole S, Maroui MA, Mascle XH, Aubry M & Chelbi-Alix MK (2013) Differential Roles of PML Isoforms. *Front Oncol* 3: 1–17

Niu G, Briggs J, Deng J, Ma Y, Lee H, Kortylewski M, Kujawski M, Kay H, Cress WD, Jove R, *et al* (2008) Signal Transducer and Activator of Transcription 3 Is Required for Hypoxia-Inducible Factor-1α RNA Expression in Both Tumor Cells and Tumor-Associated Myeloid Cells. *Mol Cancer Res* 6: 1099–1105

Nojima T, Oshiro-ideue T, Nakanoya H, Kawamura H, Morimoto T, Kawaguchi Y &

Kataoka N (2009) Herpesvirus protein ICP27 switches PML isoform by altering mRNA splicing. 37: 6515–6527

Nora EP, Lajoie BR, Schulz EG, Giorgetti L, Okamoto I, Servant N, Piolot T, van Berkum NL, Meisig J, Sedat J, *et al* (2012) Spatial partitioning of the regulatory landscape of the X-inactivation centre. *Nature* 485: 381–385

Oskarsson T, Acharyya S, Zhang XHF, Vanharanta S, Tavazoie SF, Morris PG, Downey RJ, Manova-Todorova K, Brogi E & Massagué J (2011) Breast cancer cells produce tenascin C as a metastatic niche component to colonize the lungs. *Nat Med* 17: 867–874

Pampin M, Simonin Y, Blondel B, Percherancier Y & Chelbi-Alix MK (2006) Cross Talk between PML and p53 during Poliovirus Infection: Implications for Antiviral Defense. *J Virol* 80: 8582–8592

Panagoulias I, Karagiannis F, Aggeletopoulou I, Georgakopoulos T, Argyropoulos CP, Akinosoglou K, Gogos C, Skoutelis A & Mouzaki A (2018) Ets-2 Acts As a Transcriptional Repressor of the Human Immunodeficiency Virus Type 1 through Binding to a Repressor–Activator Target Sequence of 5′-LTR. *Front Immunol* 8: 1–15

Pascual-Reguant L, Blanco E, Galan S, Le Dily F, Cuartero Y, Serra-Bardenys G, Di Carlo V, Iturbide A, Cebrià-Costa JP, Nonell L, *et al* (2018) Lamin B1 mapping reveals the existence of dynamic and functional euchromatin lamin B1 domains. *Nat Commun* 9: 3420

Peric-Hupkes D, Meuleman W, Pagie L, Bruggeman SWM, Solovei I, Brugman W, Gräf S, Flicek P, Kerkhoven RM, van Lohuizen M, *et al* (2010) Molecular Maps of the Reorganization of Genome-Nuclear Lamina Interactions during Differentiation. *Mol Cell* 38: 603–613

Politz JCR, Scalzo D & Groudine M (2013) Something silent this way forms: The functional organization of the repressive nuclear compartment. *Annu Rev Cell Dev Biol* 29: 241–270

Ponente M, Campanini L, Cuttano R, Piunti A, Delledonne GA, Coltella N, Valsecchi R, Villa A, Cavallaro U, Pattini L, *et al* (2017) PML promotes metastasis of triple-negative breast cancer through transcriptional regulation of HIF1A target genes. *JCI Insight* 2: 1–15

Prakash K & Fournier D (2018) Evidence for the implication of the histone code in building the genome structure. *Biosystems* 164: 49–59

Quinodoz SA, Ollikainen N, Tabak B, Palla A, Schmidt JM, Detmar E, Lai MM, Shishkin AA, Bhat P, Takei Y, *et al* (2018) Higher-Order Inter-chromosomal Hubs Shape 3D Genome Organization in the Nucleus. *Cell* 174: 744-757.e24

Rai TS, Cole JJ, Nelson DM, Dikovskaya D, Faller WJ, Vizioli MG, Hewitt RN, Anannya O, McBryan T, Manoharan I, *et al* (2014) HIRA orchestrates a dynamic chromatin landscape in senescence and is required for suppression of neoplasia. *Genes Dev* 28: 2712–2725

Razin S V., Borunova V V., Iarovaia O V. & Vassetzky YS (2014) Nuclear matrix and structural and functional compartmentalization of the eucaryotic cell nucleus. *Biochem* 79: 608–618

Robinson JT, Thorvaldsdóttir H, Winckler W, Guttman M, Lander ES, Getz G & Mesirov JP (2011) Integrative genomics viewer. *Nat Biotechnol* 29: 24–26

Saatci O, Kaymak A, Raza U, Ersan PG, Akbulut O, Banister CE, Sikirzhytski V, Tokat UM, Aykut G, Ansari SA, *et al* (2020) Targeting lysyl oxidase (LOX) overcomes chemotherapy resistance in triple negative breast cancer. *Nat Commun* 11: 2416

Sachini N, Arampatzi P, Klonizakis A, Nikolaou C, Makatounakis T, Lam EWF, Kretsovali A & Papamatheakis J (2019) Promyelocytic leukemia protein (<scp>PML</scp>) controls breast cancer cell proliferation by modulating Forkhead transcription factors. *Mol Oncol* 13: 1369–1387

Sadaie M, Salama R, Carroll T, Tomimatsu K, Chandra T, Young ARJ, Narita M, Pérez-Mancera PA, Bennett DC, Chong H, *et al* (2013) Redistribution of the Lamin B1 genomic binding profile affects rearrangement of heterochromatic domains and SAHF formation during senescence. *Genes Dev* 27: 1800–1808

Sahin U, Ferhi O, Jeanne M, Benhenda S, Berthier C, Jollivet F, Niwa-Kawakita M, Faklaris O, Setterblad N, de Thé H, *et al* (2014) Oxidative stress–induced assembly of PML nuclear bodies controls sumoylation of partner proteins. *J Cell Biol* 204: 931–945

Saksouk N, Barth TK, Ziegler-Birling C, Olova N, Nowak A, Rey E, Mateos-Langerak J, Urbach S, Reik W, Torres-Padilla M-E, *et al* (2014) Redundant Mechanisms to Form Silent Chromatin at Pericentromeric Regions Rely on BEND3 and DNA Methylation. *Mol Cell* 56: 580–594

Salomoni P, Bernardi R, Bergmann S, Changou A, Tuttle S & Pandolfi PP (2005) The promyelocytic leukemia protein PML regulates c-Jun function in response to DNA damage. *Blood* 105: 3686–3690

Sardiello M, Cairo S, Fontanella B, Ballabio A & Meroni G (2008) Genomic analysis of the TRIM family reveals two groups of genes with distinct evolutionary properties. *BMC Evol Biol* 8: 225

Schödel J, Oikonomopoulos S, Ragoussis J, Pugh CW, Ratcliffe PJ & Mole DR (2011) High-resolution genome-wide mapping of HIF-binding sites by ChIP-seq. *Blood* 117: e207–e217

Seifert LL, Si C, Saha D, Sadic M, de Vries M, Ballentine S, Briley A, Wang G, Valero-Jimenez AM, Mohamed A, *et al* (2019) The ETS transcription factor ELF1 regulates a broadly antiviral program distinct from the type I interferon response. *PLOS Pathog* 15: e1007634

Semenza GL (2003) Targeting HIF-1 for cancer therapy. *Nat Rev Cancer* 3: 721–732

Sharrocks AD (2001) The ETS-domain transcription factor family. *Nat Rev Mol Cell Biol* 2: 827–837

Shastrula PK, Sierra I, Deng Z, Keeney F, Hayden JE, Lieberman PM & Janicki SM

(2019a) PML is recruited to heterochromatin during S phase and represses DAXX-mediated histone H3.3 chromatin assembly. *J Cell Sci* 132

Shastrula PK, Sierra I, Deng Z, Keeney F, Hayden JE, Lieberman PM & Janicki SM (2019b) PML is recruited to heterochromatin during S phase and represses DAXX-mediated histone H3.3 chromatin assembly. *J Cell Sci* 132

Shaulian E & Karin M (2002) AP-1 as a regulator of cell life and death. *Nat Cell Biol* 4: E131–E136

Shiels C, Islam SA, Vatcheva R, Sasieni P, Sternberg MJE, Freemont PS & Sheer D (2001) PML bodies associate specifically with the MHC gene cluster in interphase nuclei. *J Cell Sci* 114: 3705–3716

Shyu YJ, Liu H, Deng X & Hu C-D (2006) Identification of new fluorescent protein fragments for bimolecular fluorescence complementation analysis under physiological conditions. *Biotechniques* 40: 61–66

Solovei I, Thanisch K & Feodorova Y (2016) How to rule the nucleus: divide et impera. *Curr Opin Cell Biol* 40: 47–59

Spirkoski J, Shah A, Reiner AH, Collas P & Delbarre E (2019) PML modulates H3.3 targeting to telomeric and centromeric repeats in mouse fibroblasts. *Biochem Biophys Res Commun* 511: 882–888

van Steensel B & Belmont AS (2017) Lamina-Associated Domains: Links with Chromosome Architecture, Heterochromatin, and Gene Repression. *Cell* 169: 780–791

Sun Y, Durrin LK & Krontiris TG (2003) Specific interaction of PML bodies with the TP53 locus in Jurkat interphase nuclei. *Genomics* 82: 250–252

Takei Y, Yun J, Zheng S, Ollikainen N, Pierson N, White J, Shah S, Thomassie J, Suo S, Eng C-HL, *et al* (2021) Integrated spatial genomics reveals global architecture of single nuclei. *Nature* 590: 344–350

Tang Y, Chen Y, Jiang H & Nie D (2010) Promotion of tumor development in prostate cancer by progerin. *Cancer Cell Int* 10: 47

Tashiro S, Muto A, Tanimoto K, Tsuchiya H, Suzuki H, Hoshino H, Yoshida M, Walter J & Igarashi K (2004) Repression of PML Nuclear Body-Associated Transcription by Oxidative Stress-Activated Bach2. *Mol Cell Biol* 24: 3473–3484

Taylor CT & McElwain JC (2010) Ancient Atmospheres and the Evolution of Oxygen Sensing Via the Hypoxia-Inducible Factor in Metazoans. *Physiology* 25: 272–279

Ulbricht T, Alzrigat M, Horch A, Reuter N, von Mikecz A, Steimle V, Schmitt E, Krämer OH, Stamminger T & Hemmerich P (2012) PML promotes MHC class II gene expression by stabilizing the class II transactivator. *J Cell Biol* 199: 49–63

Vallian S, Gäken JA, Gingold EB, Kouzarides T, Chang K-S & Farzaneh F (1998) Modulation of Fos-mediated AP-1 transcription by the promyelocytic leukemia protein. *Oncogene* 16: 2843–2853

Vancurova M, Hanzlikova H, Knoblochova L, Kosla J, Majera D, Mistrik M, Burdova K, Hodny Z & Bartek J (2019) PML nuclear bodies are recruited to persistent DNA damage lesions in an RNF168-53BP1 dependent manner and contribute to DNA repair. *DNA Repair (Amst)* 78: 114–127

Versteeg GA, Benke S, García-Sastre A & Rajsbaum R (2014) InTRIMsic immunity: Positive and negative regulation of immune signaling by tripartite motif proteins. *Cytokine Growth Factor Rev* 25: 563–576

Voon HPJ & Wong LH (2016) New players in heterochromatin silencing: histone variant H3.3 and the ATRX/DAXX chaperone. *Nucleic Acids Res* 44: 1496–1501

Wang C, Su L De, Ming Y, Zhong W, Bu N, Hao R & Ya L (2019) Involvement of PML-I in reformation of PML nuclear bodies in acute promyelocytic leukemia cells by leptomycin B. 384

Wang J, Shiels C, Sasieni P, Wu PJ, Islam SA, Freemont PS & Sheer D (2004) Promyelocytic leukemia nuclear bodies associate with transcriptionally active genomic regions. *J Cell Biol* 164: 515–526

Wang M, Wang L, Qian M, Tang X, Liu Z, Lai Y, Ao Y, Huang Y, Meng Y, Shi L, *et al* (2020) PML2-mediated thread-like nuclear bodies mark late senescence in Hutchinson–Gilford progeria syndrome. *Aging Cell* 19: 1–14

Wang P, Benhenda S, Wu H, Lallemand-Breitenbach V, Zhen T, Jollivet F, Peres L, Li Y, Chen S-J, Chen Z, *et al* (2018) RING tetramerization is required for nuclear body biogenesis and PML sumoylation. *Nat Commun* 9: 1277

Weidtkamp-Peters S, Lenser T, Negorev D, Gerstner N, Hofmann TG, Schwanitz G, Hoischen C, Maul G, Dittrich P & Hemmerich P (2008) Dynamics of component exchange at PML nuclear bodies. *J Cell Sci* 121: 2731–2743

Yang S, Wei W & Zhao Q (2020) B7-H3, a checkpoint molecule, as a target for cancer immunotherapy. *Int J Biol Sci* 16: 1767–1773

Yeung PL, Denissova NG, Nasello C, Hakhverdyan Z, Chen JD & Brenneman MA (2011) Promyelocytic leukemia nuclear bodies support a late step in DNA double-strand break repair by homologous recombination. *J Cell Biochem* 23: n/a-n/a

Zhang H, Wong CCL, Wei H, Gilkes DM, Korangath P, Chaturvedi P, Schito L, Chen J, Krishnamachary B, Winnard PT, *et al* (2012) HIF-1-dependent expression of angiopoietin-like 4 and L1CAM mediates vascular metastasis of hypoxic breast cancer cells to the lungs. *Oncogene* 31: 1757–1770

Zhang J-M, Yadav T, Ouyang J, Lan L & Zou L (2019) Alternative Lengthening of Telomeres through Two Distinct Break-Induced Replication Pathways. *Cell Rep* 26: 955-968.e3

Zhang Q, Lei L & Jing D (2020) Knockdown of SERPINE1 reverses resistance of triple-negative breast cancer to paclitaxel via suppression of VEGFA. *Oncol Rep* 44: 1875–1884

Zhang R, Poustovoitov M V., Ye X, Santos HA, Chen W, Daganzo SM, Erzberger JP, Serebriiskii IG, Canutescu AA, Dunbrack RL, *et al* (2005) Formation of

MacroH2A-Containing Senescence-Associated Heterochromatin Foci and Senescence Driven by ASF1a and HIRA. *Dev Cell* 8: 19–30

Zhang Y, Liu T, Meyer CA, Eeckhoute J, Johnson DS, Bernstein BE, Nusbaum C, Myers RM, Brown M, Li W, *et al* (2008) Model-based Analysis of ChIP-Seq (MACS). *Genome Biol* 9: R137

Zheng P, Guo Y, Niu Q, Levy DE, Dyck JA, Lu S, Sheiman LA & Liu Y (1998) Proto-oncogene PML controls genes devoted to MHC class I antigen presentation. *Nature* 396: 373–376

Zheng R, Wan C, Mei S, Qin Q, Wu Q, Sun H, Chen C-H, Brown M, Zhang X, Meyer CA, *et al* (2019) Cistrome Data Browser: expanded datasets and new tools for gene regulatory analysis. *Nucleic Acids Res* 47: D729–D735

Zhong S, Salomoni P & Pandolfi PP (2000) The transcriptional role of PML and the nuclear body. *Nat Cell Biol* 2: E85–E90